國 立 交 通 大 學

機械工程學系

碩士論文

渾沌與鳥群行為控制，渾沌廣義及交織同步與超渾沌

Chaos and Boids Control, Generalized, Symplectic Synchronization and Hyperchaos of Chaotic Systems

研 究 生：陳聰文

指導教授：戈正銘　教授

中華民國九十八年一月

渾沌與鳥群行為控制，渾沌廣義及交織同步與超渾沌

Chaos and Boids Control, Generalized, Symplectic Synchronization and Hyperchaos of Chaotic Systems

研究生：陳聰文　　Student: Tsung-Wen Chen

指導教授：戈正銘　　Advisor: Zheng-Ming Ge

國 立 交 通 大 學

機 械 工 程 研 究 所

碩 士 論 文

A Thesis

Submitted to Institute of Mechanical Engineering

College of Engineering

National Chiao Tung University

In Partial Fulfillment of the Requirement

For the Degree of master of science

In

Mechanical Engineering

January 2009

Hsinchu, Taiwan, Republic of China

中華民國九十八年一月

國立交通大學

論文口試委員會審定書

本校 機械工程 學系碩士班 陳聰文 君

所提論文(中文)渾沌與鳥群行為控制，渾沌廣義及交織同步與超渾沌

(英文) Chaos and Boids Control, Generalized, Symplectic Synchronization and Hyperchaos of Chaotic Systems

合於碩士資格水準、業經本委員會評審認可。

口試委員：許陳紘　李青一

陳鵬升　戈正銘

指導教授：戈正銘

系主任：陳仁浩 教授

中華民國 九十八 年 一 月 八 日

渾沌與鳥群行為控制，渾沌廣義及交織同步與超渾沌

學生：陳聰文　　指導教授：戈正銘

摘要

本篇論文以相圖、龐卡萊映射圖、Lyapunov 指數、分歧圖以及參數圖等數值方法研究慣性測速器系統的渾沌現象。對此系統研究應用 GYC 部分區域穩定理論來研究系統的廣義渾沌同步和渾沌控制。以非自治慣性測速器系統來模擬鳥群的渾沌行為。此外，將探討 Lorenz 系統以 Bessel 函數為參數的渾沌及超渾沌行為。最後透過非線性方法來研究非自治系統的交織同步。在以上研究中，皆可由相圖和時間歷程圖得到驗證。

Chaos and Boids Control, Generalized, Symplectic Synchronization and Hyperchaos of Chaotic Systems

Student：Tsung-Wen Chen **Advisor：Zheng-Ming Ge**

Abstract

In this thesis, the chaotic behavior in an inertial tachometer system is studied by phase portraits, time histories, Poincaré maps, Lyapunov exponents, bifurcation diagram and parametric diagram. A new strategy to achieve chaos generalized synchronization and chaos control by GYC partial region stability theory is proposed Boids control of chaos for a nonautonomous inertial tachometer system is presented. Moreover, the Lorenz system with Bessel function parameters is studied for chaotic and hyperchaotic behaviors. Finally, a new symplectic synchronization of different order nonautonomous systems via nonlinear control is studied. Numerical analysis, such as phase portraits and time histories can be provided to verfy the effectiveness in all above studies.

誌　　謝

此篇論文及碩士學業之完成，首先必須感謝指導教授　戈正銘老師的耐心指導與教誨。老師專業領域上的成就以及對於文學和史學上的熱情，都令學生印象深刻且受益匪淺。這兩年的相處，在學術研究之餘也體會到古典文學的美，這都開拓了學生不一樣的視野。

這研究的日子中，承蒙張晉銘、李仕宇、李乾豪、李式中、吳宗訓、林森生學長和翁郁婷學姐的熱心指導，同時也感謝彥賢、凱銘、俊諺、峻宇、聰文、瑜韓、志銘、育銘同學的相互勉勵和幫忙。另外也要感謝學弟泳厚、翔平、尚恩、振賓，幫忙處理煩瑣雜事，使得本篇論文能夠順利的完成。

最後感謝我的家人，讓我可以不必擔心課業以外的事物，無後顧之憂的完成學業。最後，僅以此論文獻給你們。

CONTENTS

CHINESE ABSTRACT……..…i
ABSTRACT……...…ii
ACKNOWLEDGMENT…….. iii
CONTENTS……..iv
LIST OF FIGURES……...vi

Chapter 1 Introduction…….1

Chapter 2 Chaos of an Inertial Tachometer System……..4

2.1 Preliminaries……..4

2.2 Description of an Inertial Tachometer System……..4

2.3 Computational Analysis of an Inertial Tachometer System……..…5

Chapter 3 Chaos Generalized Synchronization of Inertial Tachometer Systems with a New Mathieu-Van der Pol Systems as Functional System by GYC Partial Region Stability Theory……13

3.1 Preliminaries……13

3.2 Generalized Chaos Synchronization Strategy……13

3.3 Chaos of a New Mathieu-Van der Pol System……14

3.4 Numerical Simulations……14

Chapter 4 Chaos Control of an Inertial Tachometer System by GYC Partial Region Stability Theory……...30

4.1 Preliminaries……30

4.2 Chaos Control Scheme……30

4.3 Numerical Simulations……31

Chapter 5 Boids Control of Chaos for an Inertial Tachometer System…….41

5.1 Preliminaries……41

5.2 Boids Nonlinear Control……41

5.3 Chaos of an Inertial Tachometer……..43

5.4 Numerical Simulations of Boids Control……45

Chapter 6 Hyperchaos of a Lorenz System with Bessel Function Parameters..57

6.1 Preliminaries……57

6.2 Lorenz System with Bessel Function Parameters……...57

6.3 Numerical Simulations……58

Chapter 7 Symplectic Synchronization Scheme of Different Order Nonautonomous Systems via Nonlinear Control……..……67

7.1 Preliminaries……67

7.2 Symplectic Synchronization of Different Order Nonautonomous Chaotic Systems……...68

7.3 Numerical Results……...70

Chapter 8 Conclusions……81

Appendix A GYC Partial Region Stability Theory…….....83

References……...91

LIST OF FIGURES

Fig. 2.1 Sketch of an inertial tachometer……....6

Fig. 2.2 The bifurcation diagram for an inertial tachometer system……..6

Fig. 2.3 The Lyapunov exponents for an inertial tachometer system…….7

Fig. 2.4 Phase portrait, Poincaré map, and time histories for an inertial tachometer system with A=0.5 (period 1)…….8

Fig. 2.5 Phase portrait, Poincaré maps, and time histories for an inertial tachometer system with A=2.5 (period 2)……...9

Fig. 2.6 Phase portrait, Poincaré maps, and time histories for an inertial tachometer system with A=4.6 (period 4)…….10

Fig. 2.7 Phase portrait, Poincaré maps, and time histories for an inertial tachometer system with A=10.5 (chaos)……...11

Fig. 2.8 The parametric diagram for an inertial tachometer system…….12

Fig. 3.1 Phase portraits of new Mathieu-Van der Pol system……..23

Fig. 3.2 Time histories of the four states of new Mathieu-van der Pol system……23

Fig. 3.3 Phase portraits of four errors dynamics for Case I……..24

Fig. 3.4 Time histories of errors for Case I……..24

Fig. 3.5 Time histories of $x_1, x_2, x_3, x_4, y_1, y_2, y_3, y_4$ for Case I……...25

Fig. 3.6 Phase portraits of error dynamics for Case II…….25

Fig. 3.7 Time histories of errors for Case II…….26

Fig. 3.8 Time histories of $x_i - y_i + K$ and $-F\sin\omega t$ for Case II…….26

Fig. 3.9 Phase portraits of error dynamics for Case III……....27

Fig. 3.10 Time histories of error for Case III……...27

Fig. 3.11 Time histories of $\frac{1}{2}x_i^2 + 20$ and y_i for Case III…….. 28

Fig. 3.12 Phase portraits of error dynamics for Case IV……..28

Fig. 3.13 Time histories of errors for Case IV……..29

Fig. 3.14 Time histories of $x_i - y_i + 50$ and $-z_i$ for Case IV……...29

Fig. 4.1 Phase portraits of error dynamics for Case I…….. 37

Fig. 4.2 Time histories of errors for Case I……..37

Fig. 4.3 Phase portraits of error dynamics for Case II…….38

Fig. 4.4 Time histories of errors for Case II…….38

Fig. 4.5 Time histories of x_1, x_2, x_3, x_4 and $F \sin w_i t$ for Case II……...39

Fig. 4.6 Phase portraits of error dynamics for Case III……....39

Fig. 4.7 Time histories of errors for Case III……40

Fig. 4.8 Time histories of x_1, x_2, x_3, x_4 for Case III……..40

Fig. 5.1 Mechanical model of an inertial tachometer……...49

Fig. 5.2 Chaotic phase portrait of chaotic for inertial tachometer system……49

Fig. 5.3 Phase portrait of chaotic for inertial tachometer system…….50

Fig. 5.4 Lyapunov exponents for A between 9.1 and 10.9……...50

Fig. 5.5 Bifurcation diagram of x_1 for A between 9.1 and 10.9…….51

Fig. 5.6 Flocking of two inertial tachometer systems……..51

Fig. 5.7 Distance between two inertial tachometer systems…….52

Fig. 5.8 Synchronization of two inertial tachometer systems……..52

Fig. 5.9 Separation of two inertial tachometer systems……...53

Fig. 5.10 Distance between two inertial tachometer systems……..53

Fig. 5.11 Desynchronization of two inertial tachometer systems……54

Fig. 5.12 Obstacle avoidance for inertial tachometer system (sphere)……54

Fig. 5.13 Obstacle avoidance for inertial tachometer system (sphere)……55

Fig. 5.14 Obstacle avoidance for inertial tachometer system (cylinder)……..55

Fig. 5.15 Obstacle avoidance for inertial tachometer system (cylinder)……..56

Fig. 6.1 The time history $\sigma(t)$ ……61

Fig. 6.2 The time history of $Y_0(t+0.01)$……...61

Fig. 6.3 The time histories of the three states……...62

Fig. 6.4 The phase portrait and Poincaré map for x, y states……62

Fig. 6.5 The time histories of the x, y, z states……63

Fig. 6.6 The phase portrait of x, y, z states……..63

Fig. 6.7 The phase portrait and Poincaré map for x, y states……64

Fig. 6.8 The bifurcation diagram for $\sigma = 10 + J_0(t)$, and $b = 8/3$ ……64

Fig. 6.9 Lyapunov exponents of system (2-2) for varying k_2 ……65

Fig. 6.10 The parametric diagram of system (2-1) for varying k_1 and k_2 ……66

Fig. 6.11 Lyapunov exponents of system (2-2) for varying b, with $k_1 = 30$ and $k_2 = 28$ ……

….66

Fig. 7.1 Phase portrait of Duffing system……75

Fig. 7.2 Time histories of two states of Duffing system……..75

Fig. 7.3 Phase portrait of van der Pol system……...76

Fig. 7.4 Time histories of the two states of van der Pol system……...76

Fig. 7.5 Time history of error $e_1(t)$ for Case I……...77

Fig. 7.6 Time history of error $e_2(t)$ for Case I……..77

Fig. 7.7 Phase portrait of van der Pol system……...78

Fig. 7.8 Phase portraits of Chen-Lee system……78

Fig. 7.9 Time histories of the three states of Chen-Lee system……79

Fig. 7.10 Time history of error $e_1(t)$ for Case II……79

Fig. 7.11 Time history of error $e_2(t)$ for Case II……...80

Fig. A.1. Partial regions Ω and Ω_1 ……..90

Chapter 1

Introduction

Chaos is an interesting nonlinear phenomenon in nature and has been investigated extensively. Lorenz researched the strange changes in the atmosphere that is the first example to study chaos in 1963. In nature, most of dynamic systems are nonlinear and can be described by the nonlinear equation of motion. Chaotic system features that it has complex dynamical behaviors and sensitive behavior dependence on initial conditions.

Chaos synchronization, first proposed by Fujisaka and Yamada in 1983 [1], did not received great attention until 1990 [2]. In recent years, synchronization in chaotic dynamic system is a very interesting problem and has been widely studied [3-5]. There are different types of synchronization for interacting chaotic systems, such as complete synchronization [6], generalized synchronization [7], phase synchronization [8-9], lag synchronization [10-11], anticipating synchronization [12-13] and so on. Recently, many valuable control methods and techniques have been developed to synchronize chaotic systems, such as PC methods [2], linear error feedback control [14-18], adaptive control, active control, fuzzy control and impulsive control [19-27].

This thesis is organized as follows. In Chapter 2, the chaotic behaviors of an inertial tachometer system is studied numerically by phase portraits, time histories, Poincaré maps, Lyapunov exponents, bifurcation diagram, and parametric diagram. These methods can be used to explain that chaos exists in an inertial tachometer system.

In Chapter 3 and Chapter 4, a new strategy to achieve chaos generalized synchronization and chaos control by GYC partial region stability theory (see

Appendix A) is proposed [28-29]. By using the GYC partial region stability theory, the Lyapunov function is a simple linear homogeneous function of error states and the controllers are more simple and have less simulation error because they are in lower degree than that of traditional controllers.

In Chapter 5, boids control of chaos for a nonautonomous inertial tachometer system is presented. Boids is short for "Birdoid". Boids control [30] is an artificial life program, simulating animal motion such as congregating behavior of birds, herding behavior of land animals and moving behavior of fishes [31]. The behavior of boids can either be characterized as chaotic or orderly. The boids work in a manner similar to cellular neural networks, since each boid acts individually and references a neighborhood, as cellular neural networks do [32]. Boids control is an interesting strategy for control. Some computer simulation examples are given in this Chapter.

In Chapter 6, the chaotic behaviors in Lorenz system with Bessel function parameters is studied numerically by time histories of states, phase portraits, Poincaré maps, bifurcation diagram, Lyapunov exponents and parameter diagram. It is found that chaos and hyperchaos abundantly exist.

In Chapter 7, a new symplectic synchronization*

$$y = F(x, y, t) \tag{1-1}$$

is studied, where x, y are state vectors of the "master" and of the "slave", respectively, $F(x, y, t)$ is a given function of x, y and time. When $F(x, y, t) = F(x, t)$, Eq. (1-1) reduces to the generalized synchronization $y = F(x, t)$. Therefore the generalized synchronization is a special case of symplectic generalized synchronization. In Eq. (1-1), the final desired state y of the "slave" system [33] not only depends upon the "master" system state x but also depends upon the

*The term "symplectic" comes the Greek for "interwined". H. Weyl first introduced in 1939 in this book "The Classical Groups" (P. 165 in both the first edition, 1939, and second edition, 1946, Princeton University Press).

"slave" system state y itself. Therefore the "slave" system is not traditional pure slave obeying the "master" system completely but plays a role to determine the final desired state of the "slave" system. In other words, it plays an "interwined" role, so we call this kind of synchronization "symplectic synchronization", and call the "master" system partner A, the "slave" system partner B. By using the Barbalat lemma [34], the symplectic synchronization can be achieved. In simulation examples, Duffing system, Van der Pol system and Chen-Lee system [35] are used.

In Chapter 8, conclusions are drawn. In Appendix, GYC (Ge-Yao-Chen) partial region stability theory is given.

Chapter 2

Chaos of an Inertial Tachometer System

2.1 Preliminaries

An inertial tachometer system is studied by phase portraits, time histories, Poincaré maps, Lyapunov exponents, bifurcation diagram, and parametric diagram.

2.2 Description of an Inertial Tachometer System

The physical model of the inertial tachometer system is shown in Fig. 2.1. The mass of bent rod is neglected and the balls m_1 and m_2 are considered as two particles.

We can write the kinetic and potential energies of the system as follow：

$$T = \frac{1}{2}m_1(l^2\dot{\varphi}^2 + l^2\eta^2\sin^2\varphi) + \frac{1}{2}m_2(l^2\dot{\varphi}^2 + l^2\eta^2\cos^2\varphi) + \frac{1}{2}J\eta^2$$
$$\Pi = -gl(m_1\cos\varphi + m_2\sin\varphi) \qquad (2\text{-}1)$$

where

m_1, m_2 ：the mass of balls and $m_1 > m_2$,

J ：the moment of inertia of the shaft about vertical center axis,

l ： the length of rod,

φ ：the angle between the shaft and the rod,

η ：constant angular velocity of the tachometer,

g ：gravity acceleration,

The Lagrangian is $L = T - \Pi$, the corresponding Lagrange equations are

$$(m_1 + m_2)l^2\ddot{\varphi} - (m_1 - m_2)l^2\eta^2\sin\varphi\cos\varphi + gl(m_1\cos\varphi - m_2\cos\varphi) = -k\dot{\varphi} \qquad (2\text{-}2)$$

where k is damping coefficient in bent rod bearing.

We assume that the inertial tachometer is subjected to an external vertical vibration basement $A\sin x_3$ where x_3 is state variable, A is the amplitude of vibration. The vertical axis rotates with constant speed η. The Lagrange equation now are given in a noninertial vibrating reference frame, which is fixed with the basement. Due to the inertial force appearing in the noninertial frame, the gravity acceleration in the noninertial frame becomes $g - A\omega^2 \sin \omega t$. Let $x_1 = \varphi$, $x_2 = \dot{\varphi}$, $x_3 = A\sin \omega t$, $x_4 = \dot{x}_3$, $\omega = \eta$.

And the state equations can be written as：

$$\begin{cases} \dot{x}_1 = x_2 \\ \dot{x}_2 = \dfrac{1}{m_1 + m_2}[(m_1 - m_2)\eta^2 \cos x_1 \sin x_1 \\ \quad -\dfrac{1}{l}(g - \eta^2 x_3)(m_1 \sin x_1 - m_2 \cos x_1) - \dfrac{k}{l^2} x_2] \\ \dot{x}_3 = x_4 \\ \dot{x}_4 = -A\eta^2 \sin x_3 \end{cases} \tag{2-3}$$

2.3 Computational Analysis of an Inertial Tachometer System

For numerical analysis of computation, this system exhibits chaos when the parameters are $m_1 = 9$, $m_2 = 1$, $A = 10.5$, $\eta = 1$, $l = 0.3$, $k = 0.5$, $g = 9.81$ and the initial condition is (x_1, x_2, x_3, x_4)= (0, 0, 2, 2). The bifurcation diagram by changing parameter *A* is shown in Fig. 2.2. Its corresponding Lyapunov exponents are shown in Fig. 2.3. The phase portraits, time histories, and Poincaré maps of the systems are showed in Fig. 2.4~Fig. 2.7. As *A* =0.5, it is period 1 in Fig. 2.4. As *A* =2.5 and *A* =4.6, they are period 2 and period 4 in Fig. 2.5~Fig. 2.6. As *A* =10.5, the chaotic behavior is given in Fig. 2.7, respectively. In addition, the parametric diagram is obtained in Fig. 2.8.

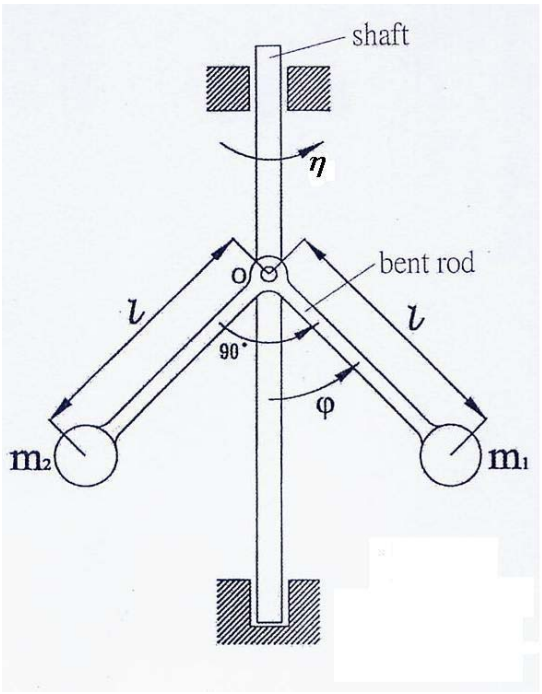

Fig. 2.1 Sketch of an inertial tachometer.

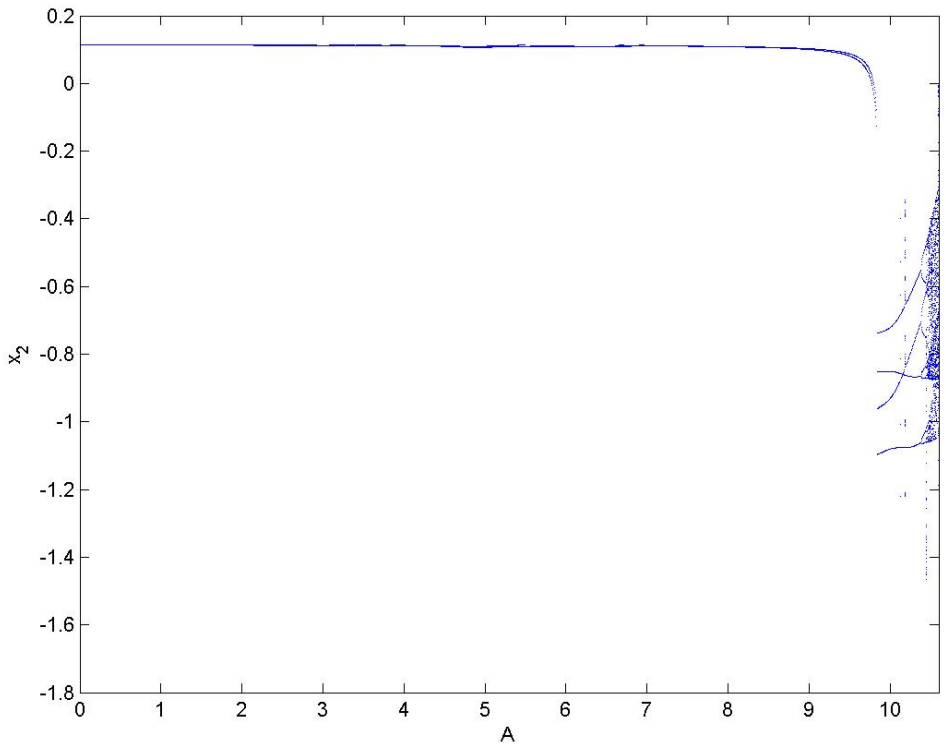

Fig. 2.2 The bifurcation diagram for an inertial tachometer system.

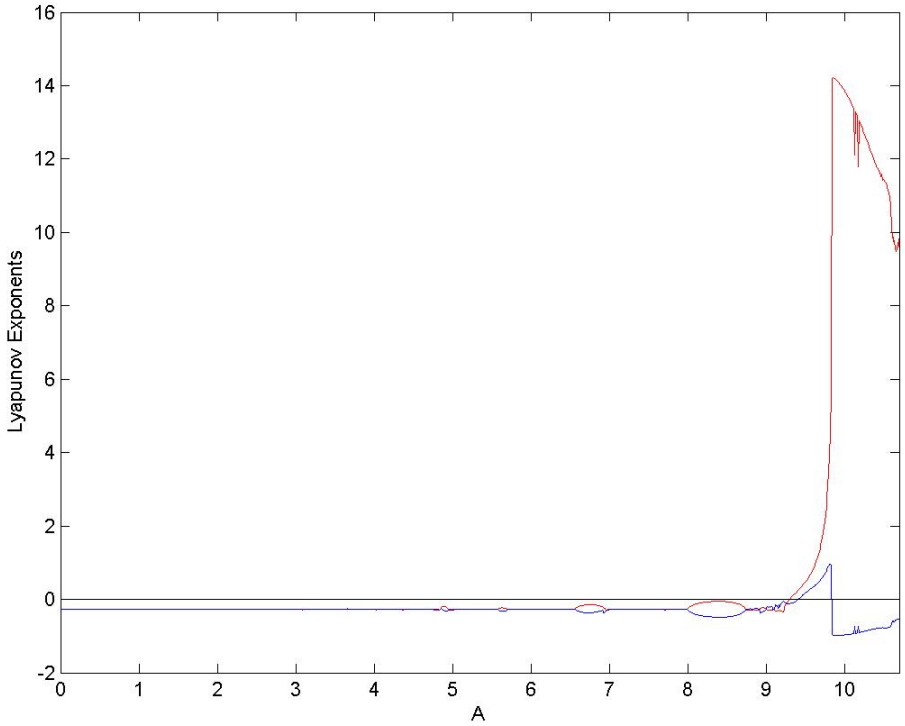

(a)

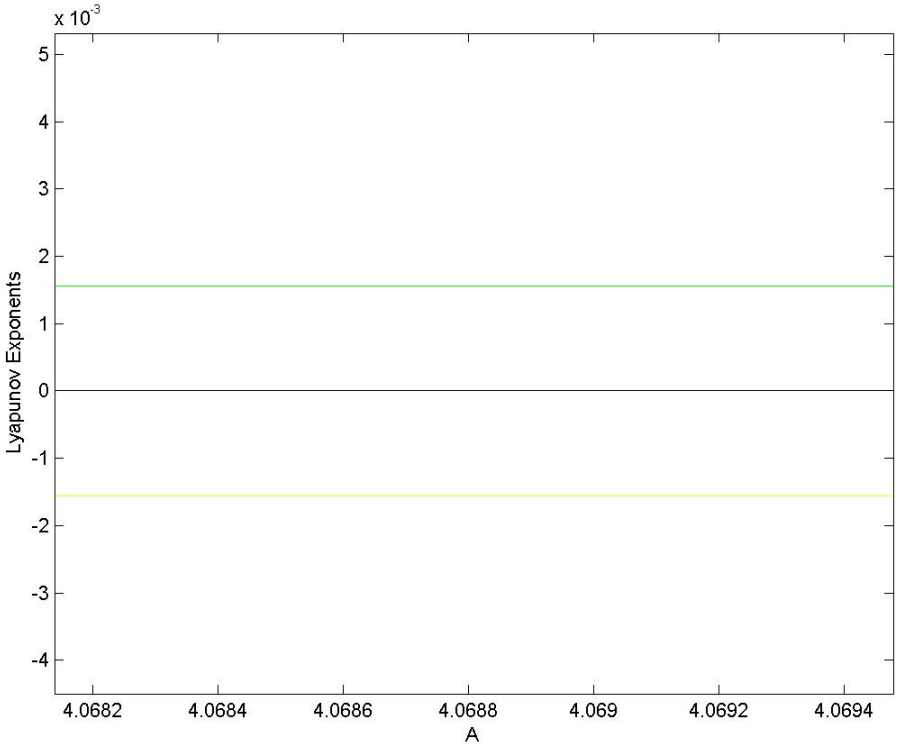

(b) Amplified diagram for (a).

Fig. 2.3 The Lyapunov exponents for an inertial tachometer system.

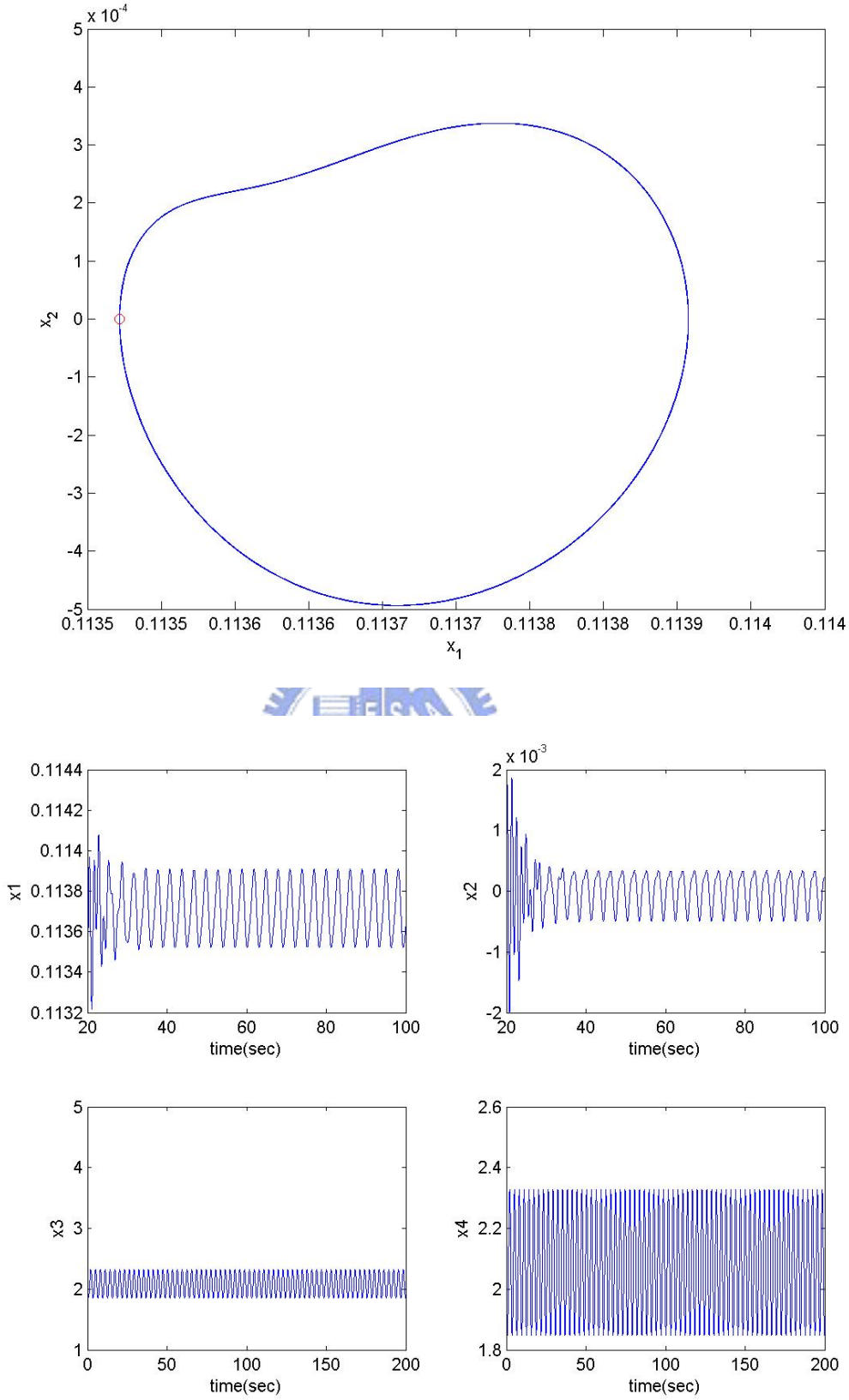

Fig. 2.4 Phase portrait, Poincaré map, and time histories for an inertial tachometer system with A=0.5 (period 1).

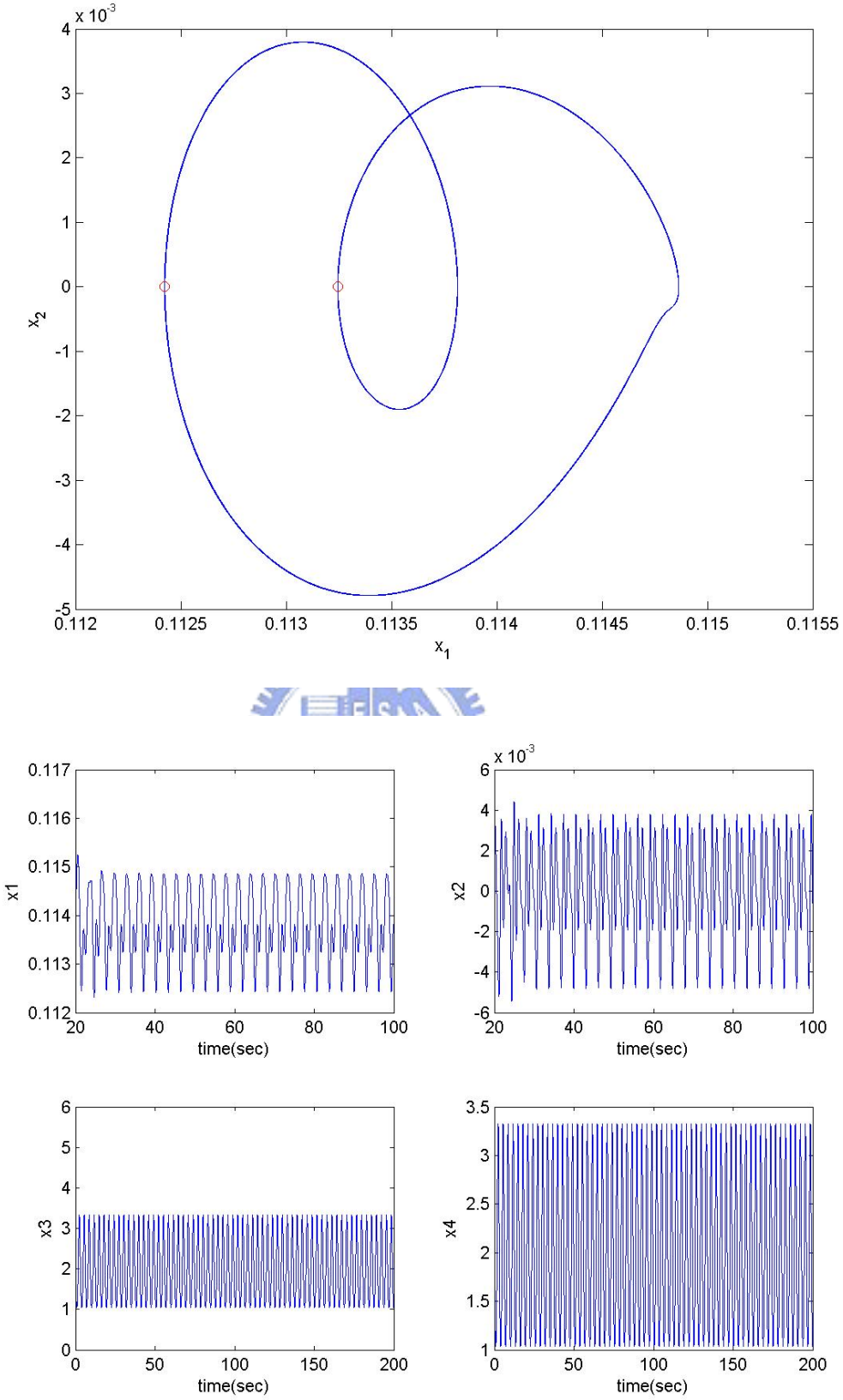

Fig. 2.5 Phase portrait, Poincaré maps, and time histories for an inertial tachometer system with A=2.5 (period 2).

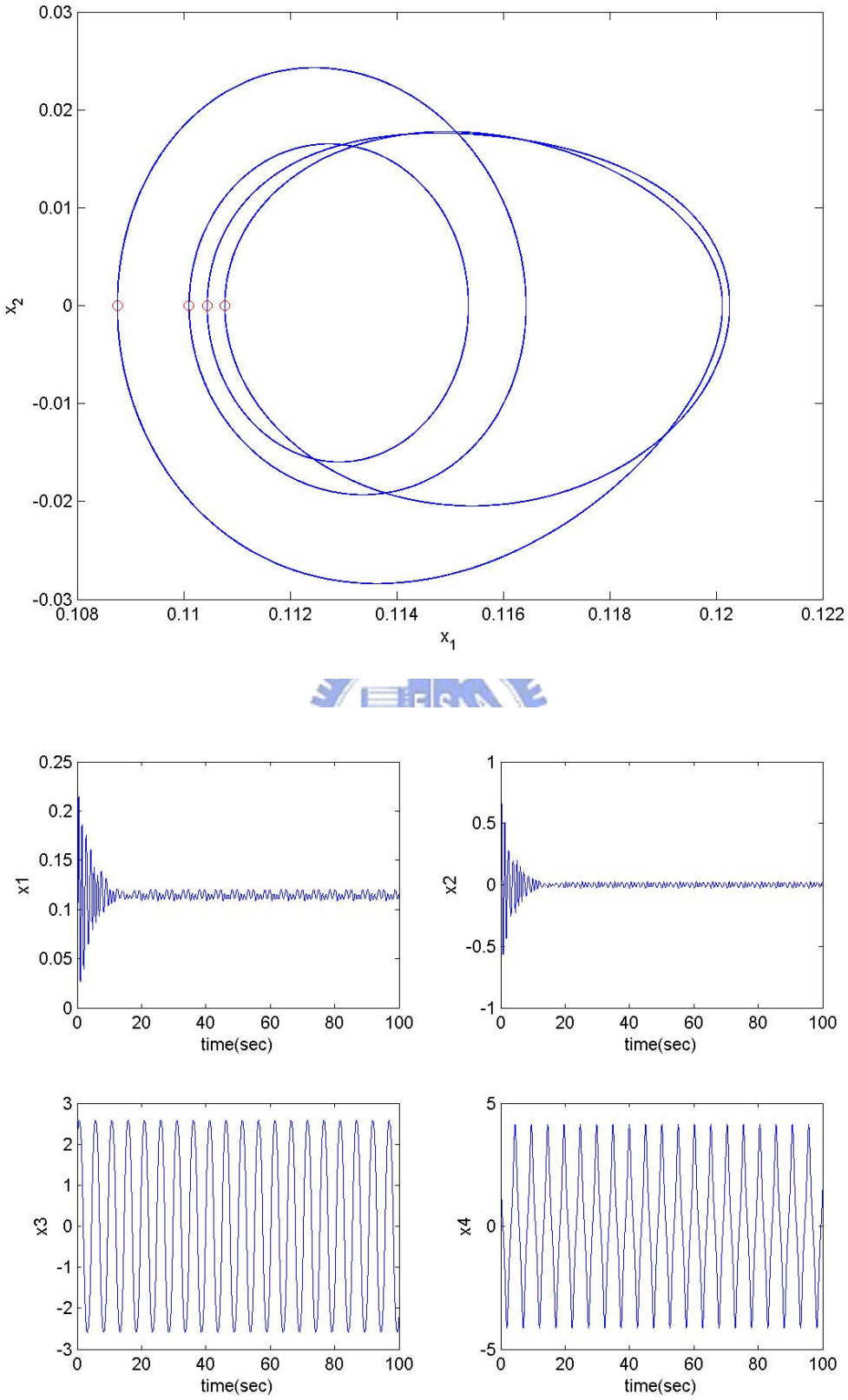

Fig. 2.6 Phase portrait, Poincaré maps, and time histories for an inertial tachometer system with A=4.6 (period 4).

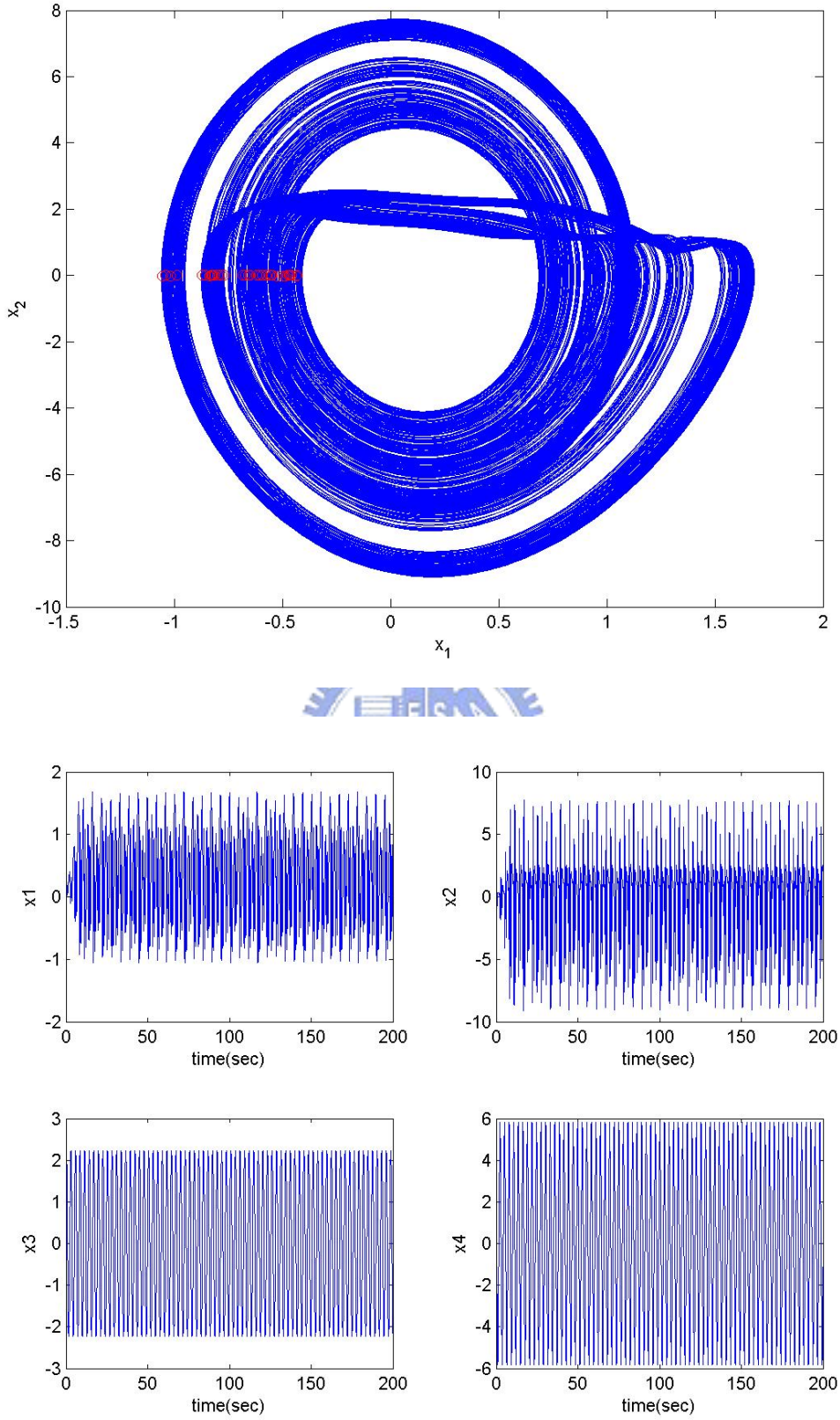

Fig. 2.7 Phase portrait, Poincaré maps, and time histories for an inertial tachometer system with A=10.5 (chaos).

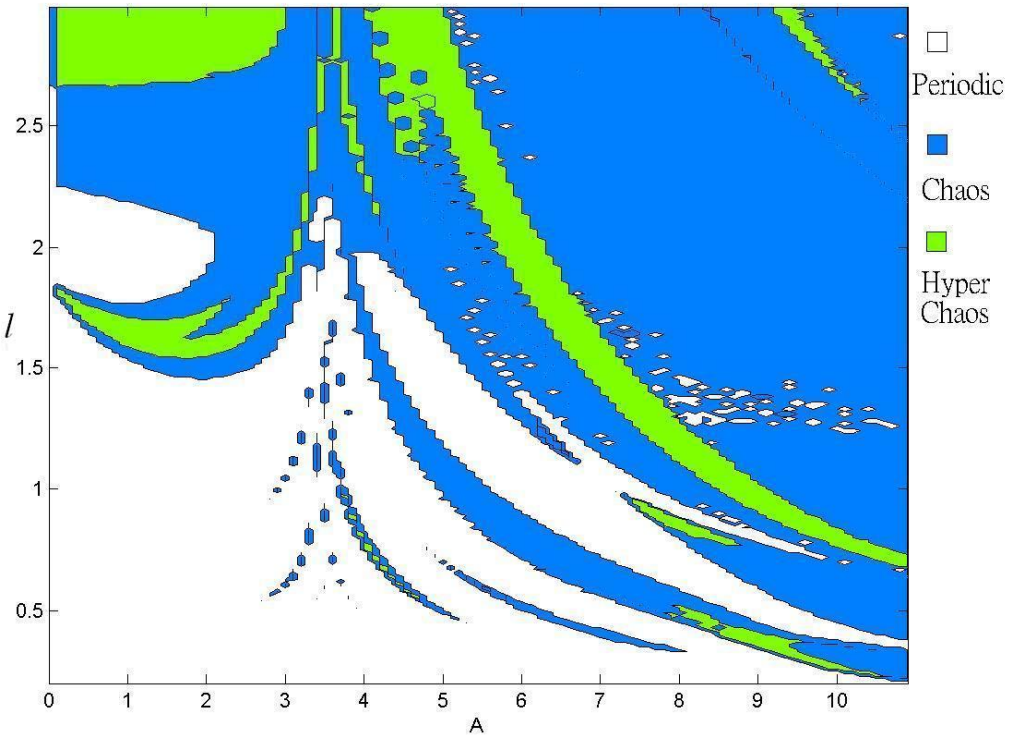

Fig. 2.8 The parametric diagram for an inertial tachometer system.

Chapter 3

Chaos Generalized Synchronization of Inertial Tachometer Systems with a New Mathieu-Van der Pol Systems as Functional System by GYC Partial Region Stability Theory

3.1 Preliminaries

A new strategy to achieve generalized chaos synchronization by GYC partial region stability theory is proposed. By using the GYC partial region stability theory the Lyapunov function is a simple linear homogeneous function of error states and the controllers are more simple and introduce less simulation error because they are in lower degree than that of traditional controllers. In simulation examples, an inertial tachometer system and Mathieu-Van der Pol system are used.

3.2 Generalized Chaos Synchronization Strategy

Consider the following unidirectional coupled chaotic systems

$$\begin{aligned} \dot{\mathbf{x}} &= \mathbf{f}(t, \mathbf{x}) \\ \dot{\mathbf{y}} &= \mathbf{h}(t, \mathbf{y}) + \mathbf{u} \end{aligned} \tag{3-1}$$

where $\mathbf{x} = [x_1, x_2, \cdots, x_n]^T \in R^n$, $\mathbf{y} = [y_1, y_2, \cdots, y_n]^T \in R^n$ denote the master state vector and slave state vector respectively, $\mathbf{f}$ and $\mathbf{h}$ are nonlinear vector functions, and $\mathbf{u} = [u_1, u_2, \cdots, u_n]^T \in R^n$ is a control input vector.

The generalized synchronization can be accomplished when $t \to \infty$, the limit of the error vector $\mathbf{e} = [e_1, e_2, \cdots, e_n]^T$ approaches zero:

$$\lim_{t\to\infty}\mathbf{e}=0 \tag{3-2}$$

where

$$\mathbf{e}=\mathbf{G}(\mathbf{x})-\mathbf{y} \tag{3-3}$$

$\boldsymbol{G}(\boldsymbol{x})$ is a given function of $\boldsymbol{x}$.

By using the partial region stability theory, the Lyapunov function is linear homogeneous function of error states. The controllers can be designed in lower degree.

3.3 Chaos of a New Mathieu- Van der Pol System

Mathieu equation and van der Pol equation are two typical nonlinear non-autonomous systems:

$$\begin{cases}\dot{z}_1=z_2\\ \dot{z}_2=-\left(a_1+b_1\sin wt\right)z_1-\left(a_1+b_1\sin wt\right)z_1^{\,3}-c_1z_2+d_1\sin wt\end{cases} \tag{3-4}$$

$$\begin{cases}\dot{z}_3=z_4\\ \dot{z}_4=-e_1z_3+f_1\left(1-z_3^{\,2}\right)z_4+g_1\sin wt\end{cases} \tag{3-5}$$

Exchanging sinwt in Eq. (3-4) with z_3 and sinwt in Eq. (3-5) with z_1, we obtain a new autonomous Mathieu-Van der Pol system：

$$\begin{cases}\dot{z}_1=z_2\\ \dot{z}_2=-\left(a_1+b_1z_3\right)z_1-\left(a_1+b_1z_3\right)z_1^{\,3}-c_1z_2+d_1z_3\\ \dot{z}_3=z_4\\ \dot{z}_4=-e_1z_3+f_1\left(1-z_3^{\,2}\right)z_4+g_1z_1\end{cases} \tag{3-6}$$

where $a_1, b_1, c_1, d_1, e_1, f_1, g_1,$ are uncertain parameters. This system exhibits chaos when the parameters of system are $a_1=10$, $b_1=3$, $c_1=0.4$, $d_1=70$, $e_1=1$, $f_1=5$, $g_1=0.1$ and the initial states of system are $(z_1, z_{,2}, z_3, z_4)$ = (0.1, -0.5, 0.1, -0.5). Its phase portraits and time histories are shown in Fig. 3.1 and Fig. 3.2.

3.4 Numerical Simulations

The following master and slave are two inertial tachometer systems with unidirectional coupling:

$$\begin{cases} \dot{x}_1 = x_2 \\ \dot{x}_2 = \dfrac{1}{m_1 + m_2}[(m_1 - m_2)\eta^2 \cos x_1 \sin x_1 \\ \quad -\dfrac{1}{l}(g - \eta^2 x_3)(m_1 \sin x_1 - m_2 \cos x_1) - \dfrac{k}{l^2} x_2] \\ \dot{x}_3 = x_4 \\ \dot{x}_4 = -A\eta^2 \sin x_3 \end{cases} \tag{3-7}$$

$$\begin{cases} \dot{y}_1 = y_2 + u_1 \\ \dot{y}_2 = \dfrac{1}{m_1 + m_2}[(m_1 - m_2)\eta^2 \cos y_1 \sin y_1 \\ \quad -\dfrac{1}{l}(g - \eta^2 y_3)(m_1 \sin y_1 - m_2 \cos y_1) - \dfrac{k}{l^2} y_2] + u_2 \\ \dot{y}_3 = y_4 + u_3 \\ \dot{y}_4 = -A\eta^2 \sin y_3 + u_4 \end{cases} \tag{3-8}$$

CASE I. The generalized synchronization error function is $e_i = x_i - y_i + 20$ $(i = 1,2,3,4)$. Our goal is $y_i = x_i + 20$, i.e.

$$\lim_{t\to\infty} e_i = \lim_{t\to\infty}(x_i - y_i + 20) = 0\,, \quad (i = 1,2,3,4) \tag{3-9}$$

The addition of 20 makes that error dynamics always happens in first quadrant.

The error dynamics becomes

$$\begin{aligned} \dot{e}_1 &= \dot{x}_1 - \dot{y}_1 = x_2 - y_2 - u_1 \\ \dot{e}_2 &= \dot{x}_2 - \dot{y}_2 = \frac{1}{m_1 + m_2}[(m_1 - m_2)\eta^2 \cos x_1 \sin x_1 \\ &\quad -\frac{1}{l}(g - \eta^2 x_3)(m_1 \sin x_1 - m_2 \cos x_1) - \frac{k}{l^2} x_2] \\ &\quad -\frac{1}{m_1 + m_2}[(m_1 - m_2)\eta^2 \cos y_1 \sin y_1 \\ &\quad -\frac{1}{l}(g - \eta^2 y_3)(m_1 \sin y_1 - m_2 \cos y_1) - \frac{k}{l^2} y_2] - u_2 \\ \dot{e}_3 &= \dot{x}_3 - \dot{y}_3 = x_4 - y_4 - u_3 \\ \dot{e}_4 &= \dot{x}_4 - \dot{y}_4 = -A\eta^2 \sin x_3 + A\eta^2 \sin y_3 - u_4 \end{aligned} \tag{3-10}$$

Let initial states be $(x_1, x_2, x_3, x_4) = (0, 0, 2, 2)$, $(y_1, y_2, y_3, y_4) = (2, 2, 0, 0)$, the error dynamics always exists in first quadrant as shown in Fig. 3.3. By GYC partial region asymptotical stability theorem, one can choose a Lyapunov function in the form of a positive definite function in first quadrant:

$$V = e_1 + e_2 + e_3 + e_4 \tag{3-11}$$

Its time derivative is

$$\begin{aligned}
\dot{V} &= \dot{e}_1 + \dot{e}_2 + \dot{e}_3 + \dot{e}_4 \\
&= (x_2 - y_2 - u_1) + \{\frac{1}{m_1 + m_2}[(m_1 - m_2)\eta^2 \cos x_1 \sin x_1 \\
&\quad -\frac{1}{l}(g - \eta^2 x_3)(m_1 \sin x_1 - m_2 \cos x_1) - \frac{k}{l^2} x_2] \\
&\quad -\frac{1}{m_1 + m_2}[(m_1 - m_2)\eta^2 \cos y_1 \sin y_1 \\
&\quad -\frac{1}{l}(g - \eta^2 y_3)(m_1 \sin y_1 - m_2 \cos y_1) - \frac{k}{l^2} y_2] - u_2\} \\
&\quad + (x_4 - y_4 - u_3) + (-A\eta^2 \sin x_3 + A\eta^2 \sin y_3 - u_4)
\end{aligned} \tag{3-12}$$

Choose

$$\begin{aligned}
u_1 &= x_2 - y_2 + e_1 \\
u_2 &= \frac{1}{m_1 + m_2}[(m_1 - m_2)\eta^2 \cos x_1 \sin x_1 \\
&\quad -\frac{1}{l}(g - \eta^2 x_3)(m_1 \sin x_1 - m_2 \cos x_1) - \frac{k}{l^2} x_2] \\
&\quad -\frac{1}{m_1 + m_2}[(m_1 - m_2)\eta^2 \cos y_1 \sin y_1 \\
&\quad -\frac{1}{l}(g - \eta^2 y_3)(m_1 \sin y_1 - m_2 \cos y_1) - \frac{k}{l^2} y_2] + e_2 \\
u_3 &= x_4 - y_4 + e_3 \\
u_4 &= -A\eta^2 \sin x_3 + A\eta^2 \sin y_3 + e_4
\end{aligned} \tag{3-13}$$

which are added at 50s.

We obtain

$$\dot{V} = -e_1 - e_2 - e_3 - e_4 < 0 \tag{3-14}$$

which is negative definite function in first quadrant. Error states versus time and time histories of states are shown in Fig. 3.4 and Fig. 3.5.

CASE II. The generalized synchronization error function is

$$e_i = x_i - y_i + F\sin wt + 20\,,\quad (i = 1,2,3,4)\,.$$

Our goal is $y_i = x_i + F\sin wt + 20$, i.e. $\lim_{t\to\infty} e_i = \lim_{t\to\infty}\left(x_i - y_i + F\sin wt + 20\right) = 0$, $(i = 1,2,3,4)$. The error dynamics becomes

$$\begin{aligned}
\dot{e}_1 &= \dot{x}_1 - \dot{y}_1 = x_2 - y_2 - u_1 + Fw\cos wt \\
\dot{e}_2 &= \dot{x}_2 - \dot{y}_2 = \frac{1}{m_1 + m_2}[(m_1 - m_2)\eta^2 \cos x_1 \sin x_1 \\
&\qquad -\frac{1}{l}(g - \eta^2 x_3)(m_1 \sin x_1 - m_2 \cos x_1) - \frac{k}{l^2}x_2] \\
&\qquad -\frac{1}{m_1 + m_2}[(m_1 - m_2)\eta^2 \cos y_1 \sin y_1 \\
&\qquad -\frac{1}{l}(g - \eta^2 y_3)(m_1 \sin y_1 - m_2 \cos y_1) - \frac{k}{l^2}y_2] - u_2 + Fw\cos wt \\
\dot{e}_3 &= \dot{x}_3 - \dot{y}_3 = x_4 - y_4 - u_3 + Fw\cos wt \\
\dot{e}_4 &= \dot{x}_4 - \dot{y}_4 = -A\eta^2 \sin x_3 + A\eta^2 \sin y_3 - u_4 + Fw\cos wt
\end{aligned} \tag{3-15}$$

Let initial states be $(x_1, x_2, x_3, x_4) = (0,\ 0,\ 2,\ 2)$, $(y_1, y_2, y_3, y_4) = (2,\ 2,\ 0,\ 0)$, and $F = 5, w = 0.1$, the error dynamic always exists in first quadrant as shown in Fig. 3.6. By GYC partial region asymptotical stability theorem, one can choose a Lyapunov function in the form of a positive definite function in first quadrant:

$$V = e_1 + e_2 + e_3 + e_4 \tag{3-16}$$

Its time derivative is

$$
\begin{aligned}
\dot{V} &= \dot{e}_1 + \dot{e}_2 + \dot{e}_3 + \dot{e}_4 \\
&= (x_2 - y_2 - u_1 + Fw\cos wt) + \{\frac{1}{m_1 + m_2}[(m_1 - m_2)\eta^2 \cos x_1 \sin x_1 \\
&\quad -\frac{1}{l}(g - \eta^2 x_3)(m_1 \sin x_1 - m_2 \cos x_1) - \frac{k}{l^2} x_2] \\
&\quad -\frac{1}{m_1 + m_2}[(m_1 - m_2)\eta^2 \cos y_1 \sin y_1 \\
&\quad -\frac{1}{l}(g - \eta^2 y_3)(m_1 \sin y_1 - m_2 \cos y_1) - \frac{k}{l^2} y_2] - u_2 + Fw\cos wt\} \\
&\quad + (x_4 - y_4 - u_3 + Fw\cos wt) + (-A\eta^2 \sin x_3 + A\eta^2 \sin y_3 - u_4 + Fw\cos wt)
\end{aligned}
\tag{3-17}
$$

Choose

$$
\begin{aligned}
u_1 &= x_2 - y_2 + Fw\cos wt + e_1 \\
u_2 &= \frac{1}{m_1 + m_2}[(m_1 - m_2)\eta^2 \cos x_1 \sin x_1 \\
&\quad -\frac{1}{l}(g - \eta^2 x_3)(m_1 \sin x_1 - m_2 \cos x_1) - \frac{k}{l^2} x_2] \\
&\quad -\frac{1}{m_1 + m_2}[(m_1 - m_2)\eta^2 \cos y_1 \sin y_1 \\
&\quad -\frac{1}{l}(g - \eta^2 y_3)(m_1 \sin y_1 - m_2 \cos y_1) - \frac{k}{l^2} y_2] + Fw\cos wt + e_2 \\
u_3 &= x_4 - y_4 + Fw\cos wt + e_3 \\
u_4 &= -A\eta^2 \sin x_3 + A\eta^2 \sin y_3 + Fw\cos wt + e_4
\end{aligned}
\tag{3-18}
$$

which are added at 50s.

We obtain

$$
\dot{V} = -e_1 - e_2 - e_3 - e_4 < 0 \tag{3-19}
$$

which is negative definite function in first quadrant. Error states versus time and time histories of $x_i - y_i + 20$ and $-F\sin wt$ are shown in Fig. 3.7 and Fig. 3.8.

CASE III. The generalized synchronization error function is

$$
e_i = \frac{1}{2} x_i^{\,2} - y_i + 20\,, (i = 1,2,3,4)\,.
$$

Our goal is $y_i = \frac{1}{2} x_i^{\,2} + 20$, i.e. $\lim_{t\to\infty} e_i = \lim_{t\to\infty}(\frac{1}{2} x_i^{\,2} - y_i + 20) = 0\,,\ (i = 1,2,3,4)$

The error dynamics becomes

$$\dot{e}_1 = x_1\dot{x}_1 - \dot{y}_1 = x_1x_2 - y_2 - u_1$$

$$\begin{aligned}\dot{e}_2 = x_2\dot{x}_2 - \dot{y}_2 = x_2 &\frac{1}{m_1+m_2}[(m_1-m_2)\eta^2\cos x_1\sin x_1 \\ &-\frac{1}{l}(g-\eta^2 x_3)(m_1\sin x_1 - m_2\cos x_1) - \frac{k}{l^2}x_2] \\ &-\frac{1}{m_1+m_2}[(m_1-m_2)\eta^2\cos y_1\sin y_1 \\ &-\frac{1}{l}(g-\eta^2 y_3)(m_1\sin y_1 - m_2\cos y_1) - \frac{k}{l^2}y_2] - u_2\end{aligned} \tag{3-20}$$

$$\dot{e}_3 = x_3\dot{x}_3 - \dot{y}_3 = x_3x_4 - y_4 - u_3$$

$$\dot{e}_4 = x_4\dot{x}_4 - \dot{y}_4 = x_4(-A\eta^2\sin x_3) + A\eta^2\sin y_3 - u_4$$

Let initial states be $(x_1, x_2, x_3, x_4) = (0, 0, 2, 2)$, $(y_1, y_2, y_3, y_4) = (2, 2, 0, 0)$, the error dynamics always exists in first quadrant as shown in Fig. 3.9. By GYC partial region asymptotical stability theorem, one can choose a Lyapunov function in the form of a positive definite function in first quadrant:

$$V = e_1 + e_2 + e_3 + e_4 \tag{3-21}$$

Its time derivative is

$$\begin{aligned}\dot{V} &= \dot{e}_1 + \dot{e}_2 + \dot{e}_3 + \dot{e}_4 \\ &= (x_1x_2 - y_2 - u_1) + \{x_2\frac{1}{m_1+m_2}[(m_1-m_2)\eta^2\cos x_1\sin x_1 \\ &\quad -\frac{1}{l}(g-\eta^2 x_3)(m_1\sin x_1 - m_2\cos x_1) - \frac{k}{l^2}x_2] \\ &\quad -\frac{1}{m_1+m_2}[(m_1-m_2)\eta^2\cos y_1\sin y_1 \\ &\quad -\frac{1}{l}(g-\eta^2 y_3)(m_1\sin y_1 - m_2\cos y_1) - \frac{k}{l^2}y_2] - u_2\} \\ &\quad + (x_3x_4 - y_4 - u_3) + [x_4(-A\eta^2\sin x_3) + A\eta^2\sin y_3 - u_4]\end{aligned} \tag{3-22}$$

Choose

$$
\begin{aligned}
u_1 &= x_1 x_2 - y_2 + e_1 \\
u_2 &= x_2 \frac{1}{m_1 + m_2}[(m_1 - m_2)\eta^2 \cos x_1 \sin x_1 \\
&\quad -\frac{1}{l}(g - \eta^2 x_3)(m_1 \sin x_1 - m_2 \cos x_1) - \frac{k}{l^2} x_2] \\
&\quad -\frac{1}{m_1 + m_2}[(m_1 - m_2)\eta^2 \cos y_1 \sin y_1 \\
&\quad -\frac{1}{l}(g - \eta^2 y_3)(m_1 \sin y_1 - m_2 \cos y_1) - \frac{k}{l^2} y_2] + e_2 \\
u_3 &= x_3 x_4 - y_4 + e_3 \\
u_4 &= x_4(-A\eta^2 \sin x_3) + A\eta^2 \sin y_3 + e_4
\end{aligned}
\tag{3-23}
$$

which are added at 50s.

We obtain

$$
\dot{V} = -e_1 - e_2 - e_3 - e_4 < 0 \tag{3-24}
$$

which is negative definite function in first quadrant. Error states versus time and time histories of $\frac{1}{2}x_i^2 + 20$ and y_i are shown in Fig. 3.10 and in Fig. 3.11.

CASE IV. The generalized synchronization error function is $e_i = x_i - y_i + z_i + 50$, where z_i $(i = 1,2,3,4)$ are chaotic states of the new Mathieu-Van der Pol system.

The functional system for synchronization is new Mathieu-Van der Pol system and initial states are $(z_1, z_{,2}, z_3, z_4)$=(0.1, -0.5, 0.1, -0.5), system parameters $a_1 = 10$, $b_1 = 3$, $c_1 = 0.4$, $d_1 = 70$, $e_1 = 1$, $f_1 = 5$, $g_1 = 0.1$.

$$
\begin{cases}
\dot{z}_1 = z_2 \\
\dot{z}_2 = -\left(a_1 + b_1 z_3\right) z_1 - \left(a_1 + b_1 z_3\right) z_1^3 - c_1 z_2 + d_1 z_3 \\
\dot{z}_3 = z_4 \\
\dot{z}_4 = -e_1 z_3 + f_1\left(1 - z_3^2\right) z_4 + g_1 z_1
\end{cases}
\tag{3-25}
$$

We have $\lim_{t\to\infty} e = \lim_{t\to\infty}(x - y + z + 50) = 0$. The error dynamics becomes

$$\dot{e}_1 = \dot{x}_1 - \dot{y}_1 + \dot{z}_1 = x_2 - y_2 + z_2 - u_1$$

$$\begin{aligned}\dot{e}_2 = \dot{x}_2 - \dot{y}_2 + \dot{z}_2 = {} & \frac{1}{m_1 + m_2}[(m_1 - m_2)\eta^2 \cos x_1 \sin x_1 \\ & -\frac{1}{l}(g - \eta^2 x_3)(m_1 \sin x_1 - m_2 \cos x_1) - \frac{k}{l^2} x_2] \\ & -\frac{1}{m_1 + m_2}[(m_1 - m_2)\eta^2 \cos y_1 \sin y_1 \\ & -\frac{1}{l}(g - \eta^2 y_3)(m_1 \sin y_1 - m_2 \cos y_1) - \frac{k}{l^2} y_2] \\ & -(a_1 + b_1 z_3) z_1 - (a + b z_3) z_1^{\,3} - c_1 z_2 + d_1 z_3 - u_2\end{aligned} \tag{3-26}$$

$$\dot{e}_3 = \dot{x}_3 - \dot{y}_3 + \dot{z}_3 = x_4 - y_4 + z_4 - u_3$$

$$\dot{e}_4 = \dot{x}_4 - \dot{y}_4 + \dot{z}_4 = -A\eta^2 \sin x_3 + A\eta^2 \sin y_3 - e_1 z_3 + f_1(1 - z_3^{\,2}) z_4 + g_1 z_1 - u_4$$

Let initial states be $(x_1, x_2, x_3, x_4) = (0, 0, 2, 2)$, $(y_1, y_2, y_3, y_4) = (2, 2, 0, 0)$ and the error dynamics always exists in first quadrant as shown in Fig. 3.12. By GYC partial region asymptotical stability theorem, one can choose a Lyapunov function in the form of a positive definite function in first quadrant:

$$V = e_1 + e_2 + e_3 + e_4 \tag{3-27}$$

Its time derivative is

$$\begin{aligned}\dot{V} = {} & \dot{e}_1 + \dot{e}_2 + \dot{e}_3 + \dot{e}_4 \\ = {} & (x_2 - y_2 + z_2 - u_1) + \{\frac{1}{m_1 + m_2}[(m_1 - m_2)\eta^2 \cos x_1 \sin x_1 \\ & -\frac{1}{l}(g - \eta^2 x_3)(m_1 \sin x_1 - m_2 \cos x_1) - \frac{k}{l^2} x_2] \\ & -\frac{1}{m_1 + m_2}[(m_1 - m_2)\eta^2 \cos y_1 \sin y_1 \\ & -\frac{1}{l}(g - \eta^2 y_3)(m_1 \sin y_1 - m_2 \cos y_1) - \frac{k}{l^2} y_2] \\ & -(a_1 + b_1 z_3) z_1 - (a + b z_3) z_1^{\,3} - c_1 z_2 + d_1 z_3 - u_2\} \\ & +(x_4 - y_4 + z_4 - u_3) \\ & +[-A\eta^2 \sin x_3 + A\eta^2 \sin y_3 - e_1 z_3 + f_1(1 - z_3^{\,2}) z_4 + g_1 z_1 - u_4]\end{aligned} \tag{3-28}$$

Choose

$$u_1 = x_2 - y_2 + z_2 + e_1$$

$$u_2 = \frac{1}{m_1 + m_2}[(m_1 - m_2)\eta^2 \cos x_1 \sin x_1$$
$$-\frac{1}{l}(g - \eta^2 x_3)(m_1 \sin x_1 - m_2 \cos x_1) - \frac{k}{l^2} x_2]$$
$$-\frac{1}{m_1 + m_2}[(m_1 - m_2)\eta^2 \cos y_1 \sin y_1 \qquad (3\text{-}29)$$
$$-\frac{1}{l}(g - \eta^2 y_3)(m_1 \sin y_1 - m_2 \cos y_1) - \frac{k}{l^2} y_2]$$
$$-(a_1 + b_1 z_3)z_1 - (a + bz_3)z_1^3 - c_1 z_2 + d_1 z_3 + e_2$$

$$u_3 = x_4 - y_4 + z_4 + e_3$$

$$u_4 = -A\eta^2 \sin x_3 + A\eta^2 \sin y_3 - e_1 z_3 + f_1(1 - z_3^2)z_4 + g_1 z_1 + e_4$$

which are added at 50s.

We obtain

$$\dot{V} = -e_1 - e_2 - e_3 - e_4 < 0 \qquad (3\text{-}30)$$

which is negative definite function in first quadrant. Error states versus time and time histories of $x_i - y_i + 50$ are shown in Fig. 3.13 and Fig. 3.14.

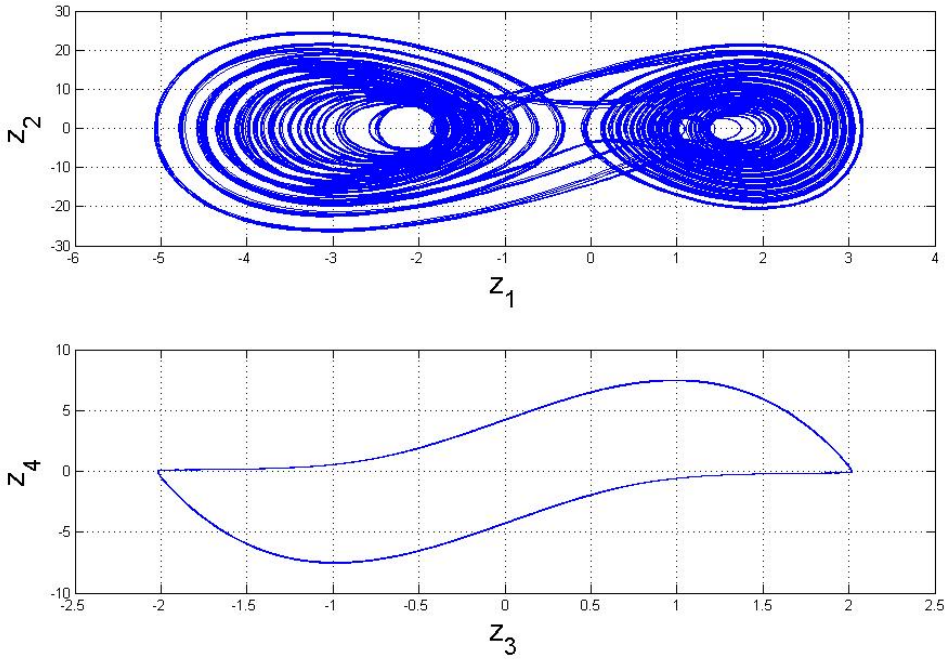

Fig. 3.1 Phase portraits of new Mathieu-Van der Pol system.

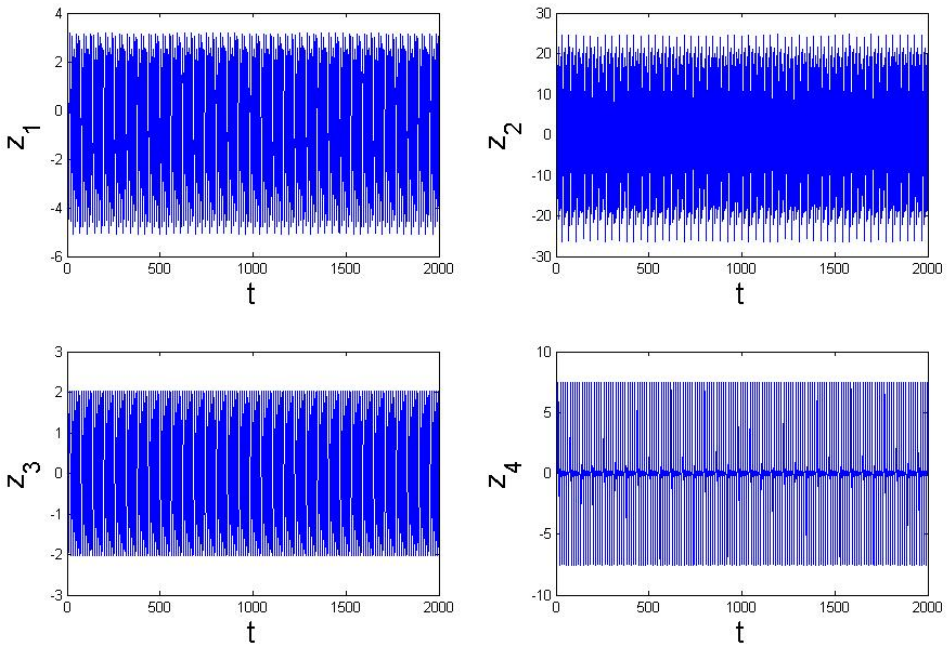

Fig. 3.2 Time histories of the four states of new Mathieu-van der Pol system.

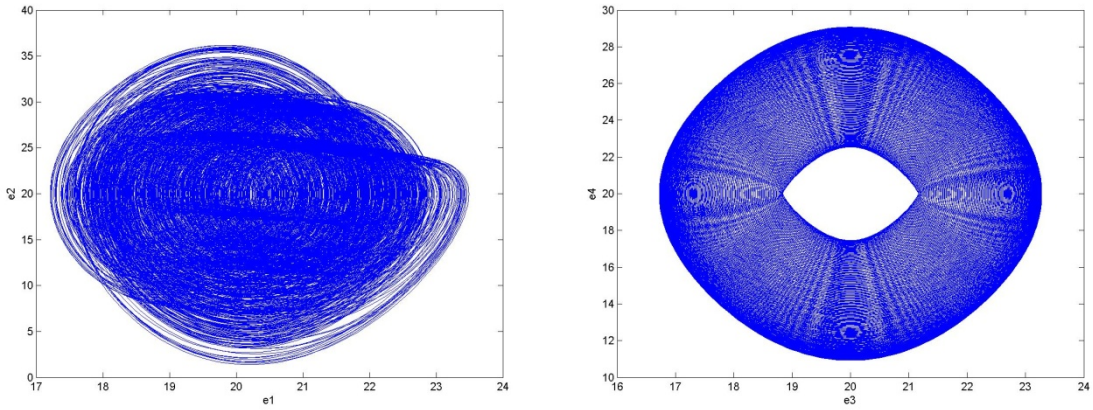

Fig. 3.3 Phase portraits of four errors dynamics for Case I.

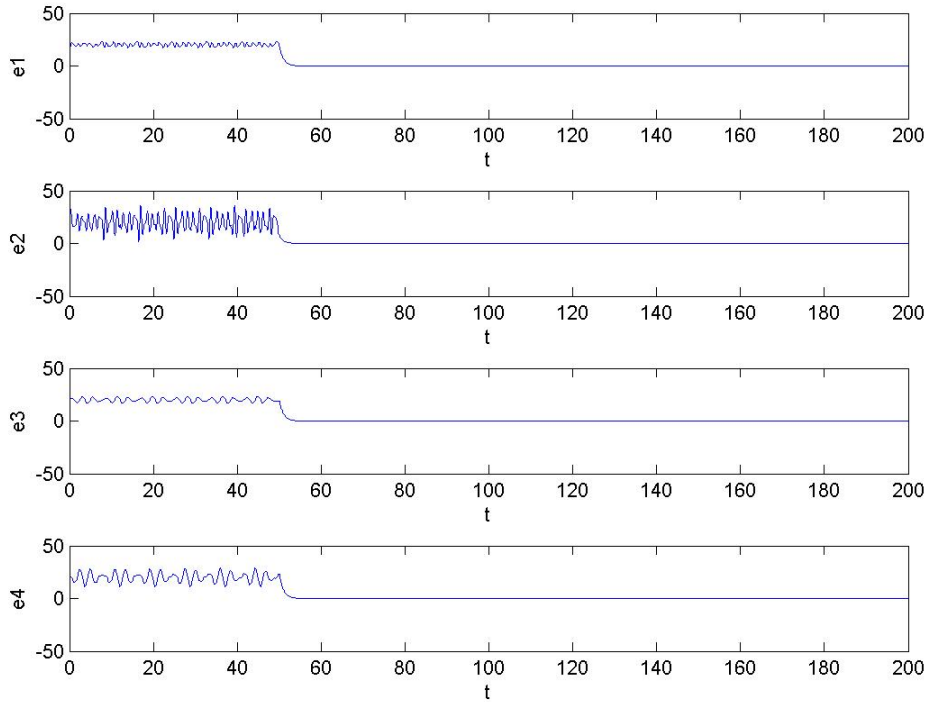

Fig. 3.4. Time histories of errors for Case I.

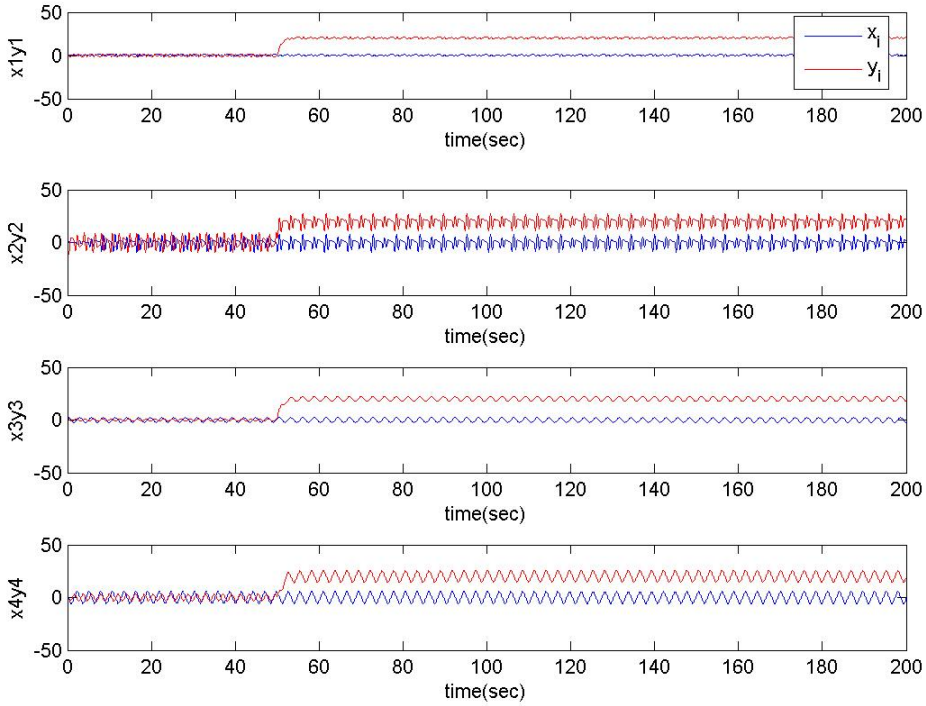

Fig. 3.5. Time histories of $x_1, x_2, x_3, x_4, y_1, y_2, y_3, y_4$ for Case I.

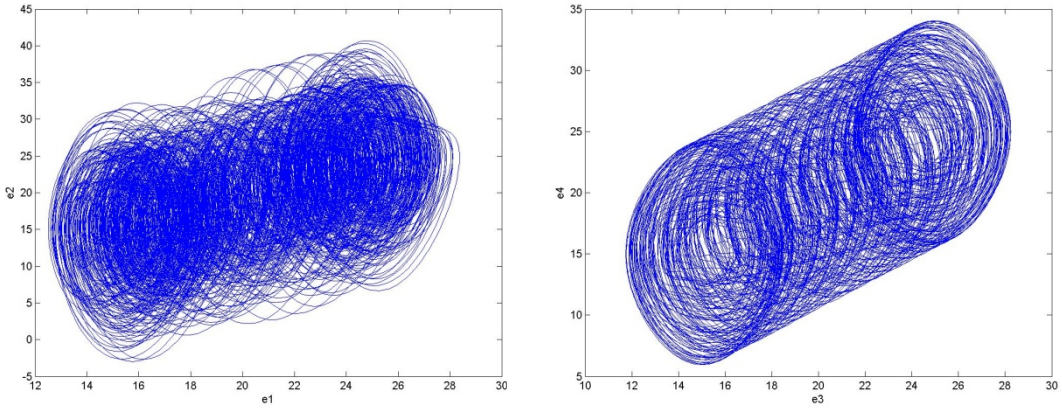

Fig. 3.6 Phase portraits of error dynamics for Case II.

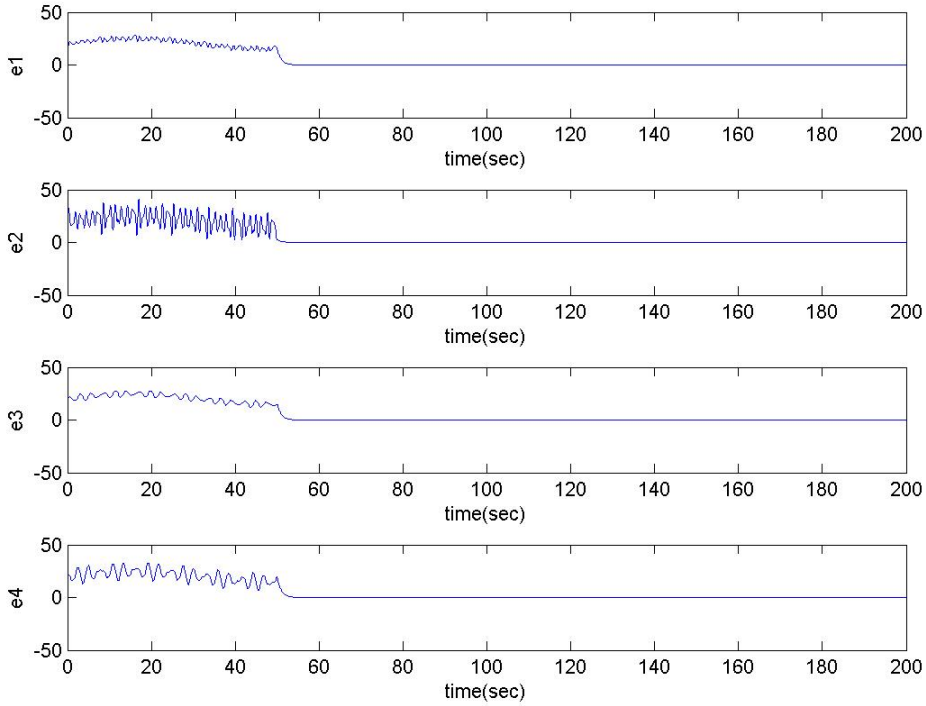

Fig. 3.7 Time histories of errors for Case II.

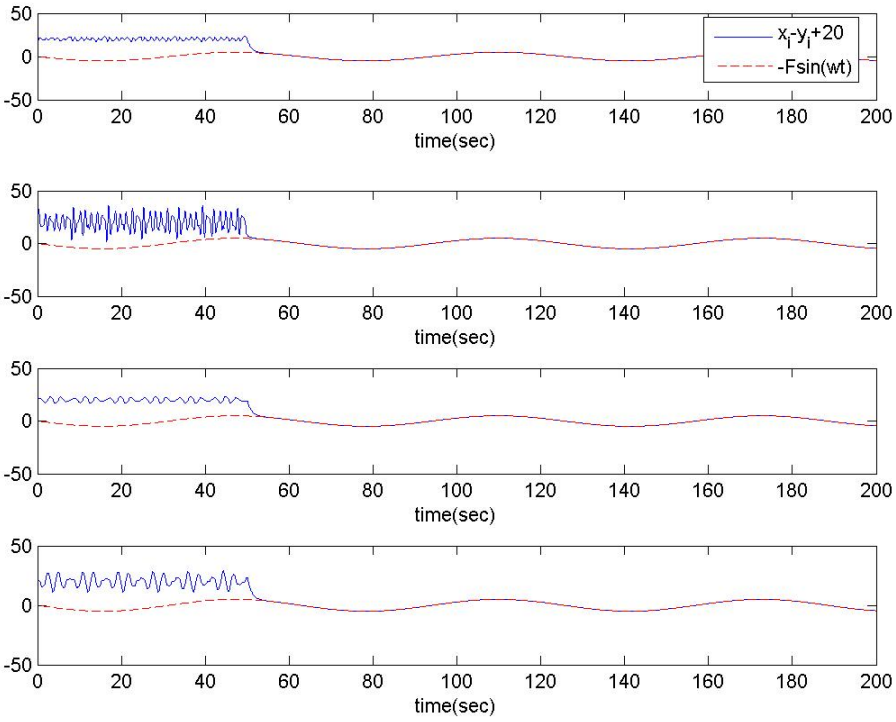

Fig. 3.8 Time histories of $x_i - y_i + 20$ and $-F\sin\omega t$ for Case II.

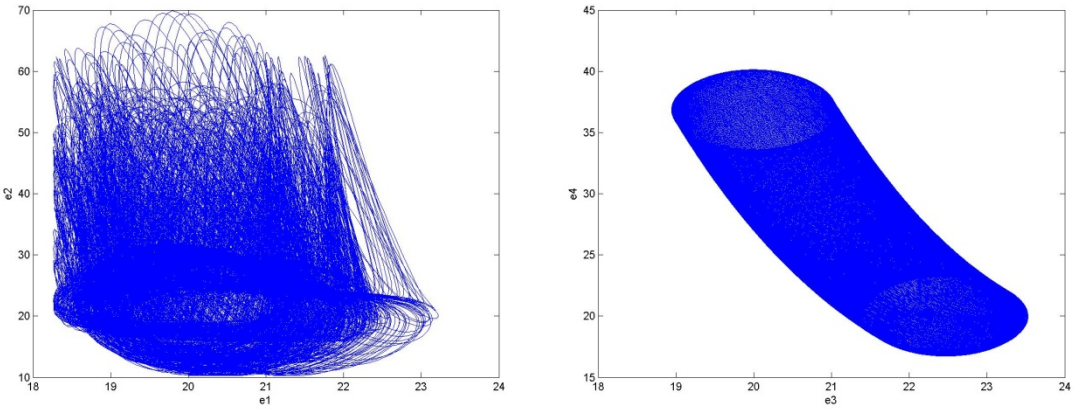

Fig. 3.9 Phase portraits of error dynamics for Case III.

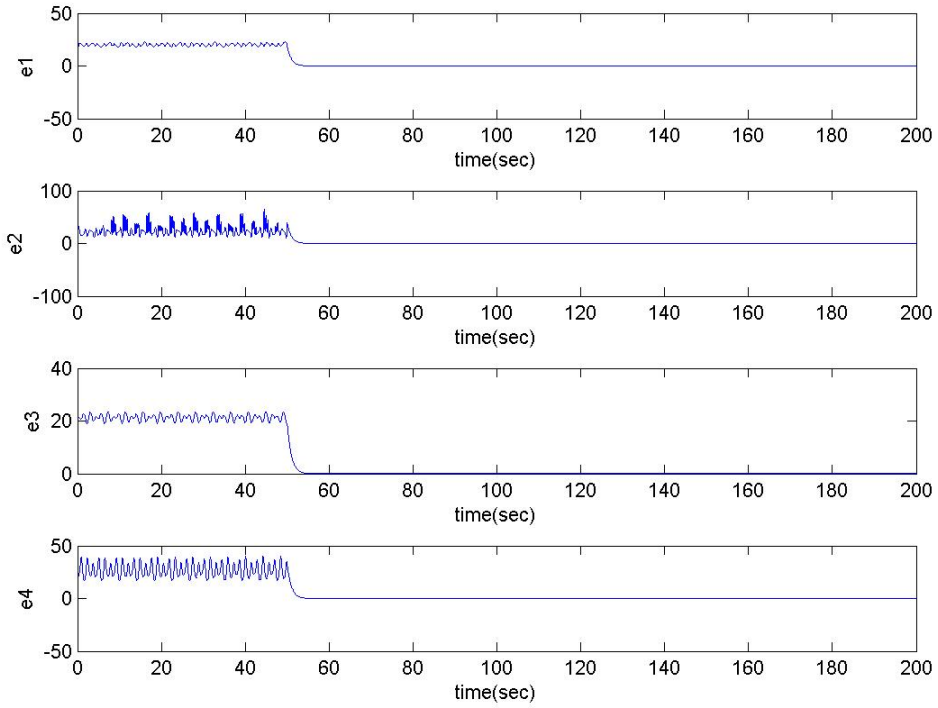

Fig. 3.10 Time histories of error for Case III.

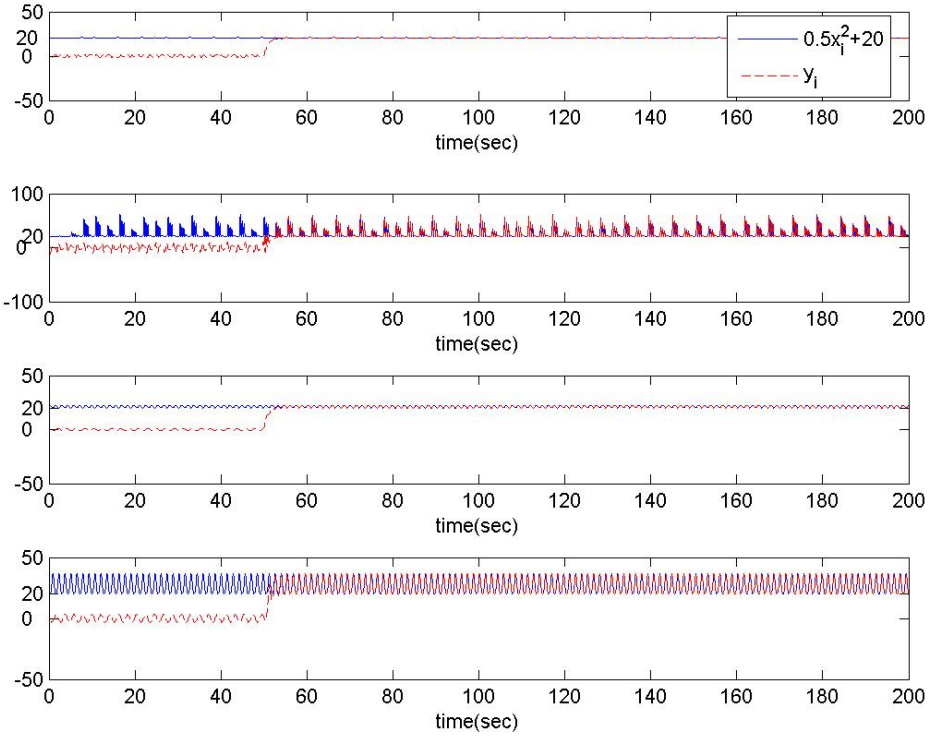

Fig. 3.11 Time histories of $\frac{1}{2}x_i^2 + 20$ and y_i for Case III.

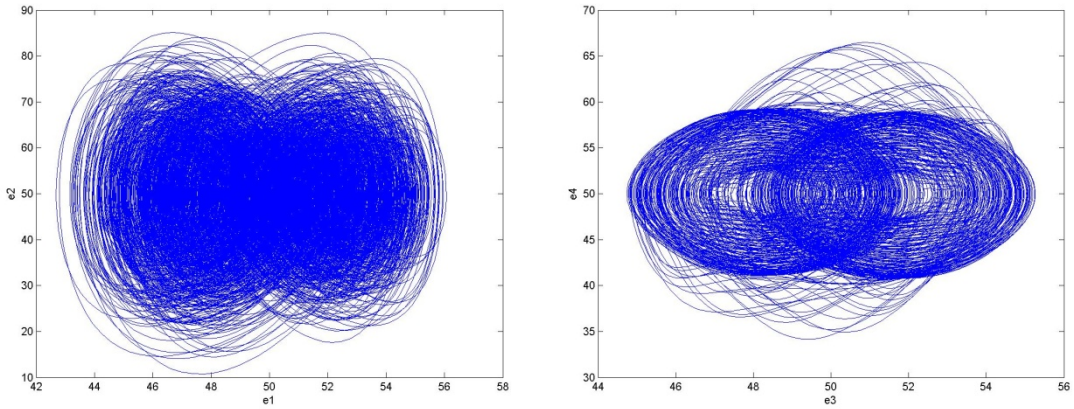

Fig. 3.12 Phase portraits of error dynamics for Case IV.

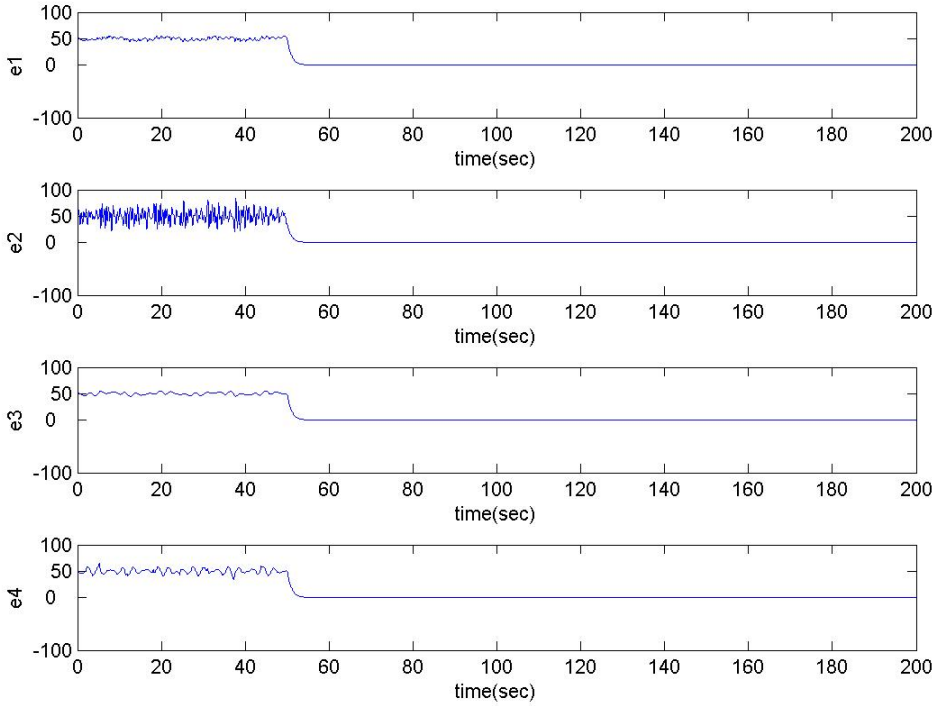

Fig. 3.13 Time histories of errors for Case IV.

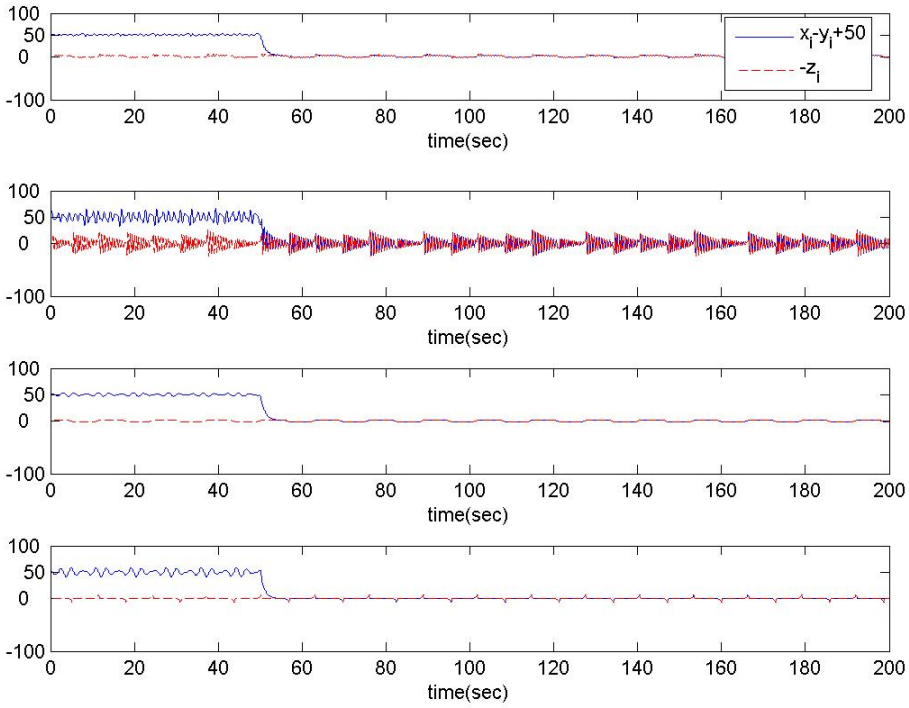

Fig. 3.14 Time histories of $x_i - y_i + 50$ and $-z_i$ for Case IV.

Chapter 4

Chaos Control of an Inertial Tachometer System by GYC Partial Region Stability Theory

4.1 Preliminaries

In this Chapter, a new technique to achieve chaos control by using GYC partial region stability theory is proposed. By using the GYC partial region stability theory, the new Lyapunov function becomes a simple linear homogeneous function of error states and the controllers are of lower degree with less simulation error. In simulation examples, an inertial tachometer system and a Mathieu-Van der Pol system are used.

4.2 Chaos Control Scheme

Consider the following chaotic systems

$$\dot{\mathbf{x}} = \mathbf{f}(t, \mathbf{x}) \tag{4-1}$$

where $\mathbf{x} = [x_1, x_2, \cdots, x_n]^T \in R^n$ is a the state vector, $\mathbf{f} : R_+ \times R^n \to R^n$ is a vector function.

The goal system which can be either chaotic or regular, is

$$\dot{\mathbf{y}} = \mathbf{g}(t, \mathbf{y}) \tag{4-2}$$

where $\mathbf{y} = [y_1, y_2, \cdots, y_n]^T \in R^n$ is a state vector, $\mathbf{g} : R_+ \times R^n \to R^n$ is a vector function.

In order to make the chaotic state $\mathbf{x}$ approaching the goal state $\mathbf{y}$, define error $\mathbf{e} = \mathbf{x} - \mathbf{y}$ as the state error. The chaos control is accomplished in the sense that :

$$\lim_{t\to\infty} \mathbf{e} = \lim_{t\to\infty} (\mathbf{x} - \mathbf{y}) = 0 \tag{4-3}$$

In this Chapter, we will use examples in which the error dynamics happens in the

first quadrant of coordinate system and use the partial region stability theory. The Lyapunov function is a simple linear homogeneous function of error states and the controllers are simpler because they are in lower degree than that of traditional controllers.

4.3 Numerical Simulations

The following chaotic system

$$\begin{cases} \dot{x}_1 = (x_2 - 20) \\ \dot{x}_2 = \dfrac{1}{m_1 + m_2}[(m_1 - m_2)\eta^2 \cos(x_1 - 20)\sin(x_1 - 20) \\ \qquad -\dfrac{1}{l}(g - \eta^2(x_3 - 20))(m_1 \sin(x_1 - 20) - m_2 \cos(x_1 - 20)) \\ \qquad -\dfrac{k}{l^2}(x_2 - 20)] \\ \dot{x}_3 = (x_4 - 20) \\ \dot{x}_4 = -A\eta^2 \sin(x_3 - 20) \end{cases} \tag{4-4}$$

is the inertial tachometer system of which old origin is translated to $(x_1, x_2, x_3, x_4) = (20, 20, 20, 20)$ in order that the error dynamics always happens in first quadrant. This system is presented as simulated examples where initial conditions are $(x_{10}, x_{20}, x_{30}, x_{40}) = (20, 20, 22, 22)$ and the parameters are $m_1 = 9$, $m_2 = 1$, $A = 10.5$, $\eta = 1$, $l = 0.3$, $k = 0.5$, $g = 9.81$.

In order to lead the states (x_1, x_2, x_3, x_4) to the goal, we add control terms u_1, u_2, u_3 and u_4 to each equation of Eq. (4-4), respectively.

$$\begin{cases} \dot{x}_1 = (x_2 - 20) + u_1 \\ \dot{x}_2 = \dfrac{1}{m_1 + m_2}[(m_1 - m_2)\eta^2 \cos(x_1 - 20)\sin(x_1 - 20) \\ \quad -\dfrac{1}{l}(g - \eta^2(x_3 - 20))(m_1 \sin(x_1 - 20) - m_2 \cos(x_1 - 20)) \\ \quad -\dfrac{k}{l^2}(x_2 - 20)] + u_2 \\ \dot{x}_3 = (x_4 - 20) + u_3 \\ \dot{x}_4 = -A\eta^2 \sin(x_3 - 20) + u_4 \end{cases} \tag{4-5}$$

CASE I. Control the chaotic motion to zero.

In this case we will control the chaotic motion of the inertial tachometer system (2.3) to zero. The goal is $y_i = 0$, $(i = 1,2,3,4)$. The state error is $e_i = x_i - y_i = x_i$,

$$\lim_{t\to\infty} e_i = \lim_{t\to\infty}(x_i - 0) = 0, \quad (i = 1,2,3,4). \tag{4-6}$$

The error dynamics becomes

$$\begin{aligned} \dot{e}_1 &= \dot{x}_1 = (x_2 - 20) + u_1 \\ \dot{e}_2 &= \dot{x}_2 = \frac{1}{m_1 + m_2}[(m_1 - m_2)\eta^2 \cos(x_1 - 20)\sin(x_1 - 20) \\ &\quad -\frac{1}{l}(g - \eta^2(x_3 - 20))(m_1 \sin(x_1 - 20) - m_2 \cos(x_1 - 20)) \\ &\quad -\frac{k}{l^2}(x_2 - 20)] + u_2 \\ \dot{e}_3 &= \dot{x}_3 = (x_4 - 20) + u_3 \\ \dot{e}_4 &= \dot{x}_4 = -A\eta^2 \sin(x_3 - 20) + u_4 \end{aligned} \tag{4-7}$$

In Fig. 4.1, we can see that the error dynamics always exists in first quadrant.

By GYC partial region stability, one can easily choose a Lyapunov function in the form of a positive definite function in first quadrant as:

$$V = e_1 + e_2 + e_3 + e_4 \tag{4-8}$$

Its time derivative through error dynamics (4-7) is

$$\dot{V} = \dot{e}_1 + \dot{e}_2 + \dot{e}_3 + \dot{e}_4$$
$$= (x_2 - 20 + u_1) + \{\frac{1}{m_1 + m_2}[(m_1 - m_2)\eta^2 \cos(x_1 - 20)\sin(x_1 - 20)$$
$$-\frac{1}{l}(g - \eta^2(x_3 - 20))(m_1 \sin(x_1 - 20) - m_2 \cos(x_1 - 20)) \quad (4\text{-}9)$$
$$-\frac{k}{l^2}(x_2 - 20)] + u_2\}$$
$$+ (x_4 - 20 + u_3) + [-A\eta^2 \sin(x_3 - 20) + u_4]$$

Choose

$$\begin{aligned} u_1 &= -(x_2 - 20) - e_1 \\ u_2 &= -\frac{1}{m_1 + m_2}[(m_1 - m_2)\eta^2 \cos(x_1 - 20)\sin(x_1 - 20) \\ &\quad -\frac{1}{l}(g - \eta^2(x_3 - 20))(m_1 \sin(x_1 - 20) - m_2 \cos(x_1 - 20)) \\ &\quad -\frac{k}{l^2}(x_2 - 20)] - e_2 \\ u_3 &= -(x_4 - 20) - e_3 \\ u_4 &= -[-A\eta^2 \sin(x_3 - 20)] - e_4 \end{aligned} \quad (4\text{-}10)$$

which are added at 50s.

We obtain

$$\dot{V} = \dot{e}_1 + \dot{e}_2 + \dot{e}_3 + \dot{e}_4 < 0$$

which is negative definite function in first quadrant. The time histories of error states are shown in Fig. 4.2. After 50 sec, the trajectories approach the origin.

CASE II. Control the chaotic motion to a regular function.

In this case we will control the chaotic motion of the inertial tachometer system (2-3) to regular function of time. The goal is $y_i = F_i \sin w_i t$, $(i = 1,2,3,4)$. The error equation

$$e_i = x_i - y_i = x_i - F_i \sin w_i t, \quad (i = 1,2,3,4) \quad (4\text{-}11)$$
$$\lim_{t\to\infty} e_i = \lim_{t\to\infty}(x_i - F_i \sin w_i t) = 0, \quad (i = 1,2,3,4)$$

where $F_1 = F_2 = F_3 = F_4 = 5$ and $w_1 = 0.1$, $w_2 = 0.2$, $w_3 = 0.3$, $w_4 = 0.4$.

The error dynamics is

$$\dot{e}_1 = \dot{x}_1 - \dot{y}_1 = (x_2 - 20) + u_1 - w_1 F_1 \cos w_1 t$$

$$\begin{aligned}\dot{e}_2 = \dot{x}_2 - \dot{y}_2 = {} & \frac{1}{m_1 + m_2}[(m_1 - m_2)\eta^2 \cos(x_1 - 20)\sin(x_1 - 20) \\ & -\frac{1}{l}(g - \eta^2(x_3 - 20))(m_1 \sin(x_1 - 20) - m_2 \cos(x_1 - 20)) \\ & -\frac{k}{l^2}(x_2 - 20)] + u_2 - w_2 F_2 \cos w_2 t\end{aligned} \tag{4-12}$$

$$\dot{e}_3 = \dot{x}_3 - \dot{y}_3 = (x_4 - 20) + u_3 - w_3 F_3 \cos w_3 t$$

$$\dot{e}_4 = \dot{x}_4 - \dot{y}_4 = -A\eta^2 \sin(x_3 - 20) + u_4 - w_4 F_4 \cos w_4 t$$

In Fig. 4.3, the error dynamics always exists in first quadrant.

By GYC partial region stability, one can easily choose a Lyapunov function in the form of a positive definite function in first quadrant as:

$$V = e_1 + e_2 + e_3 + e_4$$

Its time derivative is

$$\begin{aligned}\dot{V} = {} & \dot{e}_1 + \dot{e}_2 + \dot{e}_3 + \dot{e}_4 \\ = {} & (x_2 - 20 + u_1) - w_1 F_1 \cos w_1 t \\ & + \{\frac{1}{m_1 + m_2}[(m_1 - m_2)\eta^2 \cos(x_1 - 20)\sin(x_1 - 20) \\ & -\frac{1}{l}(g - \eta^2(x_3 - 20))(m_1 \sin(x_1 - 20) - m_2 \cos(x_1 - 20)) \\ & -\frac{k}{l^2}(x_2 - 20)] + u_2\} - w_2 F_2 \cos w_2 t \\ & + (x_4 - 20 + u_3) - w_3 F_3 \cos w_3 t \\ & + [-A\eta^2 \sin(x_3 - 20) + u_4] - w_4 F_4 \cos w_4 t\end{aligned} \tag{4-13}$$

Choose

$$\begin{aligned}u_1 = {} & -[(x_2 - 20) - w_1 F_1 \cos w_1 t] - e_1 \\ u_2 = {} & -\{\frac{1}{m_1 + m_2}[(m_1 - m_2)\eta^2 \cos(x_1 - 20)\sin(x_1 - 20) \\ & -\frac{1}{l}(g - \eta^2(x_3 - 20))(m_1 \sin(x_1 - 20) - m_2 \cos(x_1 - 20)) \\ & -\frac{k}{l^2}(x_2 - 20)] - w_2 F_2 \cos w_2 t\} - e_2 \\ u_3 = {} & -[(x_4 - 20) - w_3 F_3 \cos w_3 t] - e_3 \\ u_4 = {} & -[-A\eta^2 \sin(x_3 - 20) - w_4 F_4 \cos w_4 t] - e_4\end{aligned} \tag{4-14}$$

which are added at 50s.

We obtain

$$\dot{V} = -e_1 - e_2 - e_3 - e_4 < 0$$

which is negative definite function in first quadrant. The numerical results are shown in Fig. 4.4 and Fig. 4.5. After 50 sec., the errors approach zero and the chaotic trajectories approach to regular functions of time.

CASE III. Control the chaotic motion of the inertial tachometer system to chaotic motion of the new Mathieu-Van der pol system.

In this case we will control chaotic motion of the inertial tachometer system (2-3) to that of the new Mathieu-Van der pol system. The goal system for control is new Mathieu-Van der pol system and initial states are (0.1, -0.5, 0.1, -0.5), system parameters $a_1 = 10$, $b_1 = 3$, $c_1 = 0.4$, $d_1 = 70$, $e_1 = 1$, $f_1 = 5$, $g_1 = 0.1$.

$$\begin{cases} \dot{z}_1 = z_2 \\ \dot{z}_2 = -(a_1 + b_1 z_3) z_1 - (a_1 + b_1 z_3) z_1^3 - c_1 z_2 + d_1 z_3 \\ \dot{z}_3 = z_4 \\ \dot{z}_4 = -e_1 z_3 + f_1 (1 - z_3^2) z_4 + g_1 z_1 \end{cases} \tag{4-15}$$

The error equation is $e_i = x_i - z_i$, $(i = 1, 2, 3, 4)$ Our goal is

$$\lim_{t \to \infty} e_i = \lim_{t \to \infty} (x_i - z_i) = 0 \ (i = 1, 2, 3, 4)$$

The error dynamics become

$$\begin{aligned} \dot{e}_1 &= \dot{x}_1 - \dot{z}_1 = (x_2 - 50) + u_1 - z_2 \\ \dot{e}_2 &= \dot{x}_2 - \dot{z}_2 = \frac{1}{m_1 + m_2}[(m_1 - m_2)\eta^2 \cos(x_1 - 50)\sin(x_1 - 50) \\ &\quad -\frac{1}{l}(g - \eta^2 (x_3 - 50))(m_1 \sin(x_1 - 50) - m_2 \cos(x_1 - 50)) \\ &\quad -\frac{k}{l^2}(x_2 - 50)] + u_2 \\ &\quad -[-(a_1 + b_1 z_3) z_1 - (a_1 + b_1 z_3) z_1^2 - c z_2 + d_1 z_3] \\ \dot{e}_3 &= \dot{x}_3 - \dot{z}_3 = (x_4 - 50) + u_3 - z_4 \\ \dot{e}_4 &= \dot{x}_4 - \dot{z}_4 = -A\eta^2 \sin(x_3 - 50) + u_4 - [-e_1 z_3 + f_1 (1 - z_3^2) z_4 + g_1 z_1] \end{aligned} \tag{4-16}$$

By Fig. 4.6, we know that the error dynamics always exists in first quadrant.

By GYC partial region stability, one can easily choose a Lyapunov function in the form of a positive definite function in first quadrant as:

$$V = e_1 + e_2 + e_3 + e_4$$

Its time derivative is

$$\begin{aligned}
\dot{V} &= \dot{e}_1 + \dot{e}_2 + \dot{e}_3 + \dot{e}_4 \\
&= (x_2 - 50 + u_1) - z_2 \\
&\quad + \{\frac{1}{m_1 + m_2}[(m_1 - m_2)\eta^2 \cos(x_1 - 50)\sin(x_1 - 50) \\
&\quad - \frac{1}{l}(g - \eta^2(x_3 - 50))(m_1 \sin(x_1 - 50) - m_2 \cos(x_1 - 50)) \\
&\quad - \frac{k}{l^2}(x_2 - 50)] + u_2\} \\
&\quad - [-(a_1 + b_1 z_3)z_1 - (a_1 + b_1 z_3)z_1^2 - cz_2 + d_1 z_3] \\
&\quad + (x_4 - 50 + u_3) - z_4 \\
&\quad + [-A\eta^2 \sin(x_3 - 50) + u_4] - [-e_1 z_3 + f_1(1 - z_3^2)z_4 + g_1 z_1]
\end{aligned} \tag{4-17}$$

Choose

$$\begin{aligned}
u_1 &= -[(x_2 - 50) - z_2] - e_1 \\
u_2 &= -\frac{1}{m_1 + m_2}[(m_1 - m_2)\eta^2 \cos(x_1 - 50)\sin(x_1 - 50) \\
&\quad - \frac{1}{l}(g - \eta^2(x_3 - 50))(m_1 \sin(x_1 - 50) - m_2 \cos(x_1 - 50)) \\
&\quad - \frac{k}{l^2}(x_2 - 50)] \\
&\quad + [-(a_1 + b_1 z_3)z_1 - (a_1 + b_1 z_3)z_1^2 - cz_2 + d_1 z_3] - e_2 \\
u_3 &= -[(x_4 - 50) - z_4] - e_3 \\
u_4 &= A\eta^2 \sin(x_3 - 50) + [-e_1 z_3 + f_1(1 - z_3^2)z_4 + g_1 z_1] - e_4
\end{aligned} \tag{4-18}$$

which are added at 50s.

We obtain

$$\dot{V} = -e_1 - e_2 - e_3 - e_4 < 0$$

which is negative definite function in first quadrant. The numerical results are shown in Fig. 4.7 and Fig. 4.8. After 50 sec., the errors approach zero and the chaotic trajectories of an inertial tachometer system approach to that of the new Mathieu-Van der pol system.

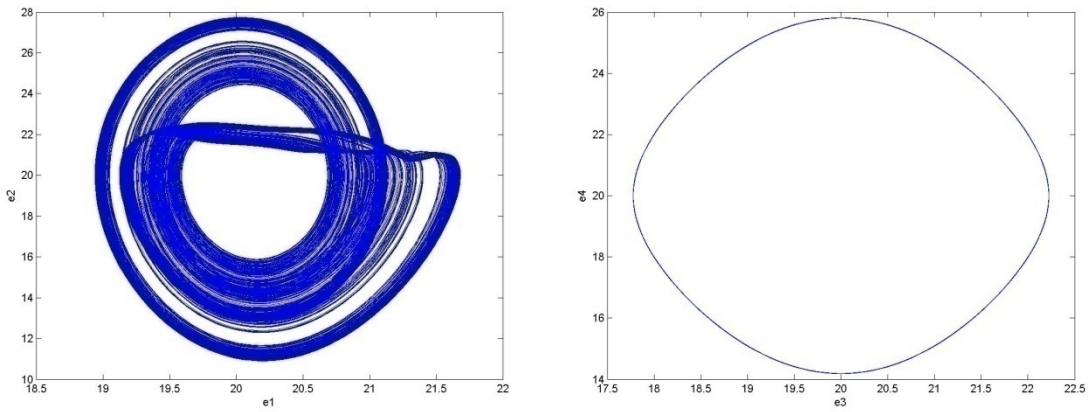

Fig. 4.1 Phase portraits of error dynamics for Case I.

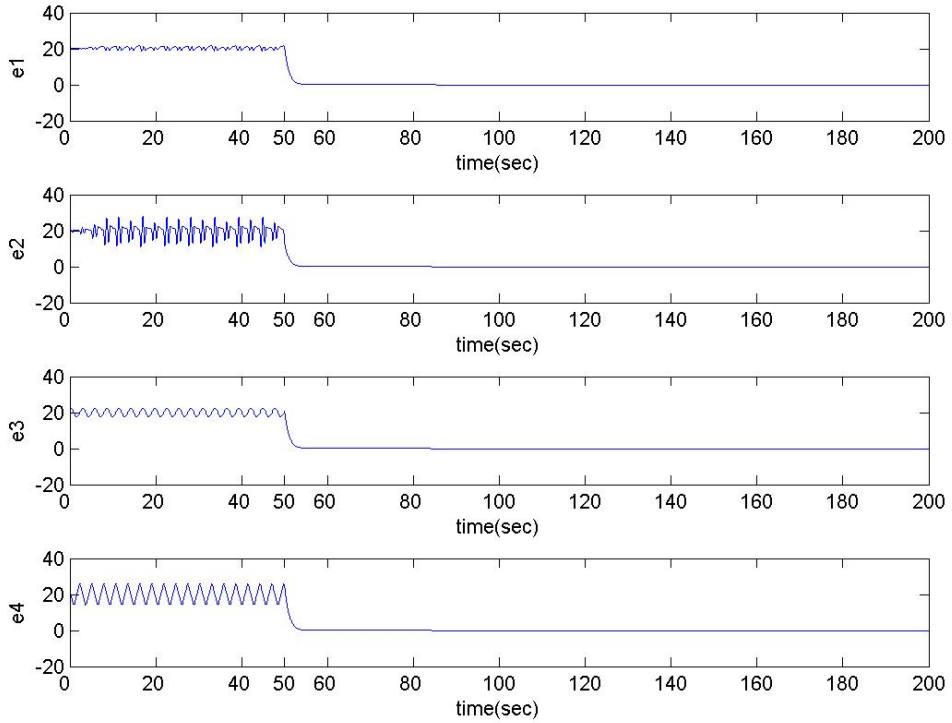

Fig. 4.2 Time histories of errors for Case I.

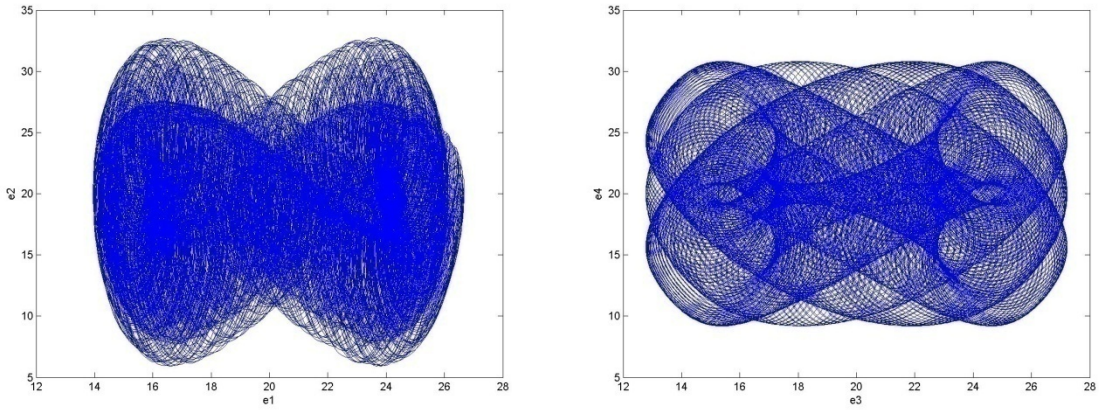

Fig. 4.3 Phase portraits of error dynamics for Case II.

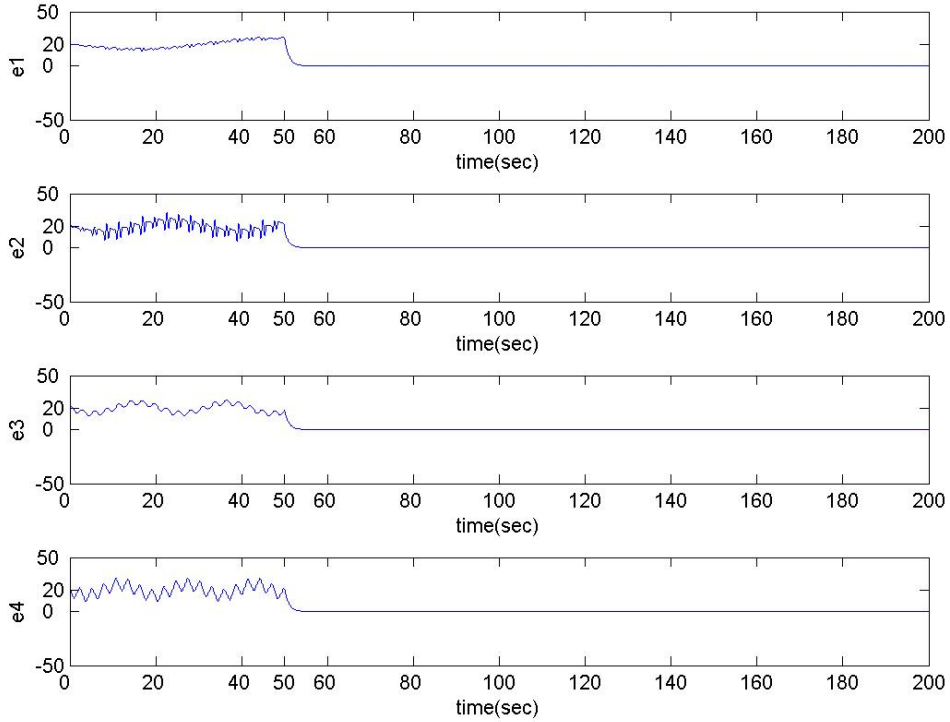

Fig. 4.4 Time histories of errors for Case II.

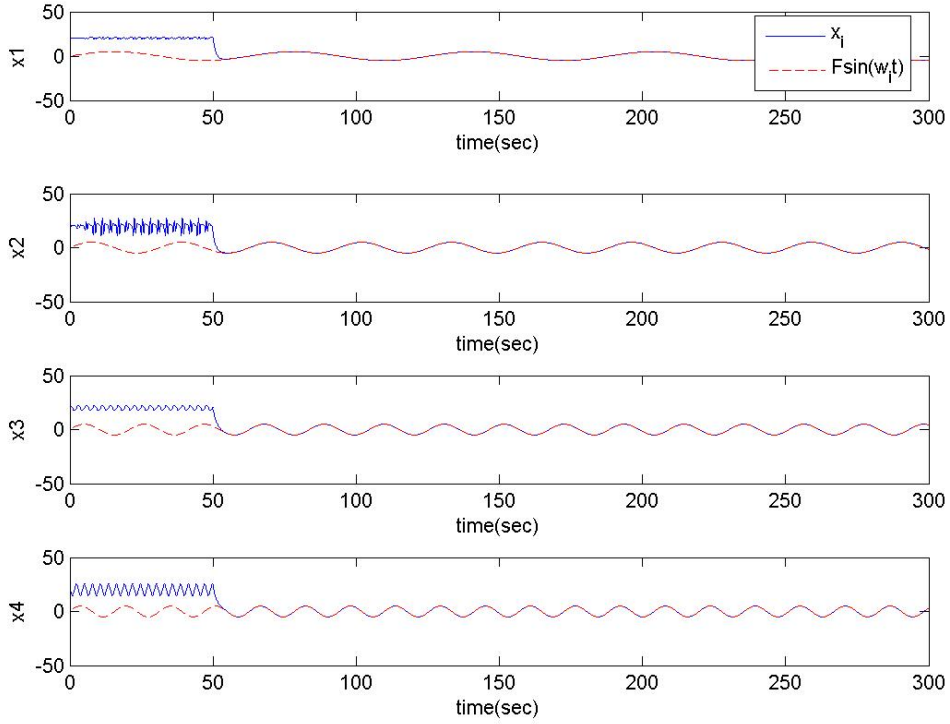

Fig. 4.5 Time histories of x_1, x_2, x_3, x_4 and $F \sin w_i t$ for Case II.

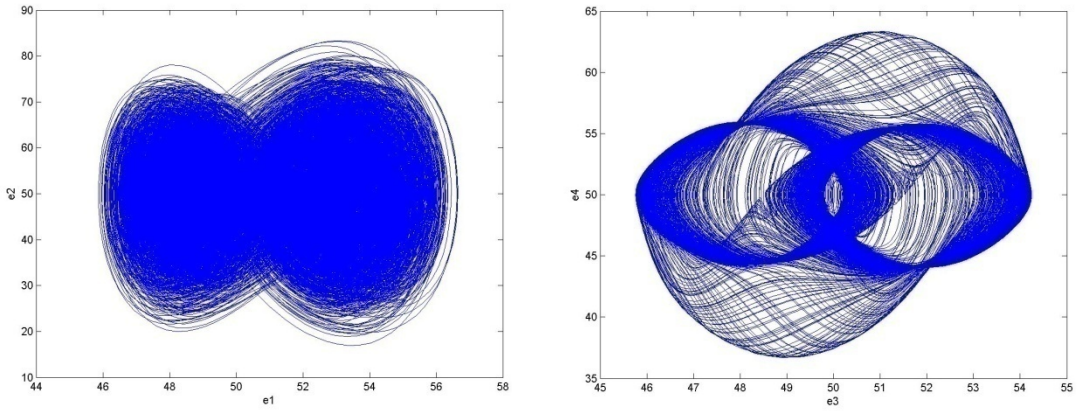

Fig. 4.6 Phase portraits of error dynamics for Case III.

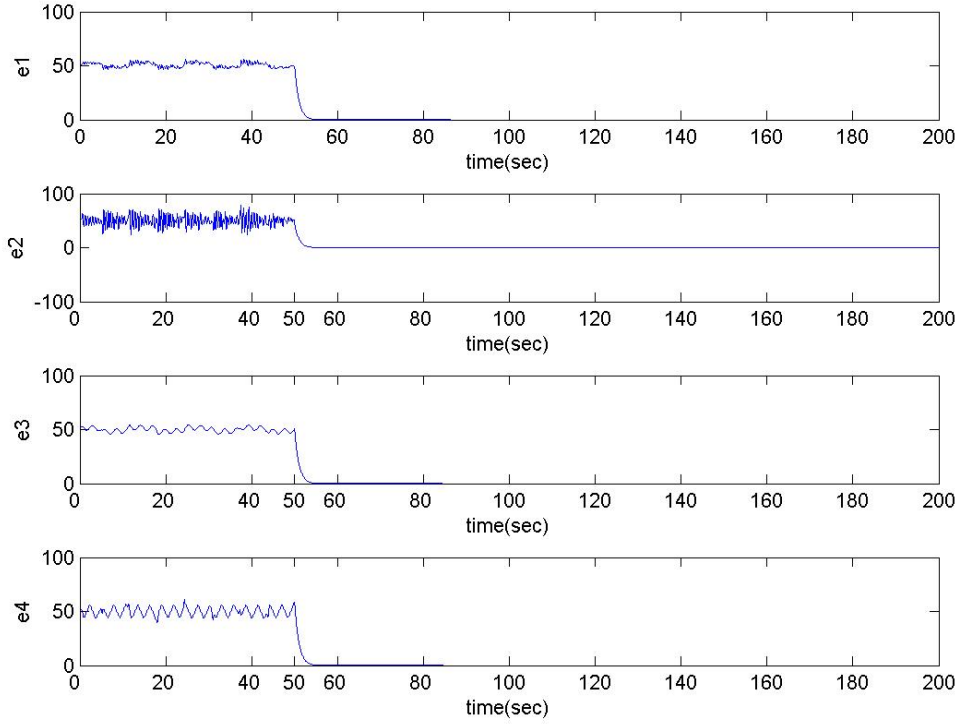

Fig. 4.7 Time histories of errors for Case III.

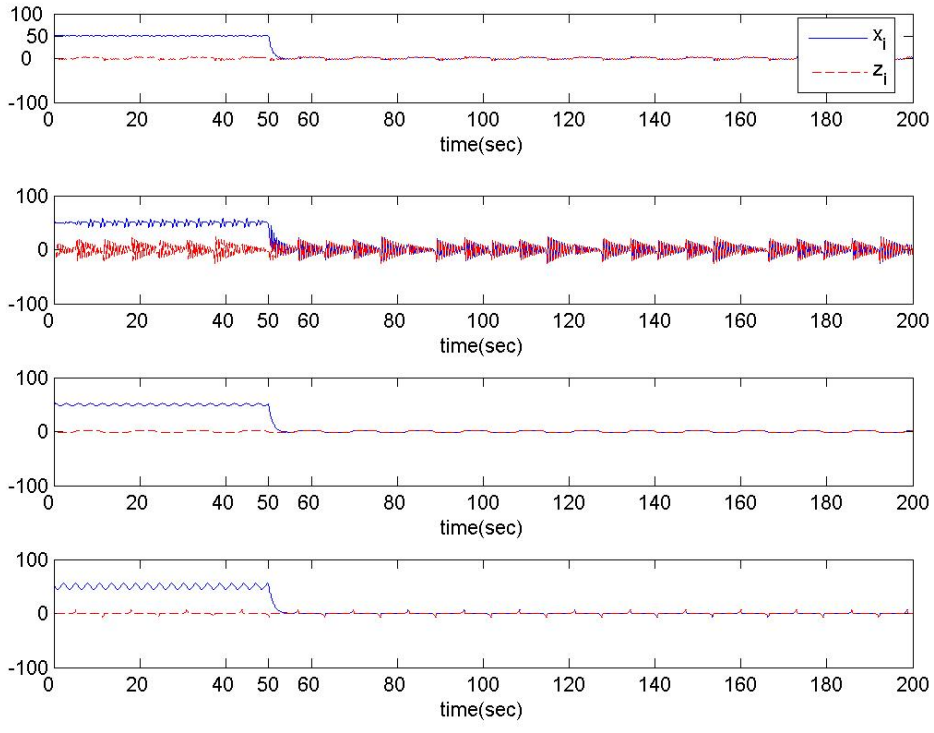

Fig. 4.8 Time histories of x_1, x_2, x_3, x_4 for Case III.

Chapter 5

Boids Control of Chaos for an Inertial Tachometer System

5.1 Preliminaries

The aggregate motion of a flock of birds or a herd of land animals is a beautiful and familiar part of the natural world. They exhibit complex and emergent behaviors such as flocking behavior, separation behavior, and obstacle avoiding behavior. This Chapter explores an approach based on simulation as an alternative to scripting the paths of each bird individually. Flock centering and separation, obstacle avoidance are studied. A nonautonomous inertial tachometer system is used for simulation example.

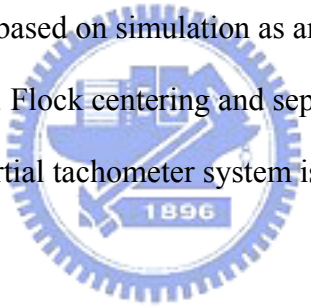

5.2 Boids Nonlinear Control

Many nonlinear systems which are known to present chaotic behavior are modeled by a set of nonlinear nonautonomous differential equations:

$$\frac{dx_i}{dt} = f_i(x_1, x_2, \cdots, x_n, t) \quad (i = 1, 2, \cdots, n) \tag{5-1}$$

where $x = (x_1(t), x_2(t), \cdots, x_n(t))$ is state variable vector, and $f(x,t) = (f_1(x,t), f_2(x,t), \cdots, f_n(x,t))$ is a nonlinear vector function of **x** and t. Given initial state $x_i^{\alpha}(0)$ at t=0, the state x_i^{α} of each isolated boid B_{α} is assumed to evolve for all $t \geq 0$ via state equations:

$$\frac{dx_i^{\alpha}}{dt} = f_i(x_1^{\alpha}, x_2^{\alpha}, \cdots, x_n^{\alpha}, t) \quad (i = 1, 2, \cdots, n) \tag{5-2}$$

We will assume for simplicity that all boids are identical and each boid is coupled locally only to those neighbor boids whose trajectories lie inside a prescribed sphere S_α of radius ε:

$$S_\alpha(\varepsilon,t)=\left\{B_\beta:\gamma_{\alpha,\beta}\ \sqrt{\sum_{i=1}^{n}(x_i^\alpha(t)-x_i^\beta(t))^2}\le\varepsilon\right\}, \tag{5-3}$$

at time t, where $\gamma_{\alpha,\beta}$ indicates the distance between the boids B_α and B_β. We will usually delete ε and t from $S_\alpha(\varepsilon,t)$ and simply write S_α to avoid clutter. Then the dynamics of the locally coupled chaotic nonlinear networks, namely, the dynamics of boids nonlinear networks is defined by

$$\frac{dx_i^\alpha}{dt}=f_i(x_1^\alpha,x_2^\alpha,\cdots,x_n^\alpha,t)+\sum_{B_\beta\in S_\alpha}D_i^\beta g_i(x_1^\beta,x_2^\beta,\cdots,x_n^\beta,t)$$
$$(i=1,2,\cdots,n,\quad \alpha=1,2,\cdots,M) \tag{5-4}$$

where D_i^β $(i=1,2,\cdots,n)$ are coupling coefficients, and $g(x,t)=(g_1(x,t),g_2(x,t),\cdots,g_n(x,t))$ is a nonlinear vector function of **x** and t.

Case I Flock Centering: Boids attempt to move toward the average position of nearby flockmates.

The center of nearby flockmates is defined by

$$\overline{x_i^\alpha}(t)=\frac{\sum_{\beta\in S\alpha}x_i^\beta(t)}{N_\alpha}, \tag{5-5}$$

where N_α indicates the number of nearby flockmates. The boids can move toward the center $\overline{x_i^\alpha}$ by using chaotic synchronization [36]. Therefore, flock centering is implemented here by imposing the control dynamics

$$\frac{dx_i^\alpha}{dt}=f_i(x_1^\alpha,x_2^\alpha,\cdots,x_n^\alpha,t)+d_i^\alpha(\overline{x_i^\alpha}-x_i^\alpha) \tag{5-6}$$

where $d_i^{\alpha} > 0$.

Case II Separation of Flocks: Boids keep a distance from different kinds of flocks.

A flock may attempt to go away from other kinds of flocks. If a flock gets close enough to a different groups of flocks, that is, if the distance between the centers of two flocks becomes less than $\varepsilon_g > 0$, boids attempt to scatter. Separation of flocks is implemented by the dynamics of chaotic desynchronization

$$\frac{dx_i^{\alpha}}{dt} = f_i(x_1^{\alpha}, x_2^{\alpha}, \cdots, x_n^{\alpha}, t) + s_i^{\alpha}(\overline{x_i^{\alpha}} - x_i^{\alpha}) \tag{5-7}$$

where $s_i^{\alpha} < 0$ and $\overline{x_i^{\alpha}}$ indicates a center of nearby flockmates.

Case III Obstacle Avoidance: Boids attempt to dodge static obstacles.

Assume that a static obstacle is defined by the equation

$$h(x_1, x_2, \cdots, x_n) = b \quad (i = 1, 2, \cdots, n) \tag{5-8}$$

where h is a scalar function of $x = (x_1, x_2, \cdots, x_n)$ and b is a constant. The normal vector at $x = (x_1, x_2, \cdots, x_n)$ on a surface $h(x_1, x_2, \cdots, x_n, t) = b$ is given by

$$\nabla h(x_1, x_2, \cdots, x_n, t) \square \left(\frac{\partial h(x_1, x_2, \cdots, x_n)}{\partial x_1}, \frac{\partial h(x_1, x_2, \cdots, x_n)}{\partial x_2}, \cdots, \frac{\partial h(x_1, x_2, \cdots, x_n)}{\partial x_n}\right). \tag{5-9}$$

If a boid gets close enough to a static obstacle, that is, if the distance between a boid and a static obstacle is less than ε_0, the boids must attempt to dodge the static obstacle. Obstacle avoidance can be implemented by switching over to a new vector field:

$$\frac{dx_i^{\alpha}}{dt} = (1 - u_i) f_i(x_1^{\alpha}, x_2^{\alpha}, \cdots, x_n^{\alpha}, t) + u_i \gamma \frac{\partial h(x_1, x_2, \cdots, x_n)}{\partial x_i} \tag{5-10}$$

where $0 \le u_i \le 1$ and $\gamma > 0$.

5.3 Chaos of an Inertial Tachometer

In this section, an inertial tachometer system is studied. The physical model of the inertial tachometer system is shown in Fig.5.1. There exists viscous damping in bent rod bearing (O point). The mass of bent rod is neglected and the balls m_1 and m_2 are considered as two particles.

We can write the kinetic and potential energies of the system as follow：

$$T = \frac{1}{2}m_1(l^2\dot{\varphi}^2 + l^2\dot{\theta}^2\sin^2\varphi) + \frac{1}{2}m_2(l^2\dot{\varphi}^2 + l^2\dot{\theta}^2\cos^2\varphi) + \frac{1}{2}J\dot{\theta}^2$$
$$\Pi = -gl(m_1\cos\varphi + m_2\sin\varphi) \tag{5-11}$$

where

m_1, m_2 ：the mass of balls and $m_1 > m_2$,

J ：the moment of inertia of the shaft about vertical center axis,

l ： the length of rod,

φ ：the angle between the shaft and the rod,

$\dot{\theta}$ ：the angular velocity of the shaft,

g ：gravity acceleration,

The Lagrangian is $L = T - \Pi$, the corresponding Lagrange equations are

$$(m_1 + m_2)l^2\ddot{\varphi} - (m_1 - m_2)l^2\dot{\theta}^2\sin\varphi\cos\varphi + gl(m_1\sin\varphi - m_2\cos\varphi) = -k\dot{\varphi}$$
$$(m_1l^2\sin^2\varphi + m_2l^2\cos^2\varphi + J)\ddot{\theta} + (m_1 - m_2)2l^2\sin\varphi\cos\varphi\dot{\theta} = 0 \tag{5-12}$$

where k is damping coefficient in bent rod bearing.

The state equation can be written as：

$$\dot{\varphi} = \psi$$
$$\dot{\psi} = \frac{1}{m_1 + m_2}[(m_1 - m_2)\cos\varphi\sin\varphi\omega^2 - \frac{g}{l}(m_1\sin\varphi - m_2\cos\varphi) - \frac{k}{l^2}\psi] \tag{5-13}$$
$$\dot{\omega} = -\frac{(m_1 - m_2)2l^2\sin\varphi\cos\varphi}{m_1l^2\sin^2\varphi + m_2l^2\cos^2\varphi + J}\psi\omega$$

where $\omega = \dot{\theta}$.

We assume that the inertial tachometer is subjected to an external vertical vibration to basement $A\sin(\eta t)$. The Lagrange equation now are given in a noninertial vibrating reference frame, which is fixed with the basement. Due to the inertial force appearing in the noninertial frame, the gravity acceleration in the noninertial frame becomes $g + A\eta^2 \sin(\eta t)$. Let $\varphi = x_1$, $\psi = x_2$, $\omega = x_3$, the equation (5-13) is rewritten in the form

$$\begin{aligned}
\dot{x}_1 &= x_2 \\
\dot{x}_2 &= \frac{1}{m_1 + m_2}\{(m_1 - m_2)\cos x_1 \sin x_1 {x_3}^2 \\
&\quad -\frac{1}{l}[g + A\eta^2 \sin(\eta t)](m_1 \sin x_1 - m_2 \cos x_1) - \frac{k}{l^2} x_2\} \\
\dot{x}_3 &= -\frac{(m_1 - m_2)2l^2 \sin x_1 \cos_1}{m_1 l^2 \sin^2 x_1 + m_2 l^2 \cos^2 x_1 + J} x_2 x_3
\end{aligned} \tag{5-14}$$

where x_1, x_2, x_3 are state variables and $m_1, m_2, A, \eta, l, k, g, J$ are parameters. This system exhibits chaos when the parameters of system are $m_1 = 9$, $m_2 = 1$, $A = 10.7$, $J = 9$, $\eta = 1$, $l = 0.3$, $k = 0.5$, $g = 9.81$ and the initial condition is (x_1, x_2, x_3) = (0, 0, 2). Its phase portraits as shown in Fig. 5.2 and Fig. 5.3. The Lyapunov exponents and the bifurcation diagram of the inertial tachometer are shown in Fig. 5.4 and Fig. 5.5 for A between 9.1 and 10.9.

5.4 Numerical Simulations of Boids Control

The inertial tachometer system is the master system:

$$\begin{cases}
\dot{x}_1 = x_2 \\
\dot{x}_2 = \frac{1}{m_1 + m_2}\{(m_1 - m_2)\cos x_1 \sin x_1 {x_3}^2 \\
\quad -\frac{1}{l}[g + A\eta^2 \sin(\eta t)](m_1 \sin x_1 - m_2 \cos x_1) - \frac{k}{l^2} x_2\} \\
\dot{x}_3 = -\frac{(m_1 - m_2)2l^2 \sin x_1 \cos x_1}{m_1 l^2 \sin^2 x_1 + m_2 l^2 \cos^2 x_1 + J} x_2 x_3
\end{cases} \tag{5-15}$$

The slave system is

$$\begin{cases} \dot{y}_1 = y_2 \\ \dot{y}_2 = \dfrac{1}{m_1+m_2}\{(m_1-m_2)\cos y_1 \sin y_1 {y_3}^2 \\ \quad -\dfrac{1}{l}[g+A\eta^2\sin(\eta t)](m_1 \sin y_1 - m_2 \cos y_1) - \dfrac{k}{l^2} y_2\} \\ \dot{y}_3 = -\dfrac{(m_1-m_2)2l^2 \sin y_1 \cos y_1}{m_1 l^2 \sin^2 y_1 + m_2 l^2 \cos^2 y_1 + J} y_2 y_3 \end{cases} \tag{5-16}$$

Case I Flock Centering: Boids attempt to move toward the average position of nearby flockmates.

Flock centering is implemented here by imposing the control dynamics:

$$\frac{dx_i^{\alpha}}{dt} = f_i(x_1^{\alpha}, x_2^{\alpha}, \cdots, x_n^{\alpha}) + d_i^{\alpha}(\overline{x_i^{\alpha}} - x_i^{\alpha}) \quad , \qquad \text{where} \quad d_i^{\alpha} > 0 \tag{5-17}$$

The slave system is rewritten as follows:

$$\begin{cases} \dot{y}_1 = y_2 + d(\dfrac{x_1+x_2+x_3}{3} - y_1) \\ \dot{y}_2 = \dfrac{1}{m_1+m_2}\{(m_1-m_2)\cos y_1 \sin y_1 {y_3}^2 \\ \quad -\dfrac{1}{l}[g+A\eta^2\sin(\eta t)](m_1 \sin y_1 - m_2 \cos y_1) - \dfrac{k}{l^2} y_2\} \\ \quad + d(\dfrac{x_1+x_2+x_3}{3} - y_2) \\ \dot{y}_3 = -\dfrac{(m_1-m_2)2l^2 \sin y_1 \cos y_1}{m_1 l^2 \sin^2 y_1 + m_2 l^2 \cos^2 y_1 + J} y_2 y_3 + d(\dfrac{x_1+x_2+x_3}{3} - y_3) \end{cases} \tag{5-18}$$

where d=0.000001.The simulations of flocking behavior of tachometer systems are shown in Figs. 5.6~5.8. The flocking of two tachometer systems are illustrated in Fig. 5.6. The distance between two systems is given in Fig. 5.7. The synchronization behavior of two tachometer systems is given in Fig. 5.8.

Case II Separation of Flocks: Boids keep a distance from different kinds of flocks.

Separation of flocks is implemented by the dynamics of chaotic

desynchronization:

$$\frac{dx_i^{\alpha}}{dt} = f_i(x_1^{\alpha}, x_2^{\alpha}, \cdots, x_n^{\alpha}) + s_i^{\alpha}(\overline{x_i^{\alpha}} - x_i^{\alpha}) \quad , \quad \text{where} \qquad s_i^{\alpha} < 0 \qquad (5\text{-}19)$$

The slave system is rewritten as follows:

$$\begin{cases} \dot{y}_1 = y_2 + d(\dfrac{x_1 + x_2 + x_3}{3} - y_1) \\ \dot{y}_2 = \dfrac{1}{m_1 + m_2}\{(m_1 - m_2)\cos y_1 \sin y_1 y_3^{\,2} \\ \quad -\dfrac{1}{l}[g + A\eta^2 \sin(\eta t)](m_1 \sin y_1 - m_2 \cos y_1) - \dfrac{k}{l^2} y_2\} \\ \quad + d(\dfrac{x_1 + x_2 + x_3}{3} - y_2) \\ \dot{y}_3 = -\dfrac{(m_1 - m_2)2l^2 \sin y_1 \cos y_1}{m_1 l^2 \sin^2 y_1 + m_2 l^2 \cos^2 y_1 + J} y_2 y_3 + d(\dfrac{x_1 + x_2 + x_3}{3} - y_3) \end{cases} \qquad (5\text{-}20)$$

where d=-0.00002. The simulations of flocking behavior of tachometer systems are shown in Figs. 5.9~5.11. The separation of two tachometer systems is illustrated in Fig. 5.9. The distance between two systems is given in Fig. 5.10. The desynchronization behavior of two tachometer systems is given in Fig. 5.11.

Case III Obstacle Avoidance: Boids attempt to dodge static obstacles.

Obstacle avoidance can be implemented by switching over to a new vector field:

$$\frac{dx_i^{\alpha}}{dt} = (1 - u_i) f_i(x_1^{\alpha}, x_2^{\alpha}, \cdots, x_n^{\alpha}) + u_i \gamma \frac{\partial h(x_1, x_2, \cdots, x_n)}{\partial x_i} \qquad (5\text{-}21)$$

Define a sphere of radius r_1 centered at (x_1, y_1, z_1) by

$$(x - x_1)^2 + (y - y_1)^2 + (z - z_1)^2 = r_1^2 \qquad (5\text{-}22)$$

and its normal vector $n = (n_x, n_y, n_z)$ at the point (x, y, z) by

$$(n_x, n_y, n_z) = (2(x - x_1), 2(y - y_1), 2(z - z_1)) \qquad (5\text{-}23)$$

Define a cylinder of radius r_2 centered at (x_2, y_2) by

$$(x - x_1)^2 + (y - y_1)^2 = r_2^2 \qquad (5\text{-}24)$$

and its normal vector $n=(n_x,n_y,n_z)$ at the point (x, y, z) by

$$(n_x,n_y,n_z)=(2(x-x_1),2(y-y_1),0) \tag{5-25}$$

Therefore, the "sphere" and the "cylinder" obstacles are specified by the parameters: (x_1,y_1,z_1,r_1) and (x_2,y_2,r_2) respectively.

CASE III-1: Obstacle Avoidance-sphere

The inertial tachometer system is rewritten as follows:

$$\begin{cases} \dot{x}_1=(1-u_1)x_2+2u_1\gamma(x_1-X_1) \\ \dot{x}_2=\dfrac{1}{m_1+m_2}\{(m_1-m_2)\cos x_1\sin x_1 x_3{}^2 \\ \quad -\dfrac{1}{l}[g+A\eta^2\sin(\eta t)](m_1\sin x_1-m_2\cos x_1)-\dfrac{k}{l^2}x_2\}+2u_2\gamma(x_2-Y_1) \\ \dot{x}_3=-\dfrac{(m_1-m_2)2l^2\sin x_1\cos x_1}{m_1l^2\sin^2 x_1+m_2l^2\cos^2 x_1+J}x_2x_3+2u_3\gamma(x_3-Z_1) \end{cases} \tag{5-26}$$

where $\gamma=0.001$, $u_1=0.2$, $u_2=0.2$, $u_3=0.1$, $X_1=6.5$, $Y_1=0$, $Z_1=0.1$, $r_1=2$, The simulations of the obstacle avoidance behavior for sphere are illustrated in Figs. 5.12~5.13.

CASE III-2: Obstacle Avoidance-cylinder

The inertial tachometer system is rewritten as follows:

$$\begin{cases} \dot{x}_1=(1-u_1)x_2+2u_1\gamma(x_1-X_2) \\ \dot{x}_2=\dfrac{1}{m_1+m_2}\{(m_1-m_2)\cos x_1\sin x_1 x_3{}^2 \\ \quad -\dfrac{1}{l}[g+A\eta^2\sin(\eta t)](m_1\sin x_1-m_2\cos x_1)-\dfrac{k}{l^2}x_2\}+2u_2\gamma(x_2-Y_2) \\ \dot{x}_3=-\dfrac{(m_1-m_2)2l^2\sin x_1\cos x_1}{m_1l^2\sin^2 x_1+m_2l^2\cos^2 x_1+J}x_2x_3 \end{cases} \tag{5-27}$$

where $\gamma=0.0001$, $u_1=0.4$, $u_2=0.2$, $u_3=0$, $X_1=1.51$, $Y_1=0$, $Z_1=1.85$, $r_2=0.3$, The simulations of the obstacle avoidance behavior for cylinder are illustrated in Figs.5.14~5.15.

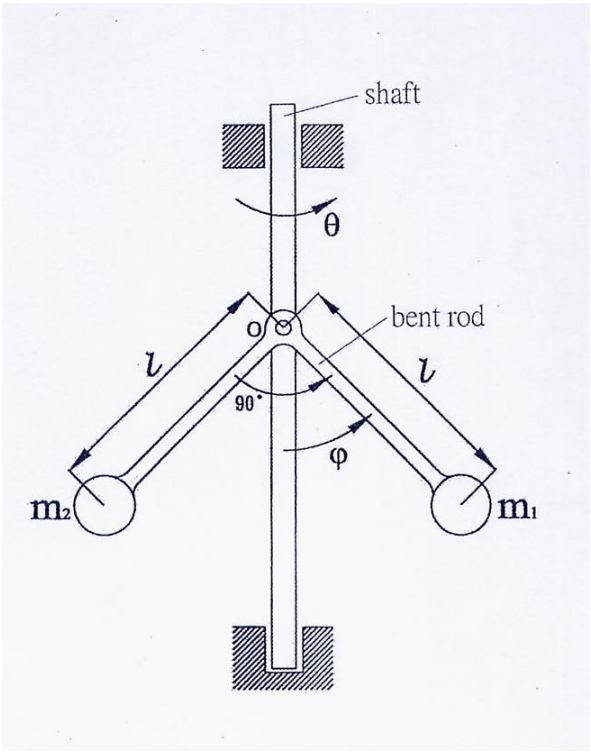

Fig. 5.1 Mechanical model of an inertial tachometer.

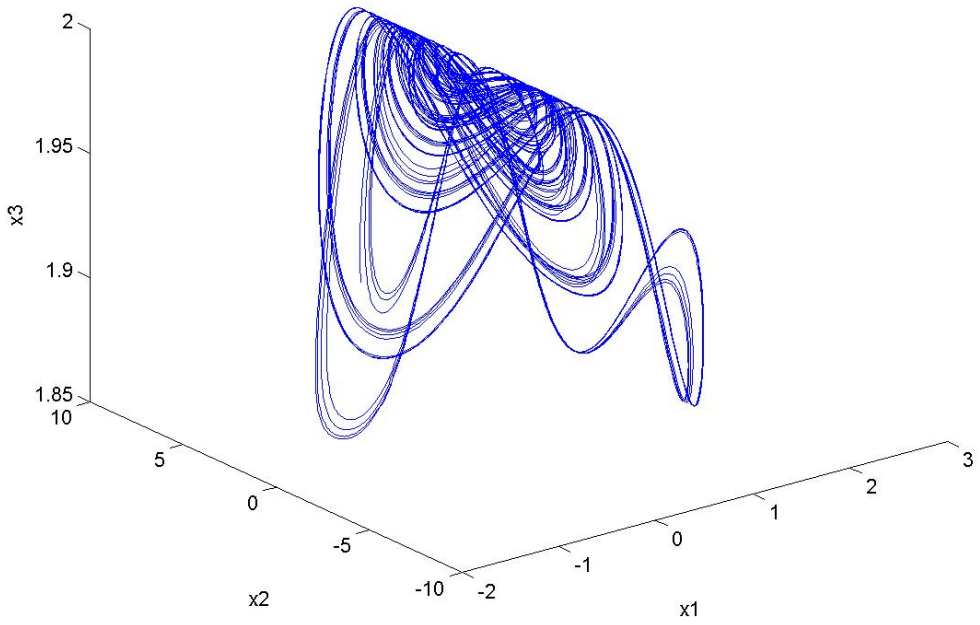

Fig . 5.2 Chaotic phase portrait for inertial tachometer system.

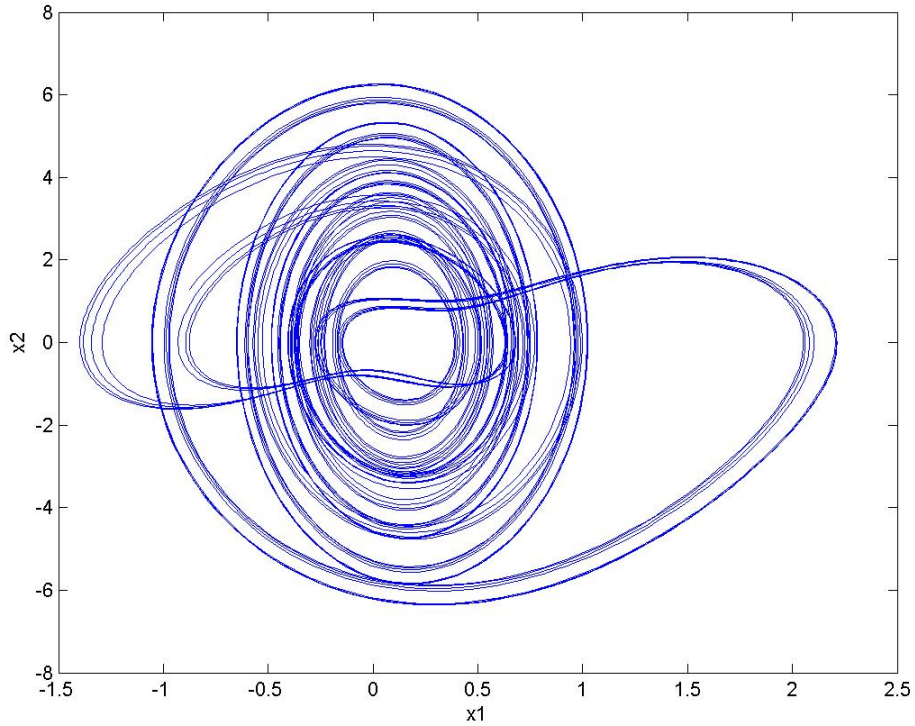

Fig . 5.3 Chaotic phase portrait for inertial tachometer system.

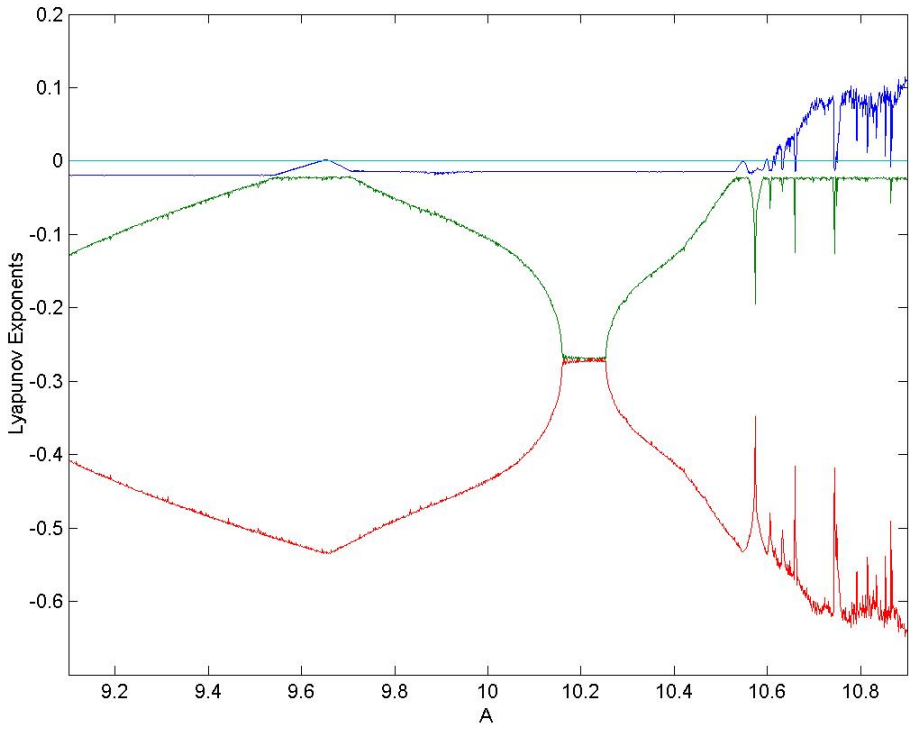

Fig. 5.4 Lyapunov exponents for A between 9.1 and 10.9.

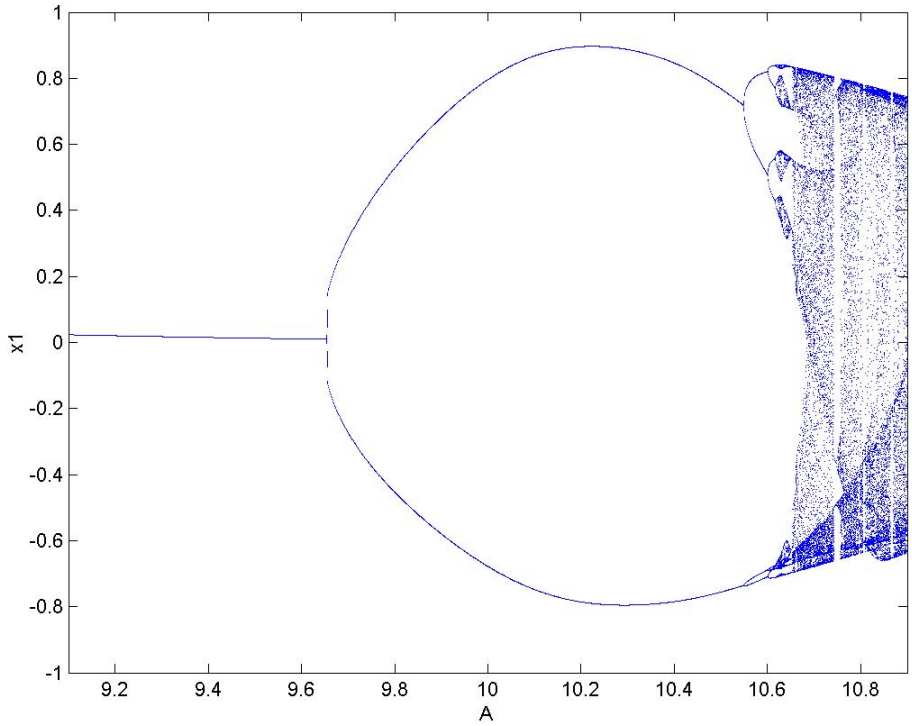

Fig. 5.5 Bifurcation diagram of x_1 for A between 9.1 and 10.9.

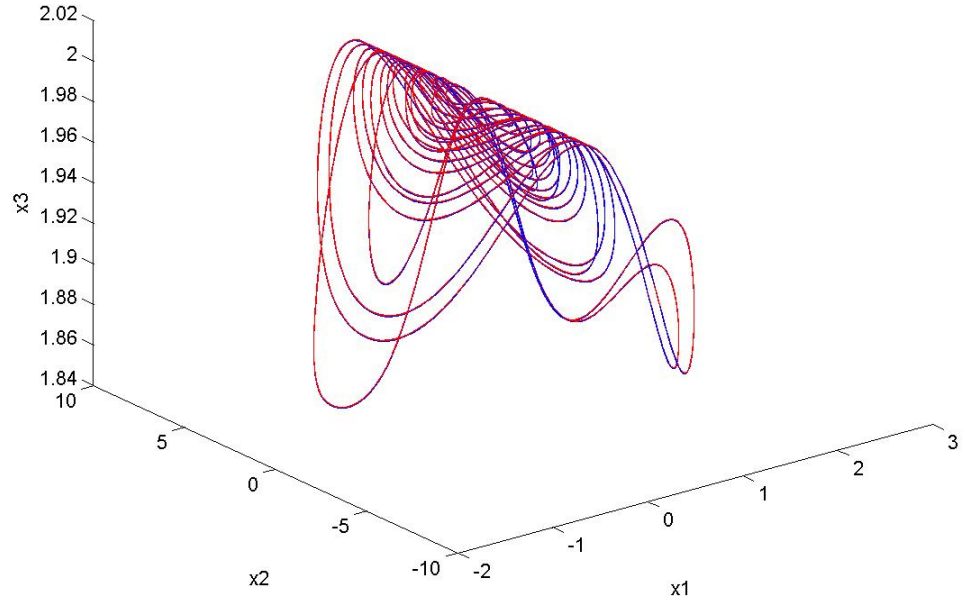

Fig. 5.6 Flocking of two inertial tachometer systems.

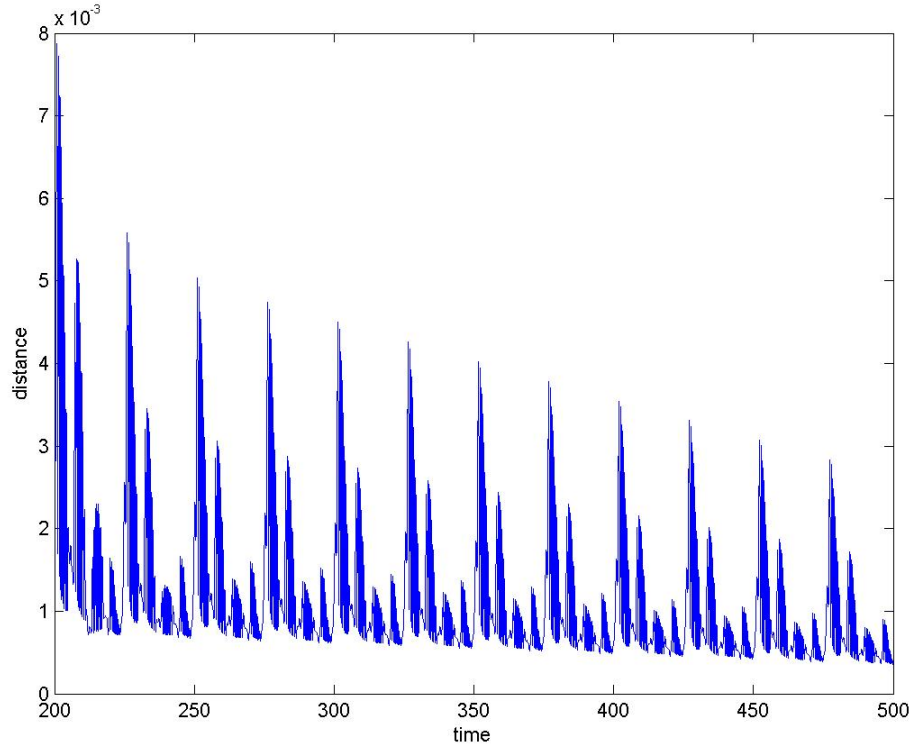

Fig. 5.7 Distance between two inertial tachometer systems.

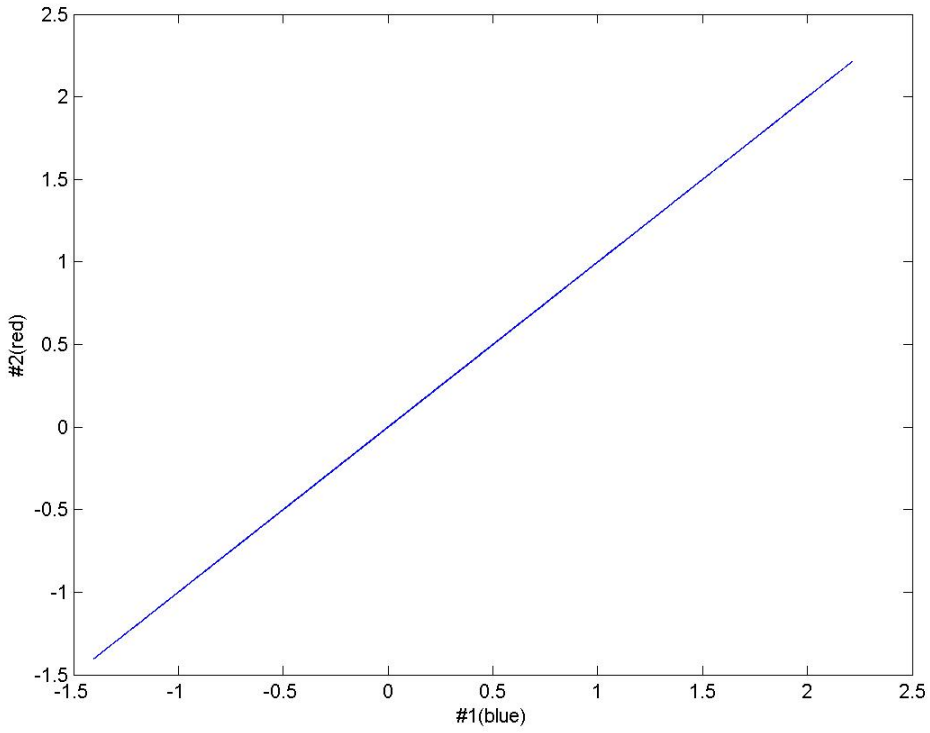

Fig. 5.8 Synchronization of two inertial tachometer systems.

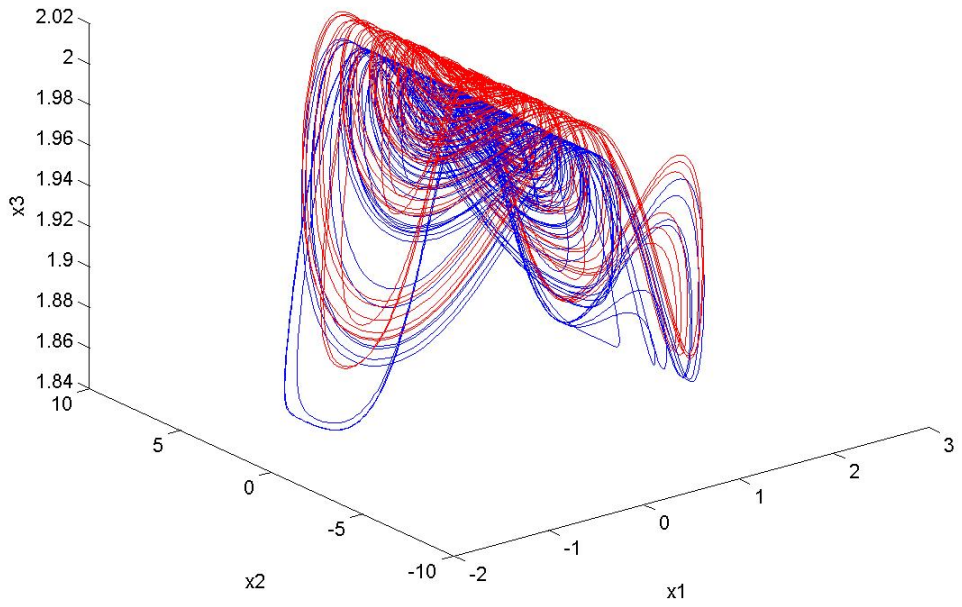

Fig .5.9 Separation of two inertial tachometer systems.

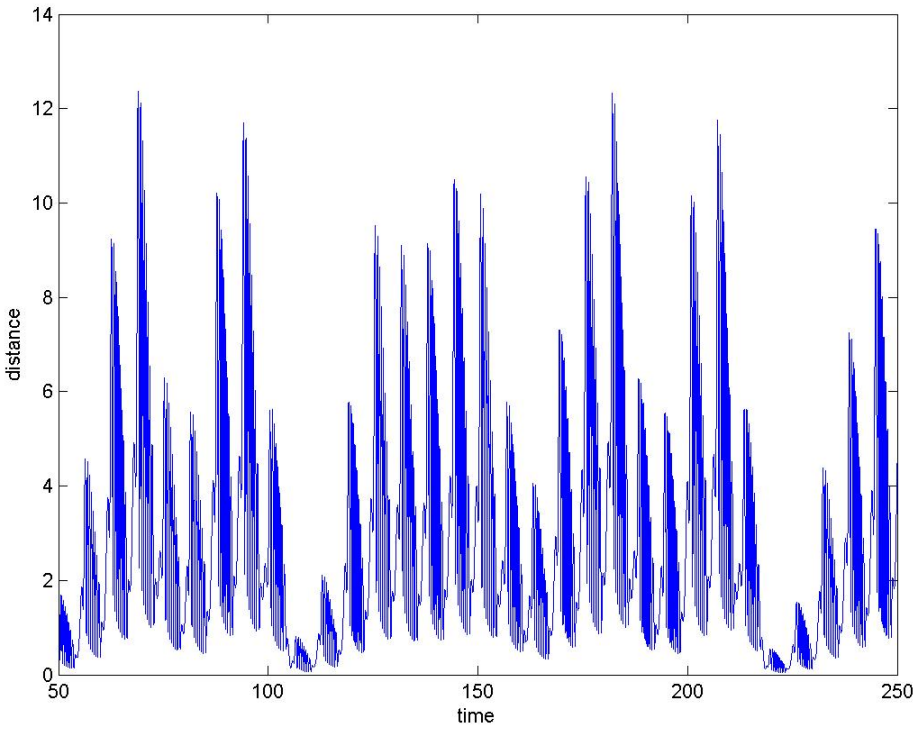

Fig. 5.10 Distance between two inertial tachometer systems.

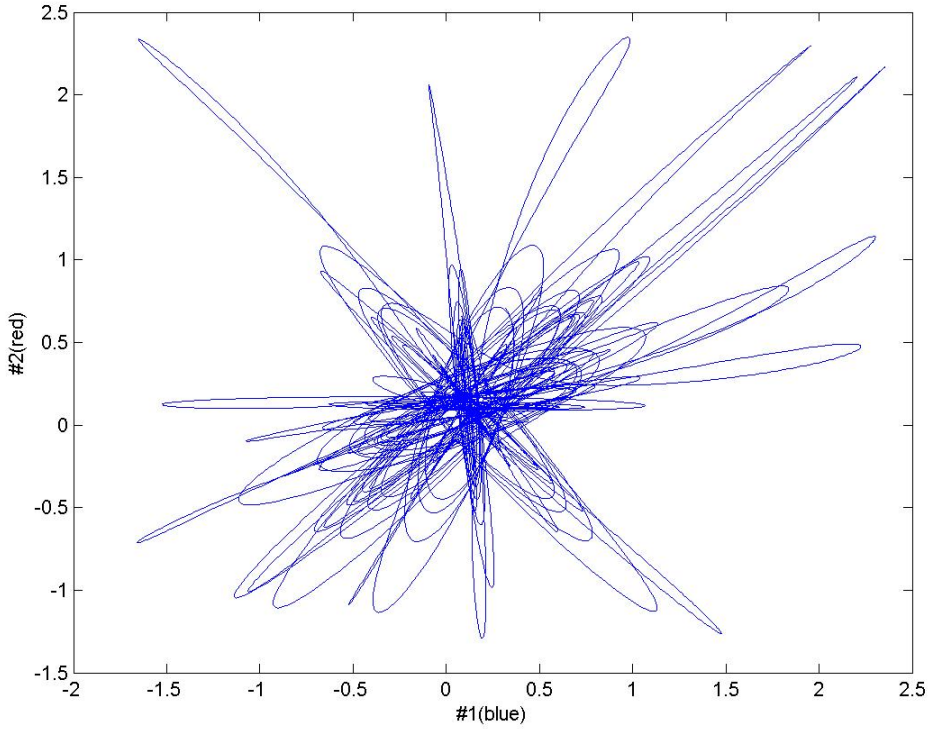

Fig. 5.11 Desynchronization of two inertial tachometer systems.

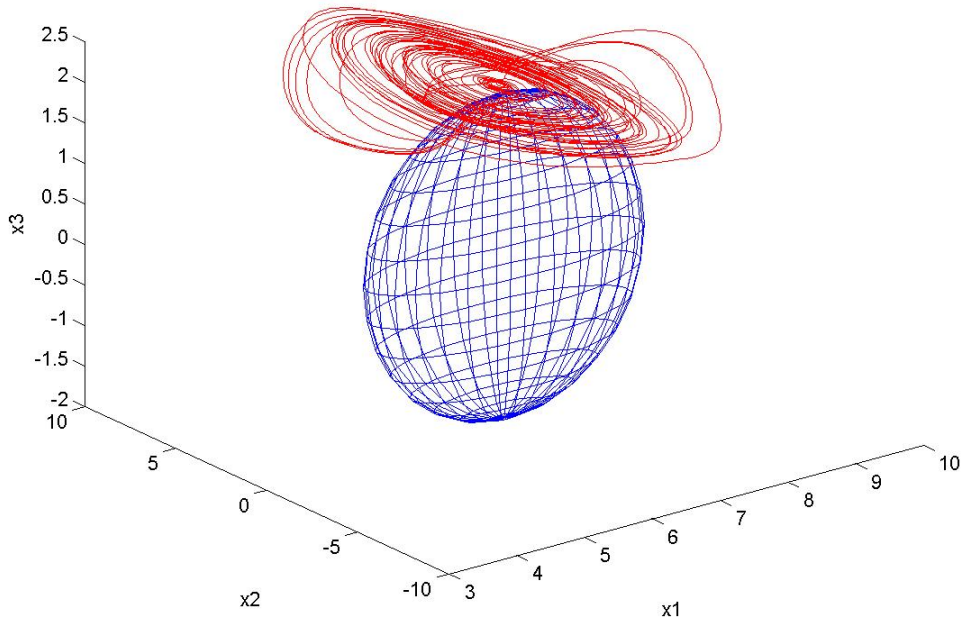

Fig. 5.12 Obstacle avoidance for inertial tachometer system (sphere).

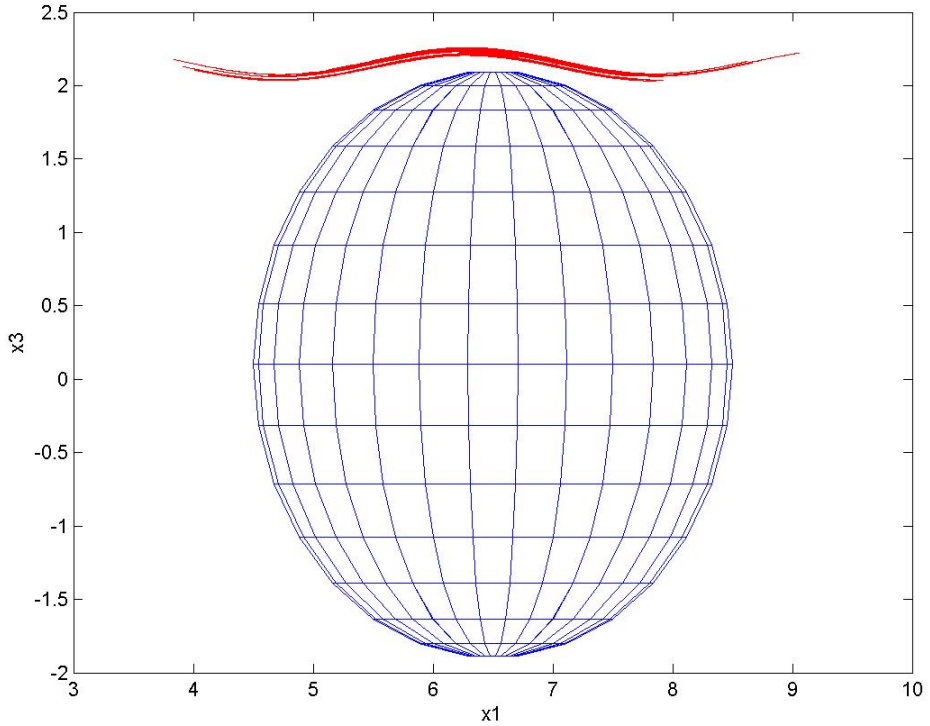

Fig. 5.13 Obstacle avoidance for inertial tachometer system (sphere).

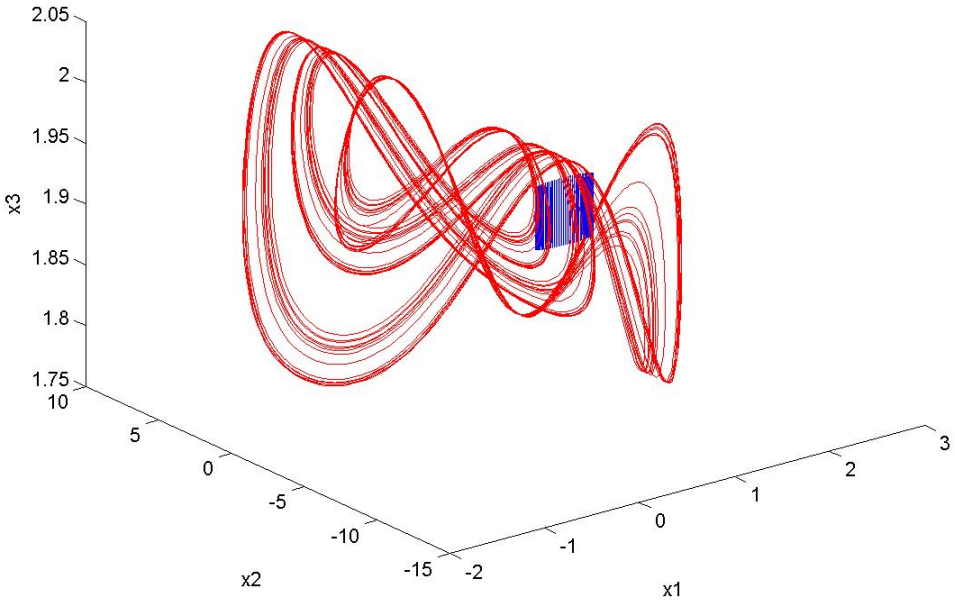

Fig. 5.14 Obstacle avoidance for inertial tachometer system (cylinder).

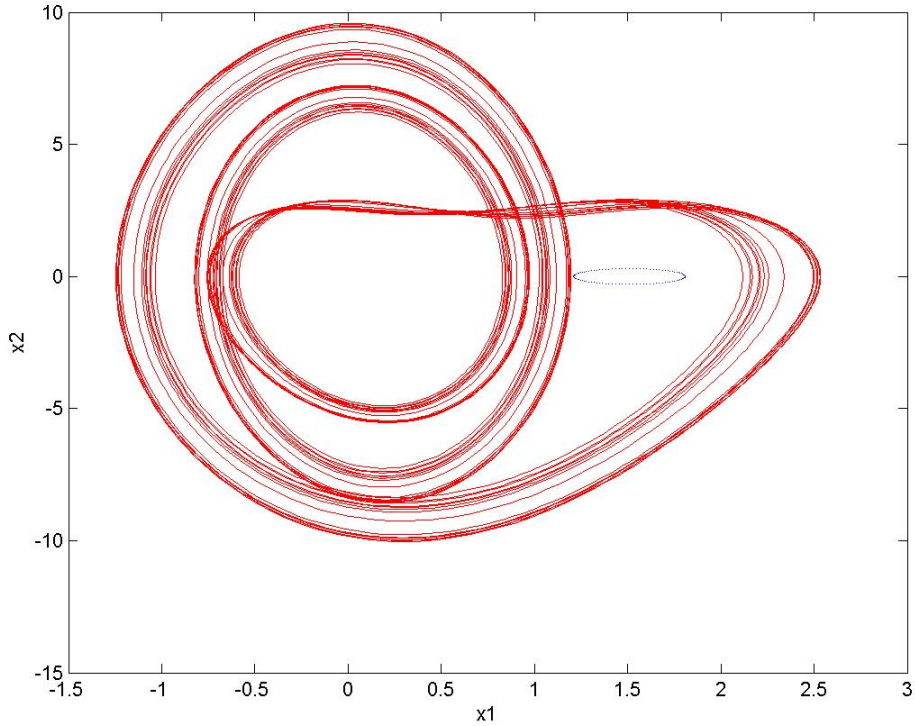

Fig. 5.15 Obstacle avoidance for inertial tachometer system (cylinder).

Chapter 6

Hyperchaos of a Lorenz System with Bessel Function Parameters

6.1 Preliminaries

The chaotic behaviors of a Lorenz system with Bessel function parameters is firstly studied numerically by time histories of states, phase portraits, Poincaré maps, bifurcation diagram, Lyapunov exponents and parameter diagram. It is found that hyperchaos and chaos exist. The hyperchaos is identified by the existence of two positive Lyapunov exponents and gives more security for secret communication.

6.2 Lorenz System with Bessel Function Parameters

The Lorenz system

$$\begin{cases} \dot{x} = \sigma(y - x) \\ \dot{y} = \gamma x - xz - y \\ \dot{z} = xy - bz \end{cases} \tag{6-1}$$

with parameters $\sigma(t)$, $\gamma(t)$, as given functions of time is a nonautonomous system, which is equivalent to a four-dimensional autonomous system.

σ, γ, b are given as：

$$\begin{cases} \sigma = 10 + k_1 J_0(t) \\ \gamma = k_2 + Y_0(t + 0.01) \\ b = 8/3 \end{cases} \tag{6-2}$$

where k_1, k_2, b are constant parameters, and

$$J_0(t) = \sum_{n=0}^{\infty} \frac{(-1)^n}{n!\Gamma(n+1)} (\frac{t}{2})^{2n} \tag{6-3}$$

$$Y_0(t+0.01)=\lim_{\mu\to 0}\frac{\cos\mu\pi J_{\mu}(t+0.01)-J_{-\mu}(t+0.01)}{\sin\mu\pi} \tag{6-4}$$

where J_0 is Bessel function of first kind, Y_0 is Bessel function of the second kind and Γ is Gamma function. The time histories of $10+J_0(t)$, $Y_0(t+0.01)$ are shown in Figs 6.1-6.2. The numerical simulations are carried out by MATLAB using the fractional operator in the Simulink environment.

6.3 Numerical Simulations

This system exhibits periodic motion when the parameters of system (6-1) are $\sigma=10+J_0(t)$, $\gamma=20.2+Y_0(t+0.01)$, $b=8/3$ and the initial condition is $(x,y,z)=(0.1,\ 10,\ 0.5)$. When the parameters are $\sigma=10+J_0(t)$, $\gamma=25+Y_0(t+0.01)$, $b=8/3$, the motion becomes chaotic. The time histories of three states, phase portraits, Poincaré maps, and bifurcation diagrams of the system are shown in Fig. 6.3~Fig 6.8.

Lyapunov exponents and parametric diagram are also given to certify the existence of hyperchaos. Let us assume Lyapunov exponents λ_i $(i=1,2,3,4)$ satisfying $\lambda_1>\lambda_2>\lambda_3$, and $\lambda_4=0$. Then the dynamics of system (6-1) can be characterized as follows:

(1) When $\lambda_{1,2,3}<0$ and $\lambda_4=0$, system (6-2) is periodic.

(2) When $\lambda_1>0,\ \lambda_{2,3}<0$, and $\lambda_4=0$, system (6-2) exhibits chaotic motion.

(3) When $\lambda_{1,2}>0,\ \lambda_3<0$, and $\lambda_4=0$, system (6-2) exhibits hyperchaotic motion.

Four cases are studied as follows.

Case I

Fix k_1, b, vary k_2. The Lyapunov exponents of the system (6-1) for $k_1=1$, and $b=8/3$ are shown in Fig. 6.9. The parametric diagram of system (6-1) for

varying k_1 and k_2 with $b = 8/3$ is shown in Fig. 6.10. The white area corresponds to periodic motion. By simulation, system is periodic when $0.01 \le k_2 \le 20.62$. The blue area corresponds to chaotic motion. And the green area corresponds to hyperchaotic motion, which is identified by the existence of two positive Lyapunov exponents, as clearly shown in Fig. 6.9. As k_2 increases to $20.63 \le k_2 \le 40$, the system displays complex behavior, with an interweaving between chaotic and hyperchaotic motions. The hyperchaotic motion becomes more and more as k_2 increases. Just like Monet's picture , Fig 6.10 gives a beautiful scene. White area is the bank of a river, blue area is the water of the river and green area is the duckweed in the river.

Case II

Fix $b = 8/3$, vary k_1, k_2. k_1 increases intermittently for increment of 10. And k_2 varies slowly for increment of 0.01. Some typical values of k_1 and k_2 that generate hyperchaos with two positive Lyapunov exponents are shown in Tables 1～3, respectively. Comparing Table 1～3, a particular phenomenon appears when k_1 increases. As k_1 increases, the value of Lyapunov exponent λ_2 becomes larger. It means that larger k_1 can arouse hyperchaotic motion. In other words, hyperchaos is aroused with enlarged Bessel function of first kind.

Table 1 Typical values of parameter k_2 that generate hyperchaos for $k_1 = 1$ and $b = 8/3$.

k_2	λ_1	λ_2	λ_3	λ_4
28.94	0.82575	0.00139	-13.82725	0
29.47	0.84172	0.00127	-13.84311	0
29.74	0.84484	0.00129	-13.84625	0
30.01	0.85157	0.00115	-13.85283	0
30.58	0.86341	0.00117	-13.86471	0
33.42	0.91705	0.00162	-13.91877	0

35.74	0.95094	0.00126	-13.95231	0

Table 2 Typical values of parameter k_2 that generate hyperchaos for $k_1 = 10$ and $b = 8/3$.

k_2	λ_1	λ_2	λ_3	λ_4
23.99	0.73925	0.00221	-13.74337	0
28.44	0.82189	0.00202	-13.82582	0
30.74	0.86354	0.00223	-13.86768	0
33.16	0.90872	0.00231	-13.91294	0
41.74	1.05732	0.00254	-14.06177	0
43.4	1.08819	0.00262	-14.09272	0

Table 3 Typical values of parameter k_2 that generate hyperchaos for $k_1 = 30$ and $b = 8/3$.

k_2	λ_1	λ_2	λ_3	λ_4
36.42	0.95411	0.00268	-13.96268	0
56.09	1.30776	0.00260	-14.31622	0
59.49	1.35049	0.00266	-14.35902	0
59.56	1.34414	0.00354	-14.35356	0
60.11	1.36281	0.00490	-14.42031	0

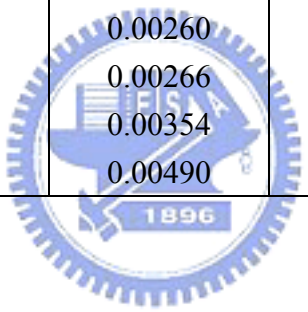

Case III

Fix $k_1 = 30$, $k_2 = 28$ and vary b. Fig. 6.11 shows the Lyapunov exponents as a function of b to classify the chaotic or periodic motions. With increasing b, the motion of system (6-1) becomes periodic when $0.01 \le b \le 0.5$. Periodic motions occur again with $b \ge 3.2$. As b increases to $0.51 \le b \le 3.19$, system displays chaotic behavior. In this case, hyperchaotic motion was not found.

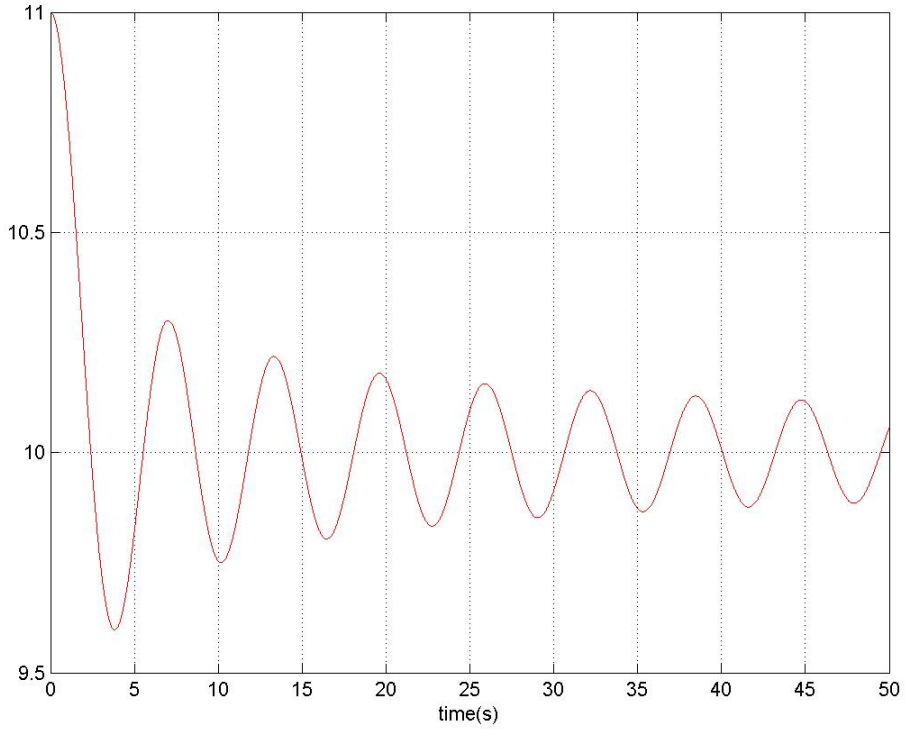

Fig. 6.1 The time history $\sigma(t)$.

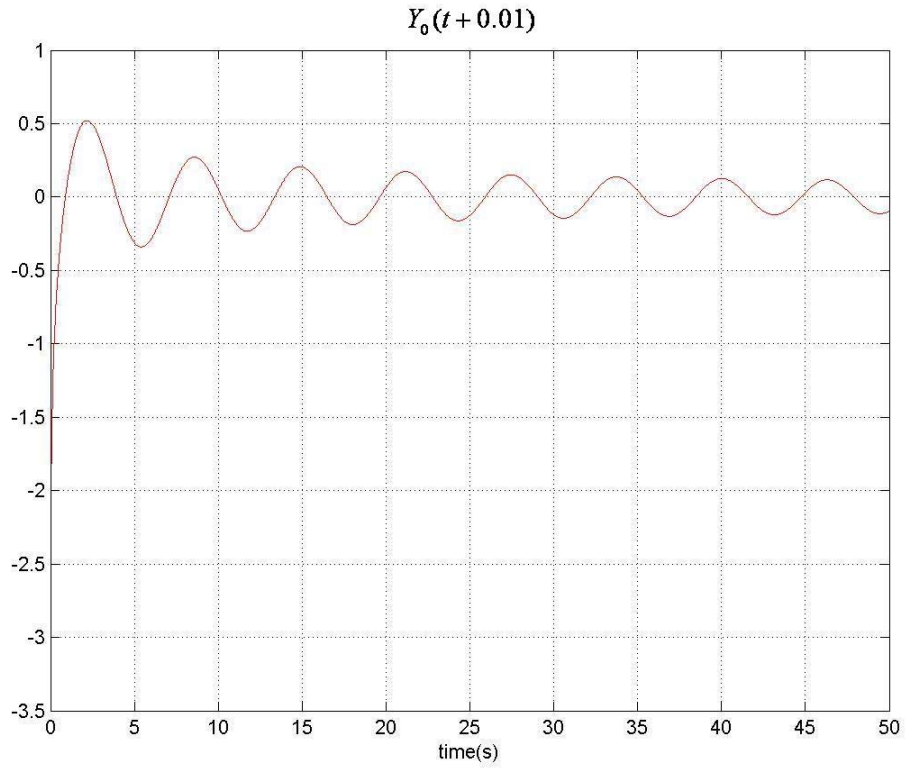

Fig . 6.2 The time history of $Y_0(t+0.01)$.

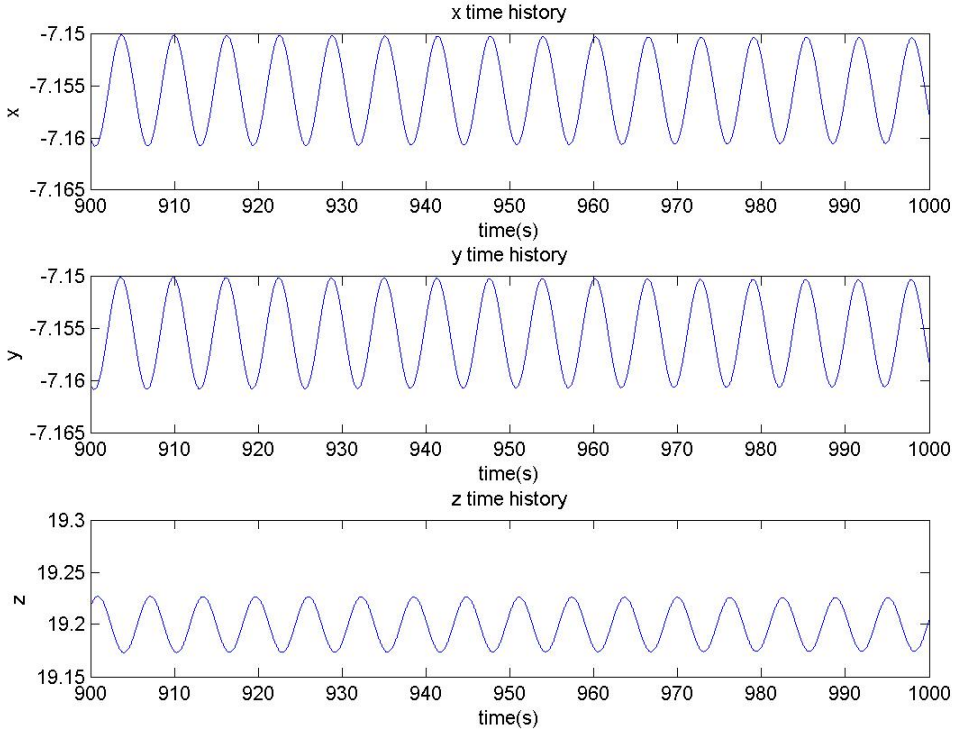

Fig . 6.3 The time histories of the three states.

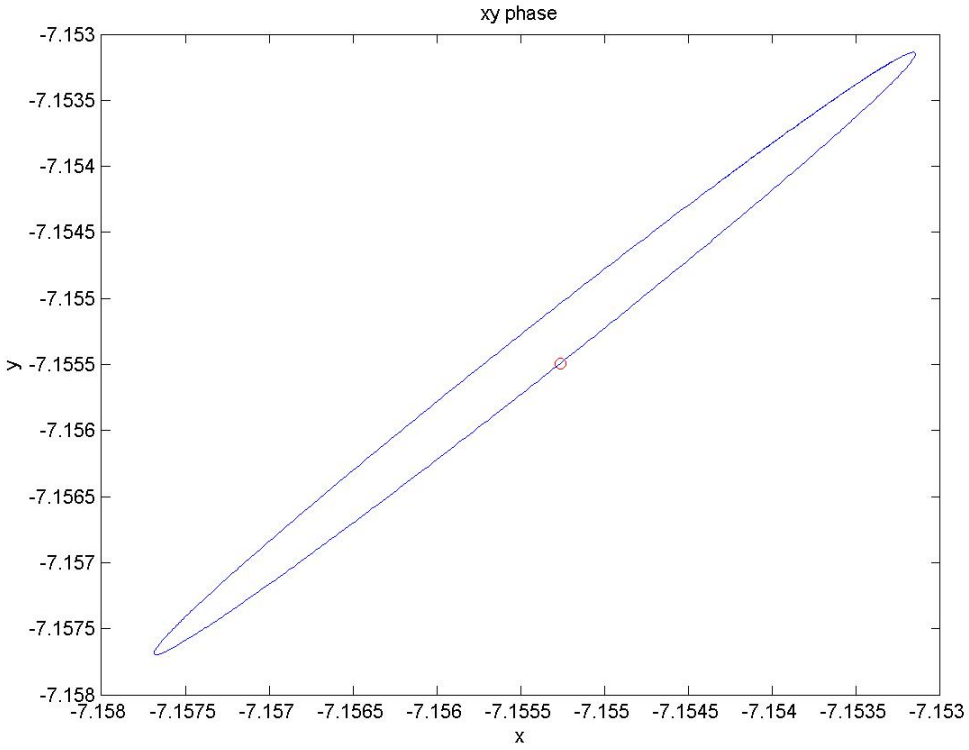

Fig. 6.4 The phase portrait and Poincaré map for x, y states.

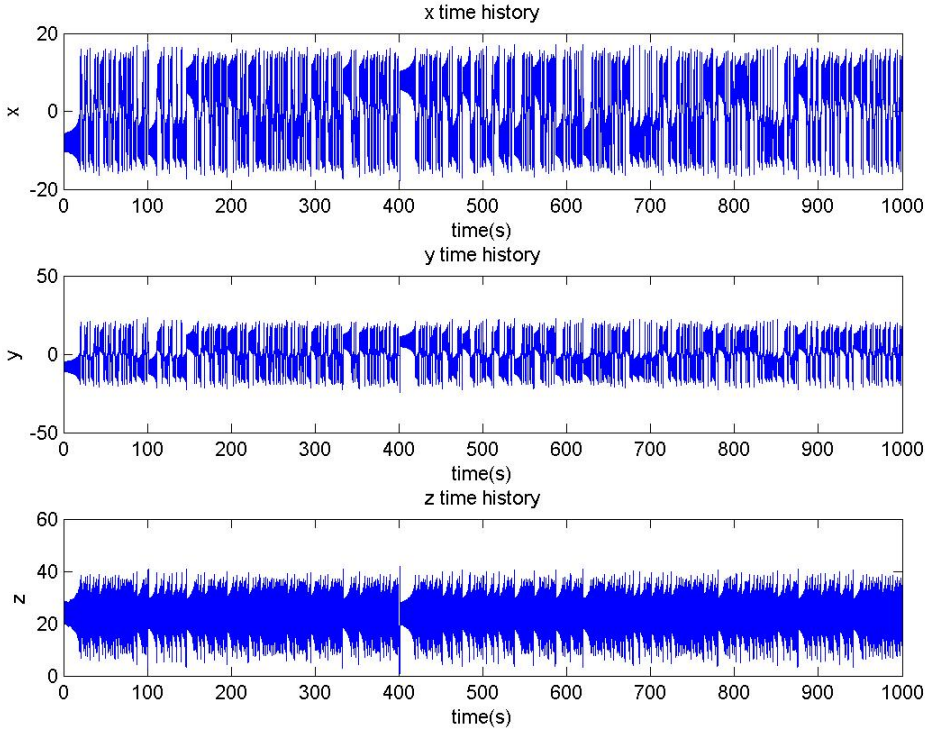

Fig . 6.5 The time histories of the x, y, z states.

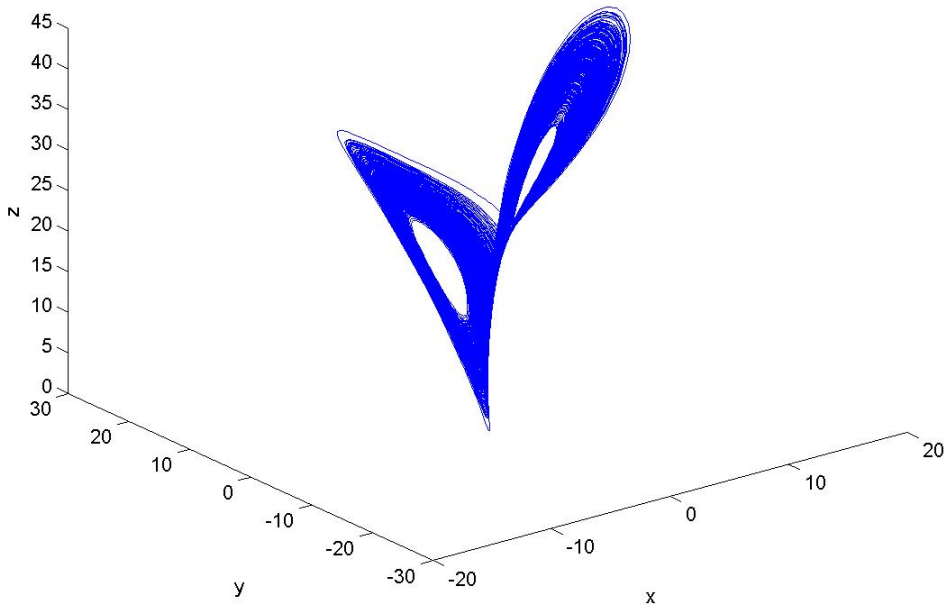

Fig. 6.6 The phase portrait of x, y, z states.

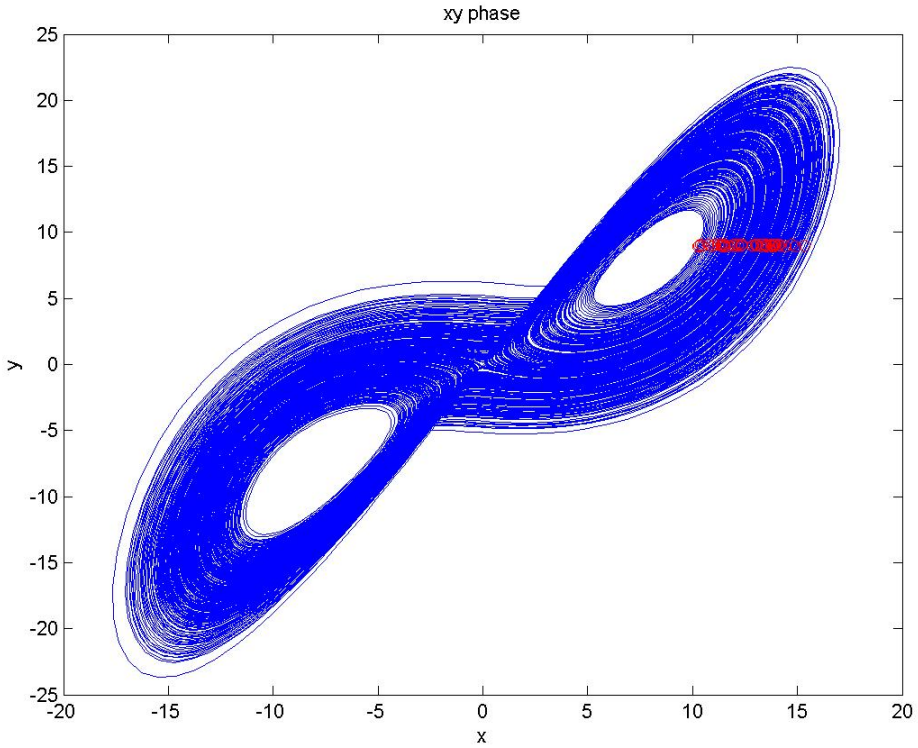

Fig. 6.7 The phase portrait and Poincaré map for x, y states.

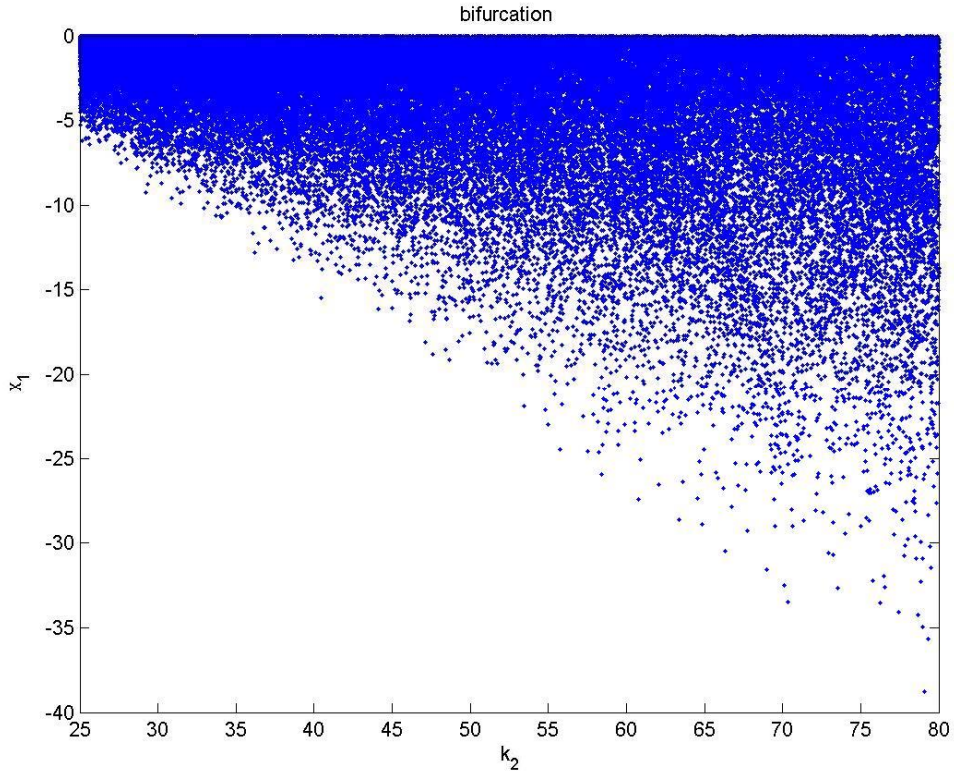

Fig. 6.8 The bifurcation diagram for $\sigma = 10 + J_0(t)$, and $b = 8/3$.

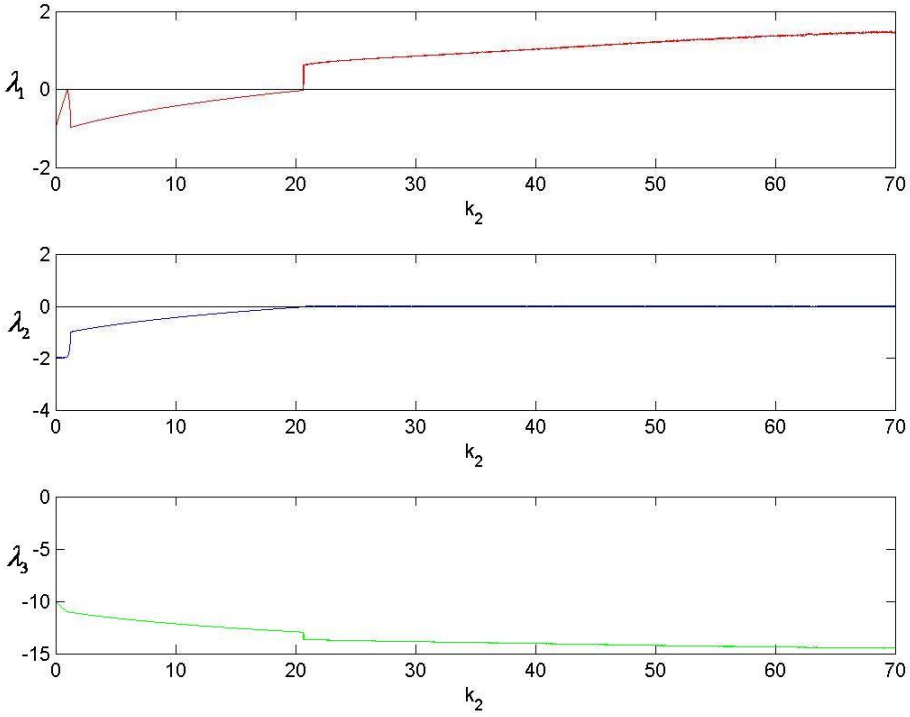

(a)

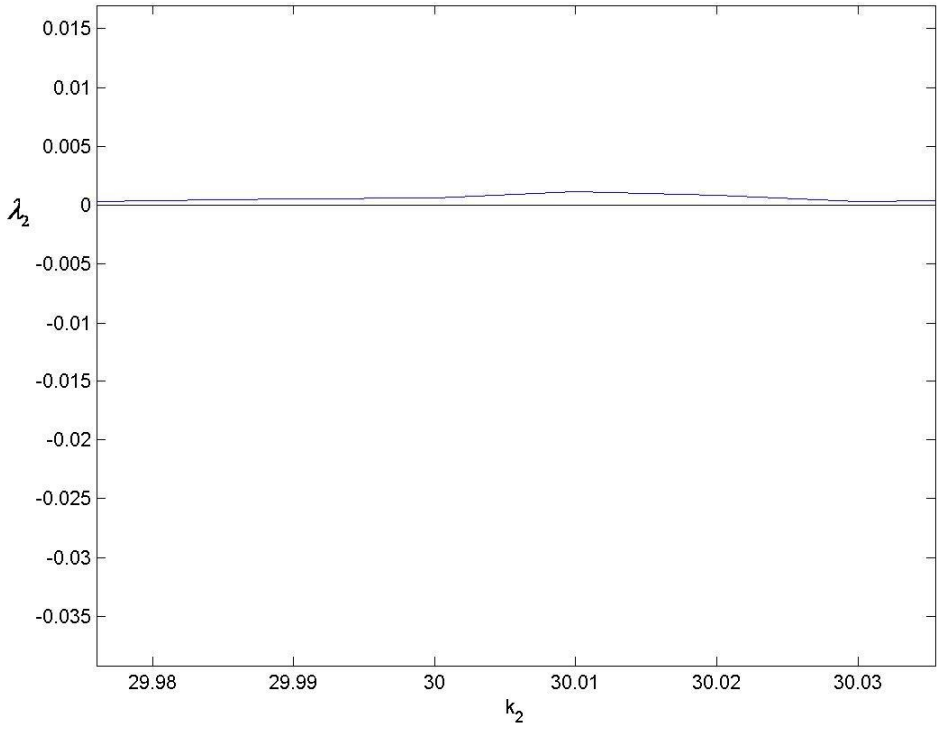

(b) Amplified diagram for λ_2

Fig. 6.9 Lyapunov exponents of system (2-2) for varying k_2.

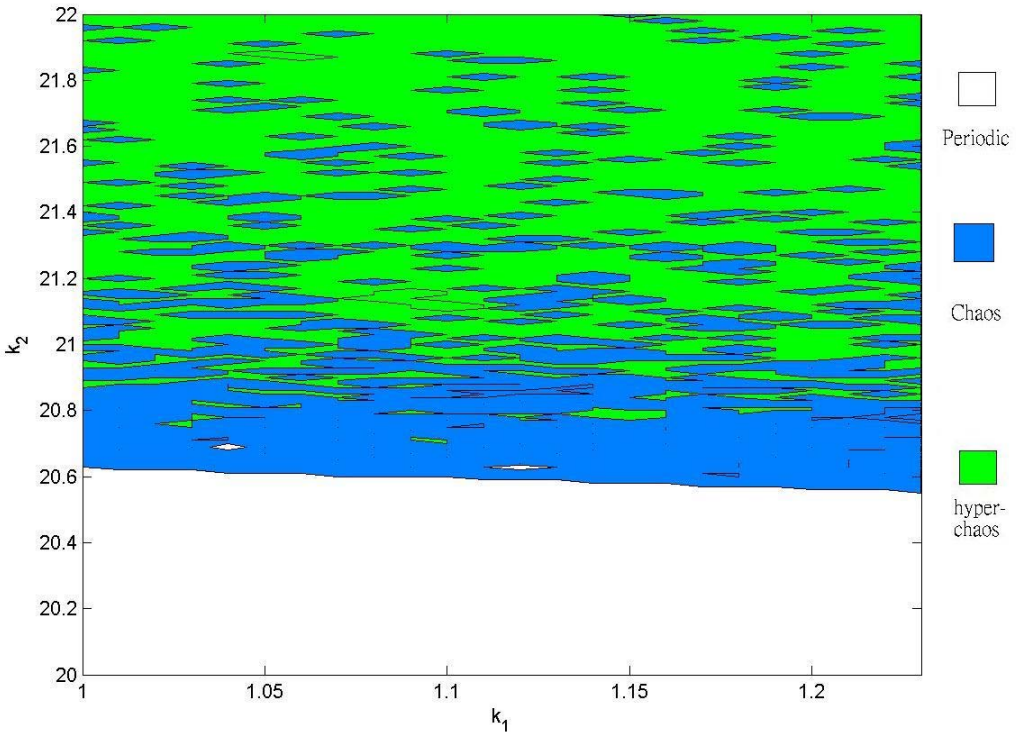

Fig. 6.10 The parametric diagram of system (2-1) for varying k_1 and k_2.

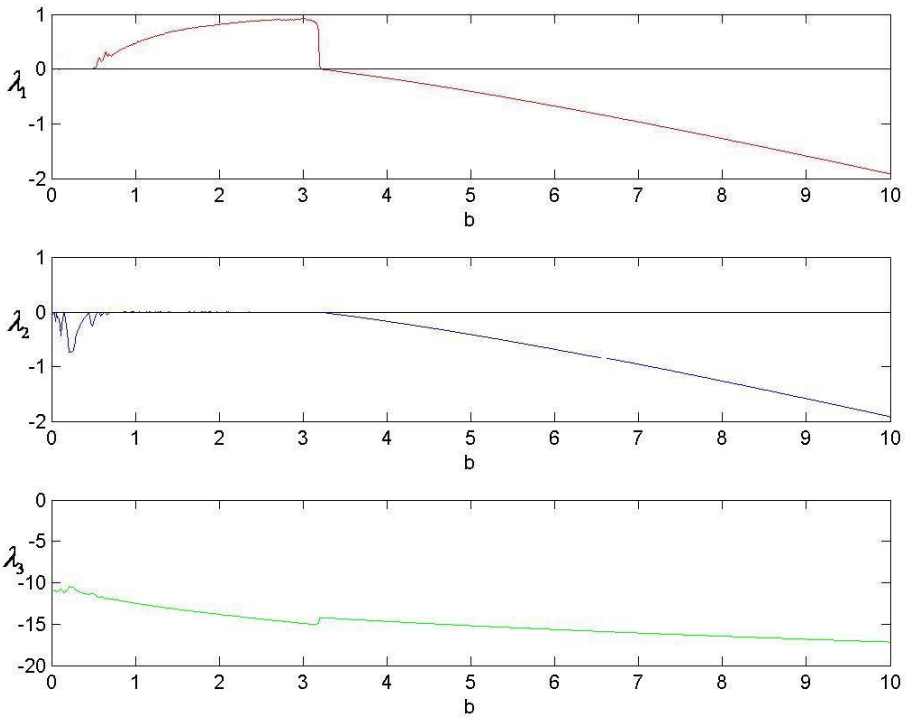

F

ig.6.11 Lyapunov exponents of system (2-2) for varying b, with $k_1 = 30$ and $k_2 = 28$.

Chapter 7

Symplectic Symchronization of Different Order Nonautonomous Systems via Nonlinear Control

7.1 Preliminaries

In this chapter, a new symplectic synchronization*

$$y = F(x, y, t) \tag{7-1}$$

is studied, where x, y are state vectors of the "master" and of the "slave", respectively, $F(x, y, t)$ is a given function of x, y and time. When $F(x, y, t) = F(x, t)$, Eq. (7-1) reduces to the generalized synchronization $y = F(x, t)$. Therefore the generalized synchronization is a special case of symplectic synchronization.

In Eq. (7-1), the final desired state y of the "slave" system not only depends upon the "master" system state x but also depends upon the "slave" system state y itself. Therefore the "slave" system is not traditional pure slave obeying the "master" system completely but plays a role to determine the final desired state of the "slave" system. In other words, it plays an "interwined" role, so we call this kind of synchronization "symplectic synchronization", and call the "master" system partner A, the "slave" system partner B.

There exists great potential of the application of the symplectic synchronization. For instance, when the symplectically synchronized chaotic signal is used as a signal carrier, the secure communication is more difficult to be deciphered. There are many control techniques to synchronize chaotic systems, such as linear error feedback

*The term "symplectic" comes the Greek for "interwined". H. Weyl first introduced in 1939 in this book "The Classical

Groups" (P. 165 in both the first edition, 1939, and second edition, 1946, Princeton University Press).

control, adaptive control, active control , fuzzy control, impulsive control [6-15].

This chapter proposes a new symplectic synchronization algorithm based on nonlinear control and Barbalat Lemma [34], which noticeably expanded the application ranges of generalized synchronization.

This chapter is organized as follow. In Section 2, symplectic synchronization scheme is proposed. In Section 3, Duffing system, Van der Pol system and Chen-Lee system [35] are used as simulated examples.

7.2 Symplectic Synchronization Scheme of Different Order Nonautonomous Chaotic Systems

Consider the nonautonomous master system :

$$\dot{x} = f_1(x,t) \tag{7-2}$$

where $x = [x_1,...,x_n]^T \in \Re^n$ is the state vector of partner A, $f_1(\cdot)$ is a continuous vector function.

The nonautonomous slave system is given by the following equation:

$$\dot{y} = C(t)y + D(t)f_2(y,t) + u \tag{7-3}$$

where $y = [y_1,...,y_m]^T \in \Re^m$ is the state vector of partner B, C and D are system matrices with proper dimensions, $f_2(\cdot)$ is a continuous vector function, and u is the controller.

Function $f_2(z,t)$ is globally Lipschitz continuous; i.e., the following condition is satisfied:

For function $f_2(z,t)$, there exists constant $L > 0$, for any two different z_1, $z_2 \in R^n$, such that

$$\left\| f_2(z_1,t) - f_2(z_2,t) \right\| < L \left\| z_1 - z_2 \right\| \tag{7-4}$$

for any t.

Our goal is to design the controller u so that the state vector y of the partner B asymptotically approaches $F(x,y,t)$. Define error vector $e(t) = [e_1, e_2, ..., e_n]^T$ and the synchronization errors are defined as

$$e = y - F(x,y,t) \tag{7-5}$$

We want

$$\lim_{t\to\infty} e = \lim_{t\to\infty} [y - F(x,y,t)] = 0 \tag{7-6}$$

From Eq. (7-5), it is obtained that

$$\dot{e} = \dot{y} - D_x F(x,y,t)\dot{x} - D_y F(x,y,t)\dot{y} - \frac{\partial F(x,y,t)}{\partial t} \tag{7-7}$$

Let the controller ***u*** is designed as

$$\begin{aligned} u = {} & D_x F(x,y,t) f_1(x,t) + D_y F(x,y,t)[C(t)y + D(t) f_2(y,t)] \\ & + \frac{\partial F(x,y,t)}{\partial t} - \eta[y - F(x,y,t)] - D(t) f_2[F(x,y,t),t] \\ & - C(t)F(x,y,t) \end{aligned} \tag{7-8}$$

where $F(x,y,t)$ corresponds to z_2 in Eq. (7-4), $\eta = diag(\eta_1, ..., \eta_m)$. $\eta_1, ..., \eta_m$ are all positive, where

$$\frac{\min(\eta_i)}{L\left\|D(t)\right\|_{\max} + \left\|C(t)\right\|_{\max}} > 1 \tag{7-9}$$

Introducing Eqs. (7-3), (7-8), into Eq. (7-7), it becomes

$$\begin{aligned} \dot{e} &= C(t)y + D(t) f_2(y,t) - \eta[y - F(x,y,t)] \\ &\quad - D(t) f_2[F(x,y,t),t] - C(t)F(x,y,t) \\ &= C(t)e - \eta e + D(t)\{f_2(y,t) - f_2[F(x,y,t),t]\} \end{aligned} \tag{7-10}$$

Construct a Lyapunov error function of the following form

$$V(t) = \frac{1}{2} e^T e = \frac{1}{2} \left\| e \right\|^2 \tag{7-11}$$

Evaluating the time derivative of $V(t)$ along the trajectory of Eq. (7-10) and

using the Lipschitz condition, we have

$$\begin{aligned}\dot{V}(t) &= e^T C(t)e - e^T \eta e + e^T D(t)\{f_2(y,t) - f_2[F(x,y,t),t]\} \\ &\le \|C(t)\|_{\max} \|e\|^2 - \min(\eta_i)\|e\|^2 + \|e\|\|D(t)\|_{\max} - \|f_2(y,t) - f_2[F(x,y,t),t]\| \\ &\le \|C(t)\|_{\max} \|e\|^2 - \min(\eta_i)\|e\|^2 + L\|D(t)\|_{\max} \|e\|^2 \\ &= [\|C(t)\|_{\max} + L\|D(t)\|_{\max} - \min(\eta_i)]\|e\|^2 \le 0\end{aligned} \tag{7-12}$$

Let $G = \min(\eta_i) - \|C(t)\|_{\max} - L\|D(t)\|_{\max} > 0$, then $\dot{V} \le -G\|e\|^2$. Thus, it is obtained that

$$V(t) \le V_0 e^{-2Gt} \tag{7-13}$$

From Eq. (7-13), we can know that $\lim_{t\to\infty} \int_0^\infty V(t)dt$ is bounded. Moreover, $V(t)$ is uniformly continuous. According to the Barbalat Lemma [34], if $f(t)$ is uniformly continuous, and $\lim_{t\to\infty} \int_0^\infty |f(\tau)|d\tau$ is bounded, then $f(t) \to 0$ when $t \to \infty$, we can get $\lim_{t\to\infty} V(t) = 0$. Namely, $\lim_{t\to\infty} \|e\| = 0$. Therefore, the error system (7-10) is asymptotically stable. The partner A and the partner B are in symplectic synchronization.

7.3 Numerical Results

Two illustrative examples are given to demonstrate the validity of the proposed scheme.

Case I Symplectic synchronization of Duffing system and van der Pol system.

Consider the following Duffing system :

$$\begin{cases} \dot{x}_1 = x_2 \\ \dot{x}_2 = -\alpha x_2 - \omega_0{}^2 x_1 - \beta x_1{}^3 + P_1 \sin \omega_1 t \end{cases} \tag{7-14}$$

where x_1, x_2, are state variables and α, $\omega_0{}^2$, β, P_1, ω_1 are constant parameters. This system exhibits chaos when the parameters of system are $\alpha = 0.7$, $\omega_0{}^2 = -1$,

$\beta = 1$, $P_1 = 0.8$, $\omega_1 = 1$, and the initial condition is $(x_1, x_2) = (0.5, 0.2)$. Its phase portrait and time histories are shown in Fig. 7.1 and Fig. 7.2.

The van der Pol system is adopted as the partner B, which is

$$\begin{cases} \dot{y}_1 = y_2 + u_1 \\ \dot{y}_2 = -\varepsilon(1 - y_1^2) y_2 - y_1 + P_2 \cos \omega_2 t + u_2 \end{cases} \tag{7-15}$$

where y_1, y_2, are state variables and ε, P_2, ω_2, are constant parameters. $u = (u_1, u_2)^T$ is the controller. This system exhibits chaos without controller when the parameters of system are $\varepsilon = 5$, $P_2 = 1.25$, $\omega_2 = 4.2$, and the initial condition is $(y_1, y_2) = (0.01, 0.5)$. Its phase portrait and time histories are shown in Fig. 7.3 and Fig. 7.4.

C, D and f_2 in Eq. (7-3) are now :

$$C = \begin{bmatrix} 0 & 1 \\ -1 & \varepsilon \end{bmatrix} = \begin{bmatrix} 0 & 1 \\ -1 & 5 \end{bmatrix}, \quad D = \begin{bmatrix} 0 & 0 \\ 0 & 1 \end{bmatrix},$$

$$f_2 = \begin{bmatrix} 0 \\ -\varepsilon y_1^2 y_2 + P_2 \cos \omega_2 t \end{bmatrix} = \begin{bmatrix} 0 \\ -5 y_1^2 y_2 + 1.25 \cos 4.2t \end{bmatrix}.$$

It can be easily verified that $\|C\|_{\max} = \|C\|_{i2} = [\lambda_{\max}(C^T C)]^{1/2} = 5.1926$ and

$\|D\|_{\max} = \|D\|_{i2} = [\lambda_{\max}(D^T D)]^{1/2} = 1$.

Let $L = 1$ and select the matrix η as :

$$\eta = \begin{bmatrix} 10 & 0 \\ 0 & 9 \end{bmatrix};$$

then we can get $\min(\eta_i) = 9$.

$G = \min(\eta_i) - \|C(t)\|_{\max} - L\|D(t)\|_{\max} = 9 - 5.1926 - 1 > 1$.

We take $F_1(x, y, t) = \frac{1}{2} x_1^2 y_1$ and $F_2(x, y, t) = x_2 y_2$. They are chaotic functions of time. By Eq. (7-6) we have

$$\lim_{t\to\infty} e_i = \lim_{t\to\infty}[y_i - F_i(x,y,t)] = 0\,,\quad i = 1,2 \tag{7-16}$$

With the parameters and initial conditions above, the controller u

$$\begin{aligned}
u &= D_x F(x,y,t)\, f_1(x,t) + D_y F(x,y,t)[C(t)y + D(t)\, f_2(y,t)] \\
&\quad + \frac{\partial F(x,y,t)}{\partial t} - \eta[y - F(x,y,t)] - D(t)\, f_2[F(x,y,t),t] \\
&\quad - C(t)F(x,y,t) \\
&= \begin{bmatrix} \frac{\partial F_1}{\partial x_1} & \frac{\partial F_1}{\partial x_2} \\ \frac{\partial F_2}{\partial x_1} & \frac{\partial F_2}{\partial x_1} \end{bmatrix} \begin{bmatrix} \dot{x}_1 \\ \dot{x}_2 \end{bmatrix} + \begin{bmatrix} \frac{\partial F_1}{\partial y_1} & \frac{\partial F_1}{\partial y_2} \\ \frac{\partial F_2}{\partial y_1} & \frac{\partial F_2}{\partial y_1} \end{bmatrix} \begin{bmatrix} \dot{y}_1 \\ \dot{y}_2 \end{bmatrix} + \begin{bmatrix} \frac{\partial F_1}{\partial t} & \frac{\partial F_1}{\partial t} \\ \frac{\partial F_2}{\partial t} & \frac{\partial F_2}{\partial t} \end{bmatrix} \\
&\quad - \begin{bmatrix} 10 & 0 \\ 0 & 9 \end{bmatrix} \begin{bmatrix} y_1 - \frac{1}{2}x_1^2 y_1 \\ y_2 - x_2 y_2 \end{bmatrix} - \begin{bmatrix} 0 & 0 \\ 0 & 1 \end{bmatrix} \begin{bmatrix} 0 \\ -\varepsilon(\frac{1}{2}x_1^2 y_1)^2 x_2 y_2 + P_2 \cos(\omega_2 t) \end{bmatrix} \\
&\quad - \begin{bmatrix} 0 & 1 \\ -1 & \varepsilon \end{bmatrix} \begin{bmatrix} \frac{1}{2}x_1^2 y_1 \\ x_2 y_2 \end{bmatrix} \\
&= \begin{bmatrix} x_1 y_1 \dot{x}_1 \\ y_2 \dot{x}_2 \end{bmatrix} + \begin{bmatrix} \frac{1}{2}x_1^2 \dot{y}_1 \\ x_2 \dot{y}_2 \end{bmatrix} - \begin{bmatrix} 10 y_1 - 5 x_1^2 y_1 \\ 9 y_2 - 9 x_2 y_2 \end{bmatrix} \\
&\quad - \begin{bmatrix} 0 \\ -5(\frac{1}{2}x_1^2 y_1)^2 x_2 y_2 + 1.25\cos(4.2t) \end{bmatrix} - \begin{bmatrix} x_2 y_2 \\ -\frac{1}{2}x_1^2 y_1 + 5 x_2 y_2 \end{bmatrix}
\end{aligned} \tag{7-17}$$

is designed according to Eq. (7-8). Fig. 7.5 and Fig. 7.6 show the time histories of error functions $e_1(t)$, $e_2(t)$, respectively. Exactly, partner A (7-14) and partner B (7-15) achieve the symplectic synchronization.

Case II Symplectic synchronization of Chen-Lee system [35] and Duffing system.

Consider the following partner A, Chen-Lee system :

$$\begin{cases} \dot{x}_1 = -x_2 x_3 + a x_1 \\ \dot{x}_2 = x_1 x_3 - b x_2 \\ \dot{x}_3 = (1/3) x_1 x_2 - c x_3 \end{cases} \tag{7-18}$$

where x_1, x_2, x_3 are state variables and a, b, c, are constant parameters. This system exhibits chaos when the parameters of system are $a = 5$, $b = 10$, $c = 3.8$,

and the initial condition is $(x_1, x_2, x_3) = (0.3, -0.02, 0.2)$. Its phase portraits and time histories as shown in Fig. 7.7 $\sim$ Fig. 7.9.

The Duffing system is adopted as partner B :

$$\begin{cases} \dot{y}_1 = y_2 + u_1 \\ \dot{y}_2 = -\alpha y_2 - \omega_0{}^2 y_1 - \beta y_1{}^3 + P_1 \sin \omega_1 t + u_2 \end{cases} \tag{7-19}$$

where y_1, y_2, are state variables and α, $\omega_0{}^2$, β, P_1, ω_1, are constant parameters. $u = (u_1, u_2)^T$ is the controller.

C, D and f_2 in Eq. (7-3) are now :

$$C = \begin{bmatrix} 0 & 1 \\ -\omega_0{}^2 & -\alpha \end{bmatrix} = \begin{bmatrix} 0 & 1 \\ 1 & -0.7 \end{bmatrix}, \quad D = \begin{bmatrix} 0 & 0 \\ 0 & 1 \end{bmatrix},$$

$$f_2 = \begin{bmatrix} 0 \\ -\beta y_1{}^3 + P_1 \sin \omega_1 t \end{bmatrix} = \begin{bmatrix} 0 \\ -y_1{}^3 + 0.8 \sin t \end{bmatrix}.$$

It can be easily verified that $\|C\|_{\max} = \|C\|_{i2} = [\lambda_{\max}(C^T C)]^{1/2} = 1.4095$ and $\|D\|_{\max} = \|D\|_{i2} = [\lambda_{\max}(D^T D)]^{1/2} = 1$.

Let $L = 1$ and select the matrix η as :

$$\eta = \begin{bmatrix} 4 & 0 \\ 0 & 8 \end{bmatrix};$$

then we can get $\min(\eta_i) = 4$.

$G = \min(\eta_i) - \|C(t)\|_{\max} - L\|D(t)\|_{\max} = 4 - 1.4095 - 1 > 1$.

We take $F_1(x, y, t) = x_1 y_1$ and $F_2(x, y, t) = 2x_2{}^2 y_2{}^2$. They are chaotic functions of time. By Eq. (7-6) we have

$$\lim_{t \to \infty} e_i = \lim_{t \to \infty} [y_i - F_i(x, y, t)] = 0, \quad i = 1, 2 \tag{7-20}$$

With the parameters and initial conditions above, the controller u

$$
\begin{aligned}
u &= D_x F(x,y,t)\, f_1(x,t) + D_y F(x,y,t)[C(t)y + D(t)\, f_2(y,t)] \\
&\quad + \frac{\partial F(x,y,t)}{\partial t} - \eta[y - F(x,y,t)] - D(t)\, f_2[F(x,y,t),t] \\
&\quad - C(t)F(x,y,t) \\
&= \begin{bmatrix} \frac{\partial F_1}{\partial x_1} & \frac{\partial F_1}{\partial x_2} \\ \frac{\partial F_2}{\partial x_1} & \frac{\partial F_2}{\partial x_1} \end{bmatrix} \begin{bmatrix} \dot{x}_1 \\ \dot{x}_2 \end{bmatrix} + \begin{bmatrix} \frac{\partial F_1}{\partial y_1} & \frac{\partial F_1}{\partial y_2} \\ \frac{\partial F_2}{\partial y_1} & \frac{\partial F_2}{\partial y_1} \end{bmatrix} \begin{bmatrix} \dot{y}_1 \\ \dot{y}_2 \end{bmatrix} + \begin{bmatrix} \frac{\partial F_1}{\partial t} & \frac{\partial F_1}{\partial t} \\ \frac{\partial F_2}{\partial t} & \frac{\partial F_2}{\partial t} \end{bmatrix} \\
&\quad - \begin{bmatrix} 4 & 0 \\ 0 & 8 \end{bmatrix} \begin{bmatrix} y_1 - x_1 y_1 \\ y_2 - 2x_2^2 y_2^2 \end{bmatrix} - \begin{bmatrix} 0 & 0 \\ 0 & 1 \end{bmatrix} \begin{bmatrix} 0 \\ -\beta(x_1 y_1)^3 + P_1 \sin(\omega_1 t) \end{bmatrix} \\
&\quad - \begin{bmatrix} 0 & 1 \\ -\omega_0^2 & -\alpha \end{bmatrix} \begin{bmatrix} x_1 y_1 \\ 2x_2^2 y_2^2 \end{bmatrix} \\
&= \begin{bmatrix} y_1 \dot{x}_1 \\ 4x_2 y_2^2 \dot{x}_2 \end{bmatrix} + \begin{bmatrix} x_1 \dot{y}_1 \\ 4x_2^2 y_2 \dot{y}_2 \end{bmatrix} - \begin{bmatrix} 4y_1 - 4x_1 y_1 \\ 8y_2 - 16x_2^2 y_2^2 \end{bmatrix} \\
&\quad - \begin{bmatrix} 0 \\ -(x_1 y_1)^3 + 0.8\sin(t) \end{bmatrix} - \begin{bmatrix} 2x_2^2 y_2^2 \\ x_1 y_1 - 1.4x_2^2 y_2^2 \end{bmatrix}
\end{aligned} \tag{7-20}
$$

is designed according to Eq. (7-8). Fig. 7.10 and Fig. 7.11 show the time histories of error functions $e_1(t)$, $e_2(t)$, respectively. Exactly, partner A (7-18) and partner B (7-19) are in symplectic synchronization.

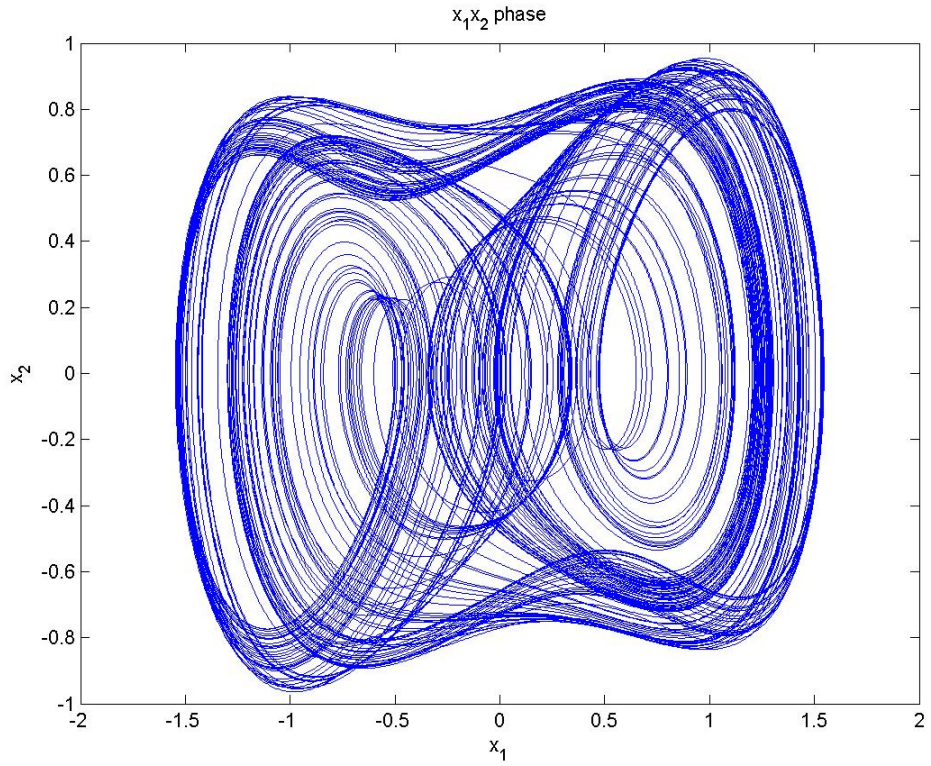

Fig. 7.1 Phase portrait of Duffing system.

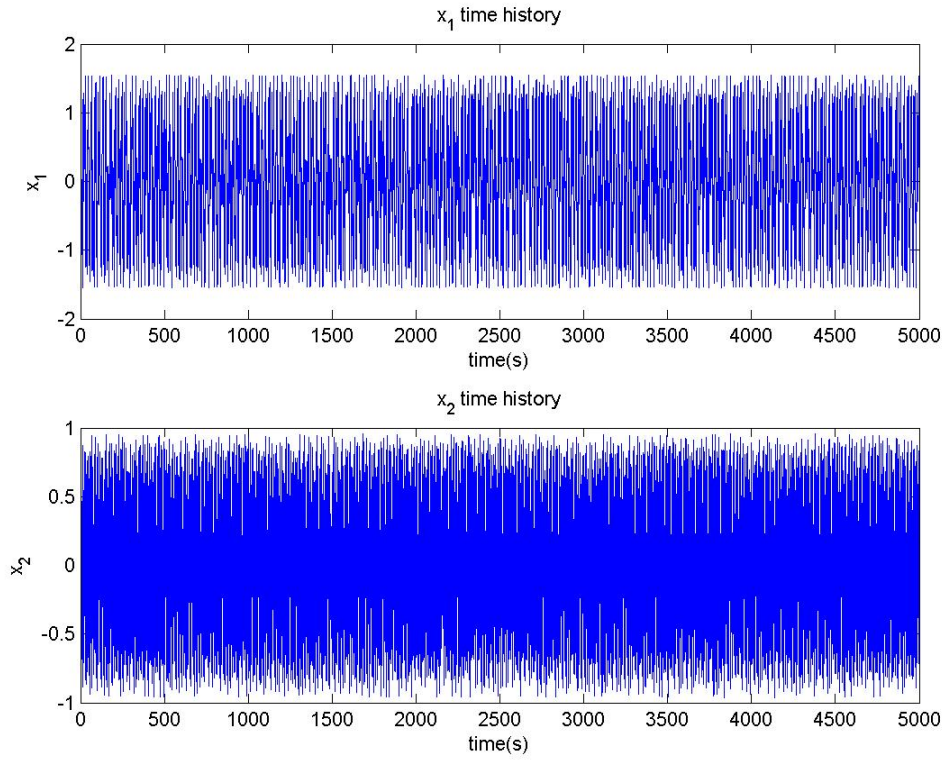

Fig. 7.2 Time histories of two states of Duffing system.

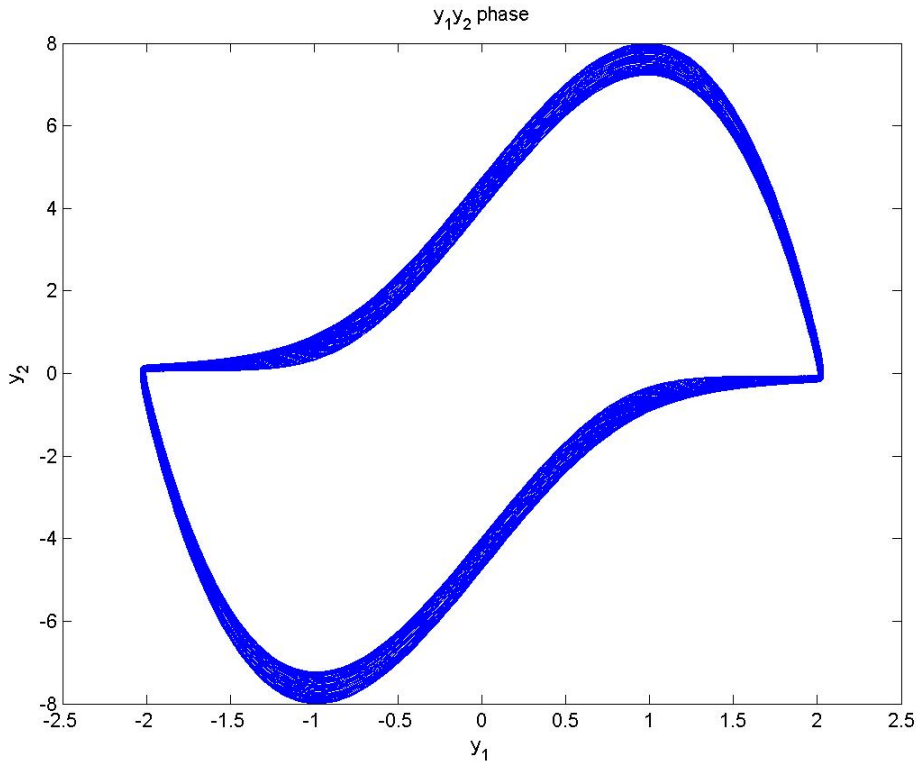

Fig. 7.3 Phase portrait of van der Pol system.

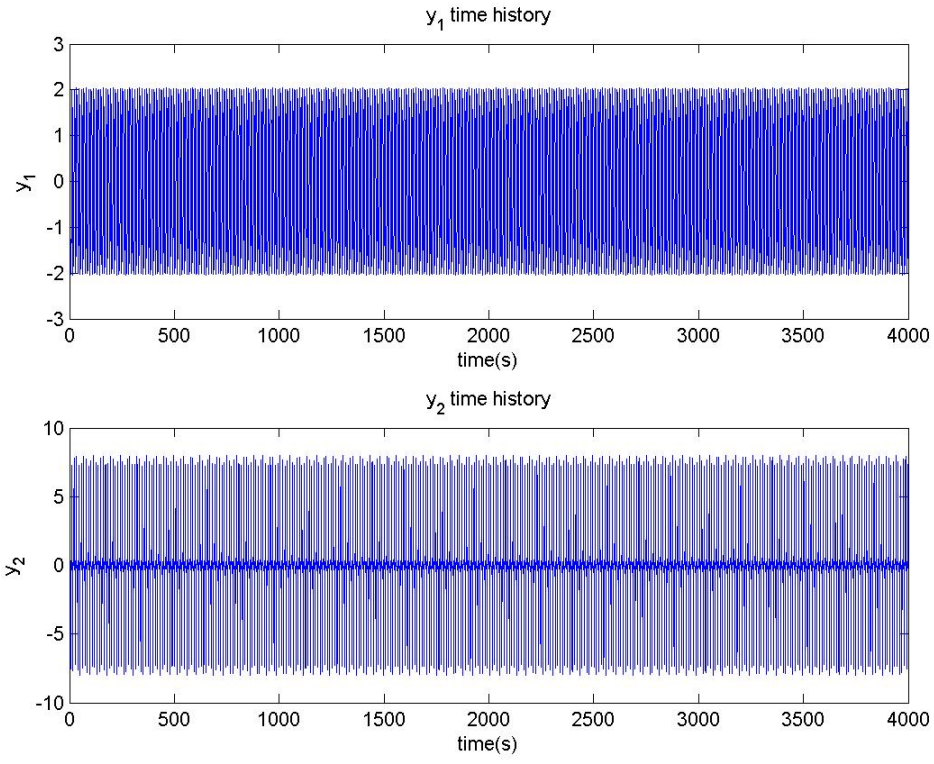

Fig. 7.4 Time histories of the two states of van der Pol system.

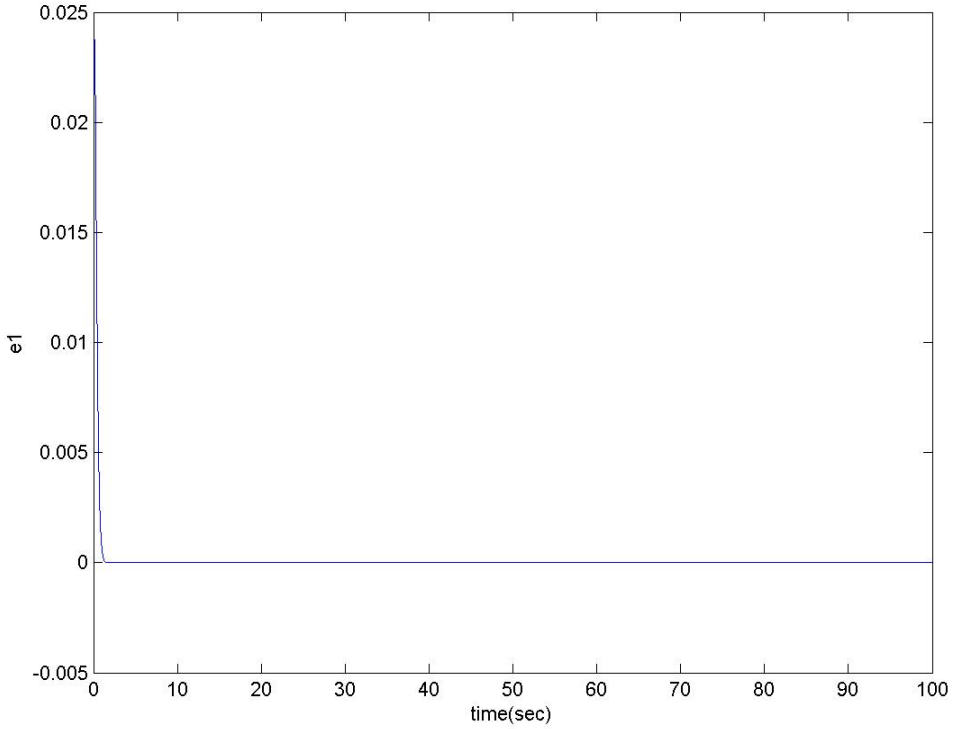

Fig. 7.5 Time history of error $e_1(t)$ for Case I.

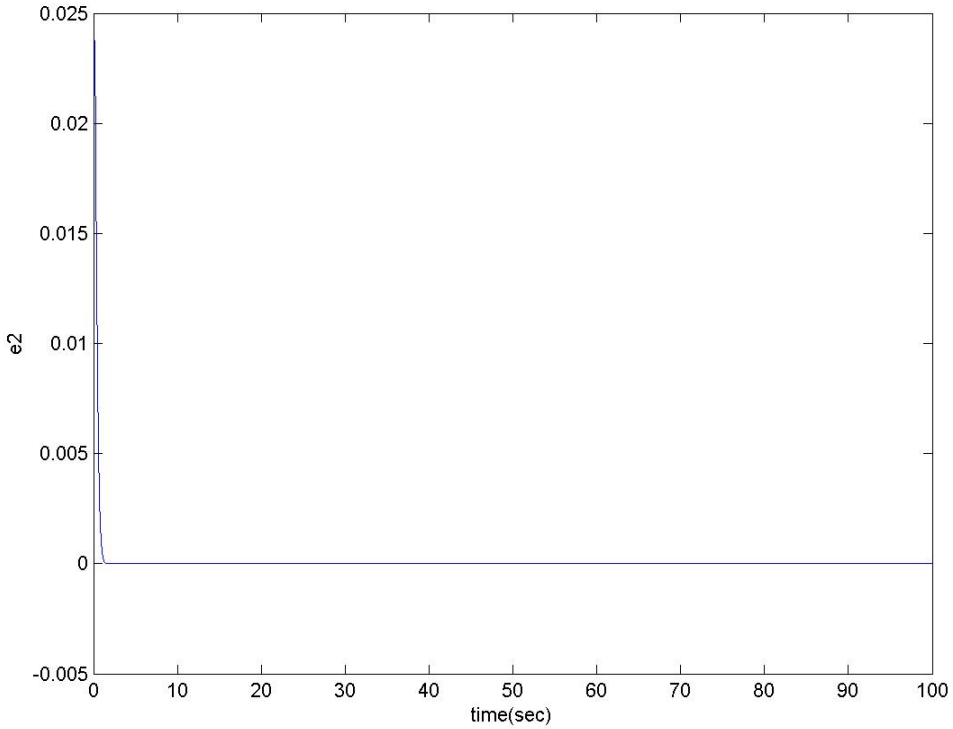

Fig. 7.6 Time history of error $e_2(t)$ for Case I.

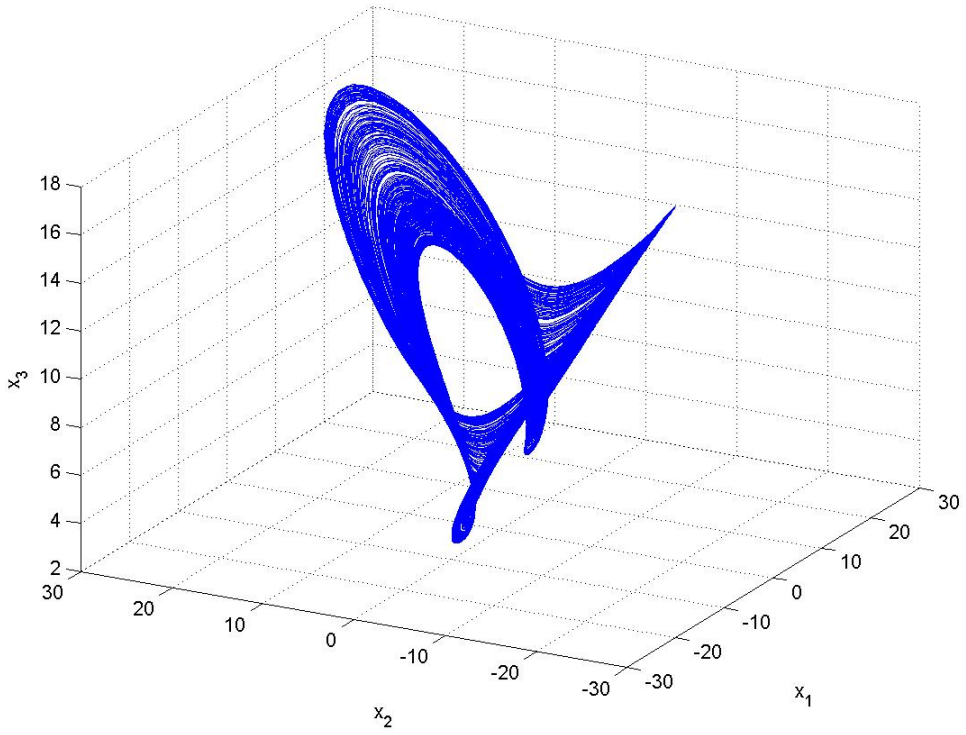

Fig. 7.7 Phase portrait of van der Pol system.

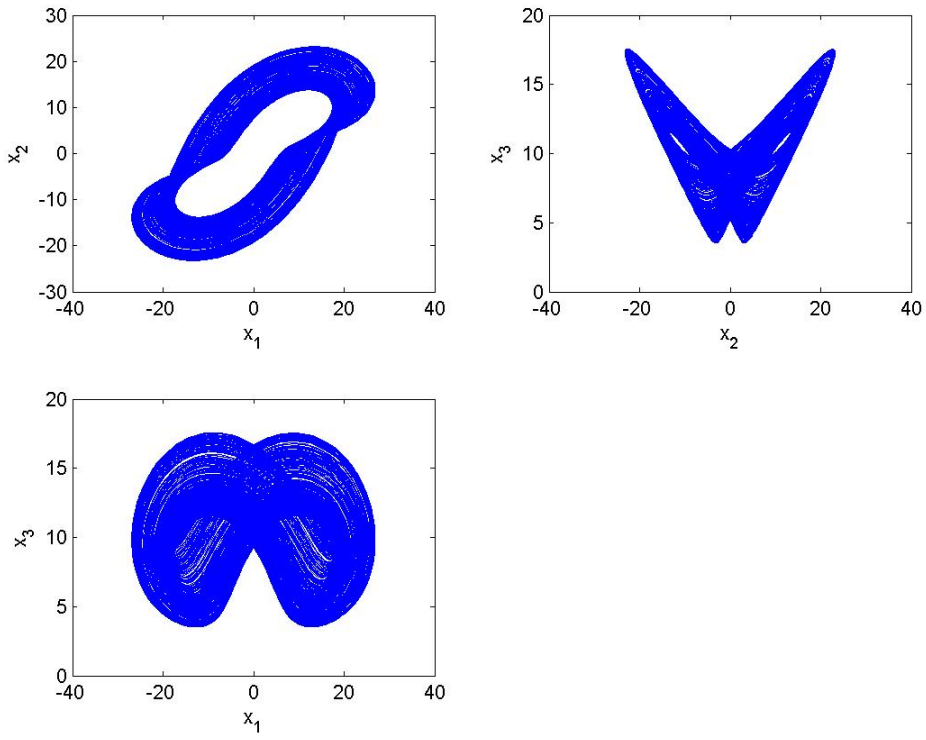

Fig. 7.8 Phase portraits of Chen-Lee system.

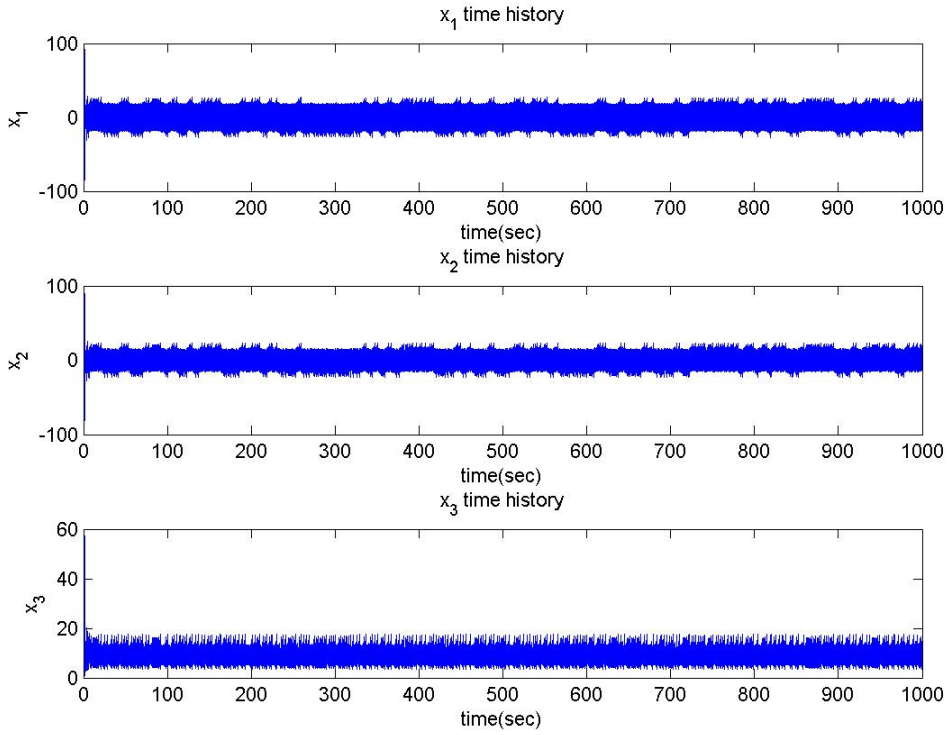

Fig. 7.9 Time histories of the three states of Chen-Lee system.

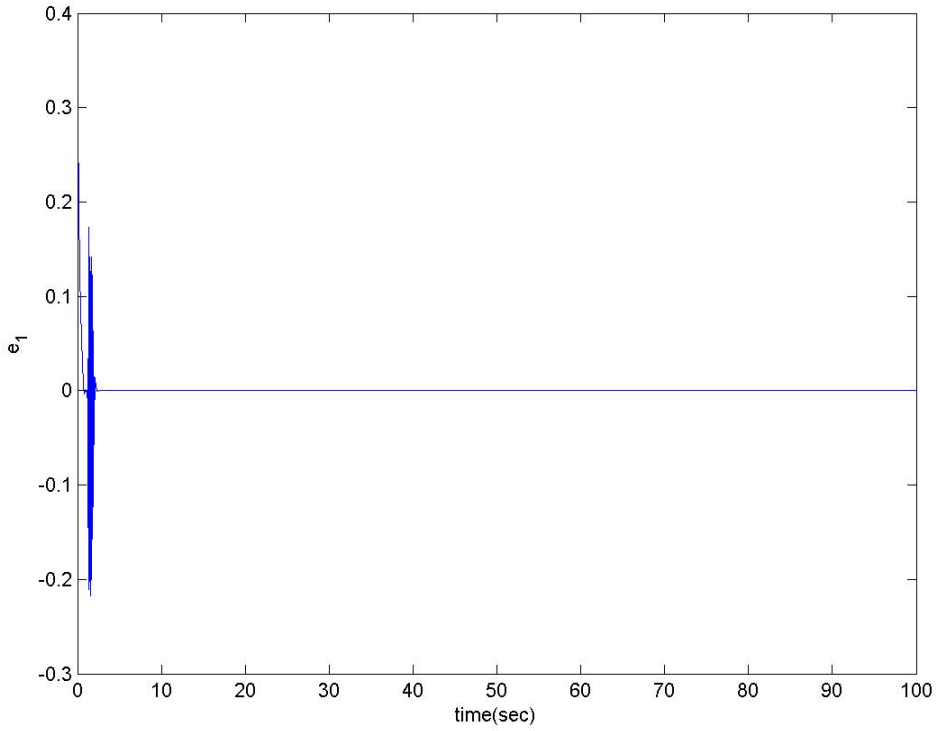

Fig. 7.10 Time history of error $e_1(t)$ for Case II.

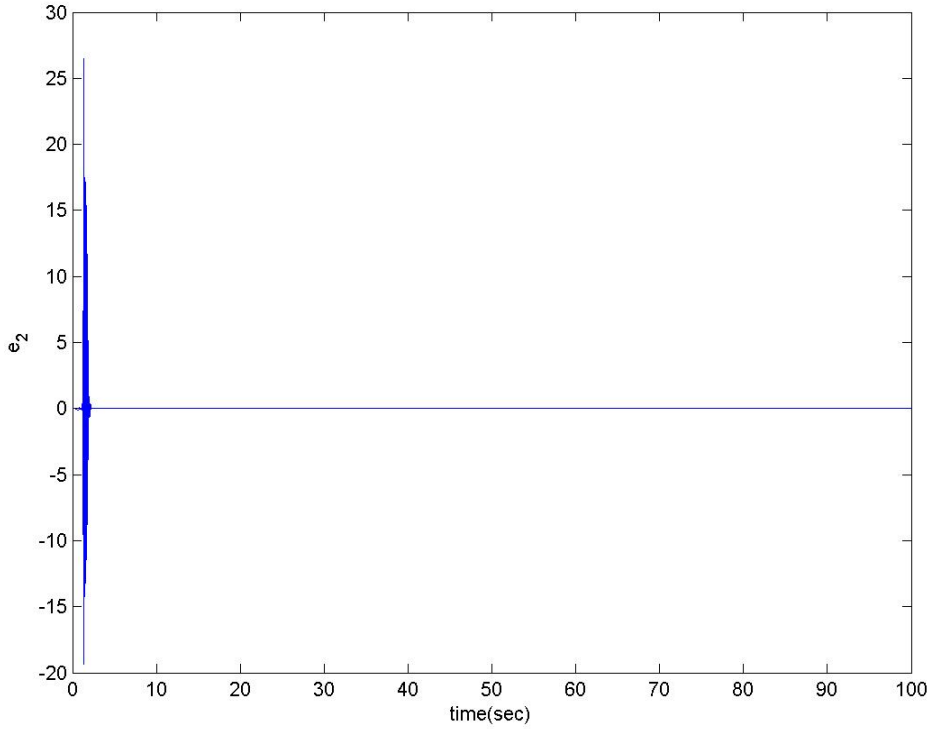

Fig. 7.11 Time history of error $e_2(t)$ for Case II.

Chapter 8

Conclusions

Chaos and boids control, generalized, symplectic synchronization and htperchaos of chaotic systems are studied in this thesis.

In Chapter 2, the chaotic behavior in an inertial tachometer system is studied by phase portraits, time history, Poincaré maps, Lyapunov exponent, bifurcation diagrams and parametric diagram.

In Chapter 3 and Chapter 4, a new strategy to achieve chaos generalized synchronization and chaos control by GYC partial region stability theory are proposed. By using the GYC partial region stability theory, the Lyapunov function is a simple linear homogeneous function of error states and the controllers are more simple and have less simulation error because they are in lower order than that of traditional controllers.

In Chapter 5, boids control that is an interesting strategy for control is presented. We have investigated several chaotic nonlinear networks controlled by several boids rules. They exhibited complex and emergent behaviors. The “synchronization” phenomenon can only be achieved with the proposed model. In this Chapter, the chaotic boids are controlled by using three state variables, and all boids are assumed to be identical for simplicity.

In Chapter 6, Lorenz system with Bessel function parameters is studied firstly. The results are verified by time histories of states, phase portraits, Poincaré maps, bifurcation analysis, Lyapunov exponents and parametric diagram. Abundant hyperchaos is found for this system. Especially enlarging the parameter with Bessel function, the hyperchaos is more obvious.

In Chapter 7, a new symplectic synchronization problems of nonautonomous chaotic systems are investigated based on Barbalat lemma [34]. Traditional generalized synchronizations are special cases of the symplectic synchronization. A sufficient condition is derived to ensure the symplectic synchronization between two different systems. The simulation results show that the proposed scheme can achieve not only the symplectic synchronization of chaotic systems with same order, but also the symplectic synchronization between chaotic systems with different orders. Symplectic synchronization may be applied to the design of secret communication with more security than generalized synchronization.

In Appendix A, GYC (Ge-Yao-Chen) partial region stability theory is given.

Appendix A

GYC Partial Region Stability Theory

Consider the differential equations of disturbed motion of a nonautonomous system in the normal form

$$\frac{dx_s}{dt} = X_s(t, x_1, \cdots, x_n), \qquad (s = 1, \cdots, n) \tag{A-1}$$

where the function X_s is defined on the intersection of the partial region Ω (shown in Fig. A-1) and

$$\sum_s x_s^2 \le H \tag{A-2}$$

and $t > t_0$, where t_0 and H are certain positive constants. X_s which vanishes when the variables x_s are all zero, is a real valued function of t, $x_1, \cdots, x_n$. It is assumed that X_s is smooth enough to ensure the existence, uniqueness of the solution of the initial value problem. When X_s does not contain t explicitly, the system is autonomous.

Obviously, $x_s = 0 \quad (s = 1, \cdots n)$ is a solution of Eq.(A-1). We are interested to the asymptotical stability of this zero solution on partial region Ω (including the boundary) of the neighborhood of the origin which in general may consist of several subregions (Fig. A.1).

Definition 1:

For any given number $\varepsilon > 0$, if there exists a $\delta > 0$, such that on the closed given partial region Ω when

$$\sum_s x_{s0}^2 \le \delta, \quad (s = 1, \cdots, n) \tag{A-3}$$

for all $t \ge t_0$, the inequality

$$\sum_s x_s^2 < \varepsilon, \quad (s = 1, \cdots, n) \tag{A-4}$$

is satisfied for the solutions of Eq.(A-27) on Ω, then the disturbed motion $x_s = 0 \quad (s = 1, \cdots n)$ is stable on the partial region Ω.

Definition 2:

If the undisturbed motion is stable on the partial region Ω, and there exists a $\delta' > 0$, so that on the given partial region Ω when

$$\sum_s x_{s0}^2 \le \delta', \quad (s = 1, \cdots, n) \tag{A-5}$$

The equality

$$\lim_{t \to \infty} \left(\sum_s x_s^2 \right) = 0 \tag{A-6}$$

is satisfied for the solutions of Eq.(A-1) on Ω, then the undisturbed motion $x_s = 0 \quad (s = 1, \cdots n)$ is asymptotically stable on the partial region Ω.

The intersection of Ω and region defined by Eq.(A-2) is called the region of attraction.

Definition of Functions $V(t, x_1, \cdots, x_n)$:

Let us consider the functions $V(t, x_1, \cdots, x_n)$ given on the intersection Ω_1 of the partial region Ω and the region

$$\sum_s x_s^2 \le h, \quad (s = 1, \cdots, n) \tag{A-7}$$

for $t \ge t_0 > 0$, where t_0 and h are positive constants. We suppose that the functions are single-valued and have continuous partial derivatives and become zero when $x_1 = \cdots = x_n = 0$.

Definition 3:

If there exists $t_0 > 0$ and a sufficiently small $h > 0$, so that on partial region Ω_1 and $t \ge t_0$, $V \ge 0$ (or ≤ 0), then V is a positive (or negative) semidefinite, in

general semidefinite, function on the Ω_1 and $t \geq t_0$.

Definition 4:

If there exists a positive (negative) definitive function $W(x_1 \ldots x_n)$ on Ω_1, so that on the partial region Ω_1 and $t \geq t_0$

$$V - W \geq 0 \ (or - V - W \geq 0), \tag{A-8}$$

then $V(t, x_1, \ldots, x_n)$ is a positive definite function on the partial region Ω_1 and $t \geq t_0$.

Definition 5:

If $V(t, x_1, \ldots, x_n)$ is neither definite nor semidefinite on Ω_1 and $t \geq t_0$, then $V(t, x_1, \ldots, x_n)$ is an indefinite function on partial region Ω_1 and $t \geq t_0$. That is, for any small $h > 0$ and any large $t_0 > 0$, $V(t, x_1, \ldots, x_n)$ can take either positive or negative value on the partial region Ω_1 and $t \geq t_0$.

Definition 6: Bounded function V

If there exist $t_0 > 0$, $h > 0$, so that on the partial region Ω_1, we have

$$\left|V(t, x_1, \ldots, x_n)\right| < L \tag{B.9}$$

where L is a positive constant, then V is said to be bounded on Ω_1.

Definition 7: Function with infinitesimal upper bound

If V is bounded, and for any $\lambda > 0$, there exists $\mu > 0$, so that on Ω_1 when $\sum_s x_s^2 \leq \mu$, and $t \geq t_0$, we have

$$\left|V(t, x_1, \ldots, x_n)\right| \leq \lambda \tag{A-10}$$

then V admits an infinitesimal upper bound on Ω_1.

Theorem 1 [28, 29]

If there can be found for the differential equations of the disturbed motion (Eq.(A-27)) a definite function $V(t, x_1, \ldots, x_n)$ on the partial region, and for which the derivative with respect to time based on these equations as given by the following :

$$\frac{dV}{dt} = \frac{\partial V}{\partial t} + \sum_{s=1}^{n} \frac{\partial V}{\partial x_s} X_s \tag{A-11}$$

is a semidefinite function on the paritial region whose sense is opposite to that of V, or if it becomes zero identically, then the undisturbed motion is stable on the partial region.

Proof:

Let us assume for the sake of definiteness that V is a positive definite function. Consequently, there exists a sufficiently large number t_0 and a sufficiently small number $h < H$, such that on the intersection Ω_1 of partial region Ω and

$$\sum_s x_s^2 \le h, \quad (s = 1, \ldots, n) \tag{A-12}$$

and $t \ge t_0$, the following inequality is satisfied

$$V(t, x_1, \ldots, x_n) \ge W(x_1, \ldots, x_n) \tag{A-13}$$

where W is a certain positive definite function which does not depend on t. Besides that, Eq. (A-7) may assume only negative or zero value in this region.

Let ε be an arbitrarily small positive number. We shall suppose that in any case $\varepsilon < h$. Let us consider the aggregation of all possible values of the quantities $x_1, \ldots, x_n$, which are on the intersection ω_2 of Ω_1 and

$$\sum_s x_s^2 = \varepsilon, \tag{A-14}$$

and let us designate by $l > 0$ the precise lower limit of the function W under this condition. by virtue of Eq. (B.5), we shall have

$$V(t, x_1, \ldots, x_n) \ge l \quad \text{for} \quad (x_1, \ldots, x_n) \quad \text{on} \quad \omega_2. \tag{A-15}$$

We shall now consider the quantities x_s as functions of time which satisfy the differential equations of disturbed motion. We shall assume that the initial values x_{s0} of these functions for $t = t_0$ lie on the intersection Ω_2 of Ω_1 and the region

$$\sum_s x_s^2 \le \delta, \tag{A-16}$$

where δ is so small that

$$V(t_0, x_{10}, \ldots, x_{n0}) < l \tag{A-17}$$

By virtue of the fact that $V(t_0, 0, \ldots, 0) = 0$, such a selection of the number δ is obviously possible. We shall suppose that in any case the number δ is smaller than ε.Then the inequality

$$\sum_s x_s^2 < \varepsilon, \tag{A-18}$$

being satisfied at the initial instant will be satisfied, in the very least, for a sufficiently small $t - t_0$, since the functions $x_s(t)$ very continuously with time. We shall show that these inequalities will be satisfied for all values $t > t_0$. Indeed, if these inequalities were not satisfied at some time, there would have to exist such an instant $t=T$ for which this inequality would become an equality. In other words, we would have

$$\sum_s x_s^2(T) = \varepsilon, \tag{A-19}$$

and consequently, on the basis of Eq. (A-9)

$$V(T, x_1(T), \ldots, x_n(T)) \geq l \tag{A-20}$$

On the other hand, since $\varepsilon < h$, the inequality (Eq.(A-4)) is satisfied in the entire interval of time [t_0, T], and consequently, in this entire time interval $\frac{dV}{dt} \leq 0$. This yields

$$V(T, x_1(T), \ldots, x_n(T)) \leq V(t_0, x_{10}, \ldots, x_{n0}), \tag{A-21}$$

which contradicts Eq. (A-12) on the basis of Eq. (A-11). Thus, the inequality (Eq.(A-1)) must be satisfied for all values of $t > t_0$, hence follows that the motion is stable.

Finally, we must point out that from the view-point of mathenatics, the stability on partial region in general does not be related logically to the stability on whole region. If an undisturbed solution is stable on a partial region, it may be either stable

or unstable on the whole region and vice versa. From the viewpoint of dynamics, we wre not interesting to the solution starting from Ω_2 and going out of Ω.

Theorem 2 [28, 29]

If in satisfying the conditions of theorem 1, the derivative $\frac{dV}{dt}$ is a definite function on the partial region with opposite sign to that of V and the function V itself permits an infinitesimal upper limit, then the undisturbed motion is asymptotically stable on the partial region.

Proof:

Let us suppose that V is a positive definite function on the partial region and that consequently, $\frac{dV}{dt}$ is negative definite. Thus on the intersection Ω_1 of Ω and the region defined by Eq. (A-4) and $t \geq t_0$ there will be satisfied not only the inequality (Eq.(A-5)), but the following inequality as will:

$$\frac{dV}{dt} \leq -W_1(x_1, \ldots x_n), \tag{A-22}$$

where W_1 is a positive definite function on the partial region independent of t.

Let us consider the quantities x_s as functions of time which satisfy the differential equations of disturbed motion assuming that the initial values $x_{s0} = x_s(t_0)$ of these quantities satisfy the inequalities (Eq. (A-10)). Since the undisturbed motion is stable in any case, the magnitude δ may be selected so small that for all values of $t \geq t_0$ the quantities x_s remain within Ω_1. Then, on the basis of Eq. (A-13) the derivative of function $V(t, x_1(t), \ldots, x_n(t))$ will be negative at all times and, consequently, this function will approach a certain limit, as *t* increases without limit, remaining larger than this limit at all times. We shall show that this limit is equal to some positive quantity different from zero. Then for all values of $t \geq t_0$ the following inequality will be satisfied:

$$V(t, x_1(t), \ldots, x_n(t)) > \alpha \tag{A-23}$$

where $\alpha > 0$.

Since V permits an infinitesimal upper limit, it follows from this inequality that

$$\sum_s x_s^2(t) \geq \lambda, \quad (s = 1, \ldots, n), \tag{B.24}$$

where λ is a certain sufficiently small positive number. Indeed, if such a number λ did not exist, that is , if the quantity $\sum_s x_s(t)$ were smaller than any preassigned number no matter how small, then the magnitude $V(t, x_1(t), \ldots, x_n(t))$, as follows from the definition of an infinitesimal upper limit, would also be arbitrarily small, which contradicts (A-14).

If for all values of $t \geq t_0$ the inequality (Eq. (A-15)) is satisfied, then Eq. (A-13) shows that the following inequality will be satisfied at all times:

$$\frac{dV}{dt} \leq -l_1, \tag{A-25}$$

where l_1 is positive number different from zero which constitutes the precise lower limit of the function $W_1(t, x_1(t), \ldots, x_n(t))$ under condition (Eq. (A-15)). Consequently, for all values of $t \geq t_0$ we shall have:

$$V(t, x_1(t), \ldots, x_n(t)) = V(t_0, x_{10}, \ldots, x_{n0}) + \int_{t_0}^{t} \frac{dV}{dt} dt \leq V(t_0, x_{10}, \ldots, x_{n0}) - l_1(t - t_0),$$

which is, obviously, in contradiction with Eq.(A-14). The contradiction thus obtained shows that the function $V(t, x_1(t), \ldots, x_n(t))$ approached zero as t increase without limit. Consequently, the same will be true for the function $W(x_1(t), \ldots, x_n(t))$ as well, from which it follows directly that

$$\lim_{t \to \infty} x_s(t) = 0, \quad (s = 1, \ldots, n), \tag{A-26}$$

which proves the theorem.

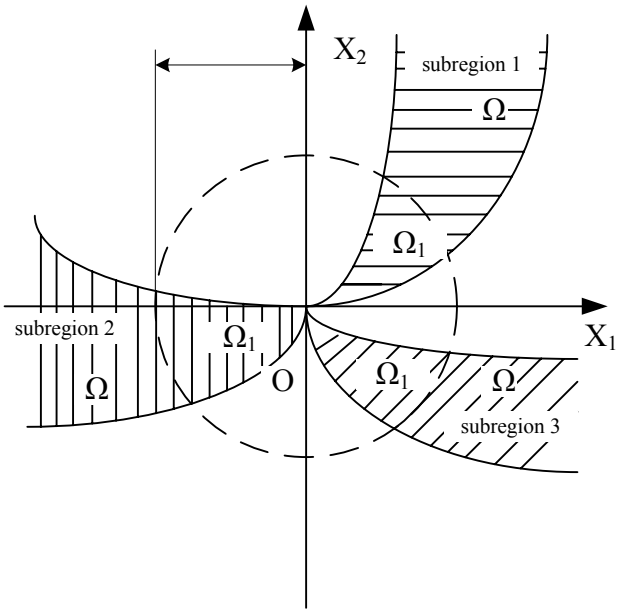

Fig. A.1. Partial regions Ω and Ω_1.

References

[1] Fujisaka H. and Yamada T., “Stability Theory of Synchronized Motion in Coupled-Oscillator Systems”, Prog. Theor. Phys., 69, 32, 1983.

[2] Pecora L.-M. and Carroll T.-L., “Synchronizations in chaotic systems”, Physical Review Letters, 64, pp.821-824, 1990.

[3] Zhou J. and Liu Z.-H., “Synchronized patterns induced by distributed time delays”, Physical Review E, 77, pp056213-1~5, 2008.

[4] Peng G.-J. and Jiang Y.-L., “Generalized projective synchronization of a class of fractional-order chaotic systems via a scalar transmitted signal”, Physics Letters A, 372, pp.3963–3970, 2008.

[5] Juan M. and Wang X.-Y., “Generalized synchronization via nonlinear control” Chaos, 18, pp.023108-1~5, 2008.

[6] Boccaletti S., “The synchronization of chaotic systems”, Phys. Rep., 366, pp.1-101, 2002.

[7] Kittel A., Parisi J. and Pyragas K., “Generalized synchronization of chaos in electronic circuit experiments”, Physica D, 112, pp.459-471, 1998.

[8] Rosenblum M., Pikovsky A. and Kurths J., “Phase synchronization of chaotic oscillators”, Physical Review Letters, 76, pp.1804-1807, 1996.

[9] Rosenblum M., Pikovsky A. and Kurths J., “Synchronization in a population of globally coupled chaotic oscillators”, Europhys. Lett., 34, pp.165-170, 1996.

[10] Pikovsky A.-S., Rowenblum M.-G., Osipov G.-V. and Kurths J., “Phase synchronization of chaotic oscillators by external driving”, Physica D, 104, pp.219-238, 1997.

[11] Barsella A. and Lepers C., “Chaotic lag synchronization and pulse-induced

transient chaos in lasers coupled by saturable absorber", Opt. Commun., 205, pp.397-403, 2002.

[12] Sivaprakasam S., Shahverdiev E.-M. Spencer P.-S. and Shore K.-A., "Experimental demonstration of anticipating synchronization in chaotic semiconductor laser with optical feedback", Physical Review Letters, 87, 154101, 2001.

[13] Chen J.-Y., Wong K.-W., Cheng L.-M. and Shuai J.-W., "A secure communication scheme based on the phase synchronization of chaotic systems", Chaos, 13, pp.508-514, 2003.

[14] Chen G. and Dong X., "On feedback control of chaotic continuous time systems", IEEE Transactions on Circuits and systems, 40, pp.591, 1993.

[15] Yassen M.-T., "Chaos control of Chen chaotic dynamical system", Chaos, Solitons and Fractals, 15, pp.271-283, 2003.

[16] Yassen M.-T., "Controlling chaos and synchronization for new chaotic system using linear feedback", Chaos, Solitons and Fractals, 26, pp.913-920, 2005.

[17] Agiza H.-N., "Controlling chaos for the dynamical system of coupled dynamos", Chaos, Solitons and Fractals, 13, pp.341-352, 2002.

[18] Lee S.-M., Ji D.-H., Park J.-H. and Won S.-C., "$H\infty$ synchronization of chaotic systems via dynamic feedback approach." Physics Letters A, 372, pp.4905-4912, 2008.

[19] Lin W., "Adaptive chaos control and synchronization in only locally Lipschitz systems", Physics Letters A, 372, pp.3195-3200, 2008.

[20] Mahmoud G.-M., Bountis T. and Mahmoud E.-E., "Active control and global synchronization of the complex Chen and Lü system."IJBC, 17, pp.4295-4308, 2008.

[21] Luo R.-Z., "Adaptive function project synchronization of Rössler hyperchaotic

system with uncertain parameters." Physics Letters A, 372, pp.3667-32671, 2008.

[22] Lian K.-Y., Huang C.-S.and Fang W.-H. and Su C.-H., "Chaotic control and chaotification using fuzzy approach." IJBC, 18, pp.263-274, 2008.

[23] Chen W.-H., Lu X.-M. and Chen F. "Impulsive synchronization of chaotic Lur'e systems via partial states." Physics Letters A, 372, pp.4210-4216. 2008.

[24] Hu M.-F., Yang Y.-Q, and Xu Z.-Y., "Impulsive control of projective synchronization in chaotic systems." Physics Letters A, 372, pp.3228-3233. 2008.

[25] Haeri M. and Dehghani M., "Impulsive synchronization of different hyperchaotic (chaotic) systems." Chaos, Solitons and Fractals, 38, pp.120-131, 2008.

[26] Ding W. and Han M.-A. "Synchronization of delayed fuzzy cellular neural networks based on adaptive control." Physics Letters A, 372, pp.4674-46812008.

[27] Lu J.-Q., Cao J.-D., Daniel and Ho W.-C., "Adaptive Stabilization and Synchronization for Chaotic Lur'e Systems With Time-Varying Delay." IEEE Transactions on Circuits and systems-I: Regular Papers, 55, pp.1347-1356, 2008.

[28] Ge Z.-M., Yao C.-W. and Chen H.-K., "Stability on Partial Region in Dynamics", Journal of Chinese Society of Mechanical Engineer, 15, No.2, pp.140-151,1994

[29] Ge Z.-M. and Chen H.-K., "Three Asymptotical Stability Theorems on Partial Region with Applications", Japanse Journal of Applied Physics, 37, pp.2762-2773, 1998 .

[30] Itoh M. and Chau L.-O., "Boids Control of Chaos", International Journal of Bifurcation and Chaos, Vol. 17, N0.2, pp.427-444, 2007.

[31] Chua L.-O., "*CNN: A Paradigm for Complexity*", World Scientific, Singapore, 1998.

[32] Chua L.-O., and Roska T., *Cellular Neural Networks and Visual Computing*,

Cambridge University Press, Cambridge, 2002.

[33] Ge Z.-M. and Yang C.-H., "Symplectic synchronization of Different Chaotic Systems", accepted by Chaos, Solitons and Fractals, 2007.

[34] Slotine and Li, *Applied nonlinear control,* Prentice-Hall, New Jersey, 1991.

[35] Chen H.-K., Lee C.-.I., "Anti-control of chaos in rigid body motion." Chaos, Solitons & Fractals, 21, pp.957-965, 2004.

[36] Itoh M. and Chua L.-O., "Star cellular neural networks for associative and dynamic memories", International Journal of Bifurcation and Chaos, Vol.14, pp.1725–1772, 2004.